NSWC/WOL/TR 75-63

NSWC/WOL/TR 75-63

NSWC TECHNICAL REPORT

WHITE OAK LABORATORY

EXPERIMENTAL INVESTIGATION OF A FIN-CONE INTERFERENCE FLOW FIELD AT MACH 5

BY
Joseph D. Gillerlain, Jr.

8 APRIL 1976

NAVAL SURFACE WEAPONS CENTER
WHITE OAK LABORATORY
SILVER SPRING, MARYLAND 20910

- Approved for public release; distribution unlimited

NAVAL SURFACE WEAPONS CENTER
WHITE OAK, SILVER SPRING, MARYLAND 20910

UNCLASSIFIED

SECURITY CLASSIFICATION OF THIS PAGE *(When Data Entered)*

REPORT DOCUMENTATION PAGE

READ INSTRUCTIONS BEFORE COMPLETING FORM

REPORT NUMBER: NSWC/WOL/TR-75-63	2. GOVT ACCESSION NO.
3. RECIPIENT'S CATALOG NUMBER	
4. TITLE *(and Subtitle)*: EXPERIMENTAL INVESTIGATION OF A FIN-CONE INTERFERENCE FLOW FIELD AT MACH 5.	5. TYPE OF REPORT & PERIOD COVERED: Technical rept.
	6. PERFORMING ORG. REPORT NUMBER
7. AUTHOR(s): Joseph D. Gillerlain, Jr	8. CONTRACT OR GRANT NUMBER(s)
9. PERFORMING ORGANIZATION NAME AND ADDRESS: Naval Surface Weapons Center, White Oak Laboratory, White Oak, Silver Spring, Maryland 20910	10. PROGRAM ELEMENT, PROJECT, TASK AREA & WORK UNIT NUMBERS: A320-320C/WF32-322-205
11. CONTROLLING OFFICE NAME AND ADDRESS	12. REPORT DATE: 8 Apr 1976
	13. NUMBER OF PAGES: 67
14. MONITORING AGENCY NAME & ADDRESS *(if different from Controlling Office)*: 71p.	15. SECURITY CLASS. *(of this report)*: UNCLASSIFIED
	15a. DECLASSIFICATION/DOWNGRADING SCHEDULE

16. DISTRIBUTION STATEMENT *(of this Report)*

Approved for public release; distribution unlimited

WF32-322 WF32-322-205

17. DISTRIBUTION STATEMENT *(of the abstract entered in Block 20, if different from Report)*

18. SUPPLEMENTARY NOTES

Excerpts presented at the Tenth Navy Symposium on Aeroballistics, 15-17 July 1975, Fredericksburg, Virginia

19. KEY WORDS *(Continue on reverse side if necessary and identify by block number)*

Interference heating
Fin-body interference
Phase-change paints
Pressure distributions
Oil-flow patterns

20. ABSTRACT *(Continue on reverse side if necessary and identify by block number)*

The general purpose of this investigation was to study the separated flow field associated with a fin-body juncture. Specific objectives included: (a) determining the severity and extent of aerodynamic heating, (b) providing flow visualization results to illustrate the flow structure, and (c) obtaining a data base of heat-transfer and surface-pressure measurements upon which to develop future analytical relations to predict peak interference heating levels. → OVER

DD FORM 1 JAN 73 1473 EDITION OF 1 NOV 65 IS OBSOLETE
S/N 0102-014-6601

UNCLASSIFIED

SECURITY CLASSIFICATION OF THIS PAGE *(When Data Entered)*

391 596

Tests were conducted at Mach 5 over a unit Reynolds number range of 4.5 to 26 million per foot. A fin-cone model was used. The data consist of surface-pressure distributions, heat-transfer measurements using the phase-change paint technique, and schlieren and oil-flow photographs. Results are presented for several fin-cone geometries to include fin sweep and fin-cone gap. Where possible, comparisons are made with fin-flat-plate data.

NSWC/WOL/TR 75-63 8 April 1976

EXPERIMENTAL INVESTIGATION OF A FIN-CONE INTERFERENCE FLOW FIELD AT MACH 5

This report documents a fin-body aerodynamic interference study conducted at the Naval Surface Weapons Center, White Oak Laboratory. Experimental results were obtained at Mach 5 for several Reynolds numbers and several fin-cone geometries.

This project was performed for the Naval Air Systems Command under AIRTASK No. A320-320C/WF32-322-205.

The author acknowledges the assistance of personnel in the Experimental Aerodynamics and Facility Engineering Support Branches in performing these tests and in preparing this report. Mr. Robert G. Ball deserves special credit for his photographic work.

K. R. ENKENHUS
By direction

CONTENTS

ILLUSTRATIONS

ILLUSTRATIONS (Cont'd)

ILLUSTRATIONS (Cont'd)

SYMBOLS

d	fin leading-edge diameter, fin thickness
h	heat-transfer coefficient
M_∞	free-stream Mach number
p	static pressure
p_o	total or supply pressure
p_∞	free-stream static pressure
Re_∞/ft	free-stream unit Reynolds number (per foot)
T_o	total or supply temperature
x	distance along cone ray
z	distance along cone surface normal

INTRODUCTION

Advanced high-speed flight vehicles which utilize fins as control surfaces may be subject to loss of control effectiveness due to flow separation or to possible loss of structural integrity as the result of fin-body interference heating. Depending on such geometrical factors as fin leading-edge sweep and bluntness, the bow shock of a control fin will interact strongly with the centerbody surface boundary layer, which is typically turbulent. The fin shock may cause the boundary layer to separate well upstream of the fin leading edge, resulting in an extensive separated flow region. Areas of substantially increased surface pressures accompanied by corresponding regions of high heat transfer may occur in the separated flow region. Designing around these problems usually results in overdesign with its consequential weight penalties. It would, therefore, be helpful to the designer to have information necessary to make reasonable estimates of peak pressure levels, peak heating rates, and the extent of flow separation.

References (1) and (2) cite over 900 studies of problems related to separated flow phenomena. Most investigations of the fin-body problem to date have dealt with fin-flat-plate configurations; for examples, see References (3)-(5). More recently, Bramlette (6) and Coleman and Lemmon (7) have investigated aeroheating phenomena associated with small roll-control fins on conical vehicles. In spite of these numerous studies, the ability to predict separated

---

(1) Ryan, B. M., "Summary of the Aerothermodynamic Interference Literature," Naval Weapons Center TN 4061-160, Apr 1969

(2) Korkegi, R. H., "Survey of Viscous Interactions Associated with High Mach Number Flight," AIAA Journal, Vol. 9, No. 5, May 1971, p. 771

(3) Kaufman, L. G., II, Korkegi, R. H., and Morton, L. C., "Shock Impingement Caused by Boundary Layer Separation Ahead of Blunt Fins," ARL Report 72-0118, Aug 1972, and AIAA Paper 73-236

(4) Winkelmann, A. E., "Experimental Investigations of a Fin Protuberance Partially Immersed in a Turbulent Boundary Layer at Mach 5," NOLTR 72-33, Jan 1972

(5) Winkelmann, A. E., "Flow Visualization Studies on a Fin Protuberance Partially Immersed in a Turbulent Boundary Layer at Mach 5," NOLTR 70-93, May 1970

(6) Bramlette, T. T., "A Study of Fin-Induced Laminar Interactions on Sharp and Spherically Blunted Cones," AIAA Paper 73-235, Jan 1973

(7) Coleman, H. W., and Lemmon, E. C., "Prediction of Turbulent Heat Transfer and Pressure on Swept Leading Edges," Journal of Spacecraft and Rockets, Vol. 11, No. 6, Jun 1974, pp. 376-381

flow phenomena either by mears of analytical solutions or on the basis of subscale tests is still very limited.

The general purpose of this investigation was to study the separated flow field associated with a general fin-body or wing-body juncture. Specific objectives included: (a) determining the severity and extent of interference heating, (b) providing flow visualization experiments to illustrate the flow structure, and (c) gathering a data base of heat-transfer and surface-pressure measurements upon which to develop future analytical relations to predict peak interference heating and peak pressure levels. A fin-cone configuration was tested at Mach 5 over a range of several Reynolds numbers. Heat transfer in the interference flow field was measured using the phase-change paint technique. Surface pressures were measured on the fin leading edge and on the cone ahead of th fin. These quantitative measurements were used in conjunction with both schlieren and oil-flow photographs in an effort to characterize the fin-cone interference flow field.

MODELS AND TEST PROCEDURES

Tests were conducted in the NAVSURFWPNCEN, White Oak Laboratory, Hypersonic Tunnel (Ref. (8)) at a nominal free-stream Mach number of 5 over a range of free-stream unit Reynolds numbers of about 4.5, 13, and 26 million per foot. Two geometrically identical fin-cone models were fabricated from existing conical models, one made of Teflon with a metal insert and a stainless-steel tip and the other of stainless steel. Both models consisted of a sharp, five-degree half-angle cone with two aft-mounted, cylindrically blunted fins 180 degrees apart, one unswept and one swept 60 degrees with respect to the cone surface normal. A schematic diagram of the models is shown in Figure 1. Photographs of both models are provided in Figures 2 and 3. The fins are adjustable by means of setscrews in a direction normal to the cone surface to simulate a control hinge configuration. For all test conditions, the cone was maintained at zero angle of attack and zero yaw and the fins were at zero cant. In all of the tests the models were injected into the flow rapidly using the hydraulic ram feature of the Hypersonic Tunnel after the desired test conditions had been established in the test cell. The Teflon model was utilized in the phase-change paint heat-transfer tests and in the oil-flow visualization experiments. The extension and fins were made of dark gray Teflon to provide better contrast with the paints, many of which dry to a light opaque color. The stainless-steel model was used in the pressure distribution tests. Further details of both models are included in Appendix A.

(8) Baltakis, F. P., "Performance Capability of the NOL Hypersonic Tunnel," NOLTR 68-187, Oct 1968

HEAT-TRANSFER MEASUREMENTS

Heat transfer in the interference flow field was measured by means of a temperature-sensitive paint method, specifically the phase-change paint technique pioneered by Jones and Hunt (Ref. (9)) at the NASA, Langley Research Center. In recent years the technique has evolved into a useful diagnostic tool which is considered capable of providing reliable quantitative heat-transfer data. It is especially applicable to complex geometries with interference heating patterns of unknown severity and extent. The phase-change paint technique and extensions of the method are well documented; for example, see References (9) and (10). Use of the technique at NAVSURFWPNCEN, White Oak Laboratory, is documented in Reference (11). Basically, the method consists of coating a model with a paint which is rated to change phase, i.e., melt, from a dry crystalline opaque solid to a clear liquid irreversibly at a specific rated temperature. The model is injected into the flow and progression of the melt-line location is recorded on movie film. This time input used in conjunction with the thermophysical properties of the model material determines the heat-transfer coefficient, h, in the data-reduction scheme. The model is assumed to behave like a semi-infinite slab and to undergo a step increase in heat transfer to a constant value of heat-transfer coefficient at any given point on its surface upon being exposed to the flow. The data reduction is based further on the assumption that the coating and the model surface are at the same temperature at the same time. Therefore, only a very thin (0.001 inch or less) coating is necessary. To achieve this condition, the paints were thinned using a special thinner specified by the manufacturer (Tempilaq Thinner and Tempilaq Phase-Change Paints by the Tempil Corporation), and were applied fairly uniformly to the model by means of an airbrush. These particular temperature-sensitive paints are considered well suited for short-duration high-speed wind-tunnel tests. They have been found to be insensitive to ambient pressures or heating rates in exhibiting their rated melting temperatures (9). Calibration checks (11) at NAVSURFWPNCEN, White Oak Laboratory, showed the paints to melt at temperatures in good agreement with those specified by the manufacturer.

Another necessary input for the phase-change paint data-reduction scheme is the initial temperature of the model. This information was provided by four embedded thermocouples in the Teflon model, one in each fin and one in the cone ahead of each fin.

(9) Jones, R. A., and Hunt, J. L., "Use of Fusible Temperature Indicators for Obtaining Quantitative Aerodynamic Heat-Transfer Data," NASA TR R-230, Feb 1966

(10) Hunt, J. L., Pitts, J. I., and Richie, C. B., "Application of Phase-Change Technique to Thin Sections with Heating on Both Surfaces," NASA TN D-7193

(11) Gillerlain, J. D., Jr., "Use of Phase-Change Paints to Study Fin-Body Interference Heating, NSWC/WOL/TR 75-62, Apr 1976

Secondarily, these thermocouples provided a check on when the semi-infinite slab approximation was violated. (See Appendix A, Fig. A-1.)

Teflon was chosen as the model material partly because of its low thermal diffusivity which enhanced its semi-infinite slab behavior. In addition, Teflon was strong enough to withstand the loading associated with rapid injection of the model, and it had a fairly high melting temperature. Also, lateral conduction effects were minimized due to its thermophysical properties. Typical values of the thermophysical properties of Teflon are given in Reference (11) as determined from other sources. Additional information may be found in Reference (12).

PRESSURE MEASUREMENTS

The stainless-steel model was instrumented with pressure taps on the fin leading edges and on the cone ahead of the fins extending about six fin thicknesses (leading-edge diameters) upstream on the fin centerline. (See Appendix A, Fig. A-2.) Each tap had its own strain-gage-type pressure transducer mounted in a multiple transducer bank. Selected pressure taps were monitored during a test run to assure that the data reflected full response of the taps.

OIL-FLOW TESTS

Oil-flow tests in general provide visual data on surface shear directions on a model surface. A 350-centistokes silicone oil (Dow 200 dielectric fluid) was used with titanium oxide powder in suspension to provide white pigmentation. A mixture of one part silicone oil to one part titanium oxide with five or six drops of oleic acid was found to be suitable for the range of Reynolds numbers tested. The oil mixture was applied to the model in a direction transverse to the free-stream flow direction. The model was rapidly injected into the flow and photographs were taken with the tunnel running once the desired patterns had developed.

SCHLIEREN PHOTOGRAPHS

Schlieren photographs were obtained using the flow visualization system of the Hypersonic Tunnel (Ref. (8)).

EXPERIMENTAL RESULTS AND DISCUSSION

Results are presented for several fin-cone configurations: (a) the fins mounted flush on the cone, (b) a fin-cone gap of 0.060 inch, and, (c) a fin-cone gap of 0.125 inch. A free-stream unit Reynolds number range of about 4.5, 13 and 26 million per foot is represented. The lowest Reynolds number condition comprises the most complete set of overall data, mainly because the fin side-heating data are considered reliable for this case.

(12) Wentink, T., Jr., "High Temperature Behavior of Teflon," AFBMD-TN-59-15, Jul 1959

SCHLIEREN AND OIL-FLOW PHOTOGRAPHS

Examination of the flow visualization data provides insight to the heat-transfer and pressure distribution patterns to be presented subsequently. Schlieren photographs are shown in Figure 4 for the flush-mounted fins, in Figure 5 for a 0.060-inch fin-cone gap, and in Figure 6 for the 0.125-inch fin-cone gap. The cone bow shock did not impinge on the fins in any of the tests, by design. Figure 4 shows that the flush-mounted unswept fin with its strong bow shock causes a separation-induced shock wave which impinges on the fin leading edge. The flush 60-degree-swept fin is sufficiently swept that very little upstream separation is apparent. When the fins are gapped off the surface, as they might be in a control-hinge configuration, in both Figures 5 and 6 the flow displays complex inlet flow patterns in the gap. The unswept fin displays a very complex pattern of reflected shocks in the gap. The swept fin shows flow attachment at its leading tip. In all of the schlieren photographs, weak shock waves are seen to propagate from the interface of the original cone and the finned extension.

Figure 7 shows a side-view oil-flow target pattern. The oil mixture was brushed on the model transverse to the flow direction. A side-view oil-flow photograph for the flush-mounted fins is shown in Figure 8. Recall that the oil is swept away in regions of high shear and pools along lines of flow separation. The lateral extent of the separated flow region associated with the unswept fin is immediately obvious. An oil accumulation line on the side of the unswept fin indicates flow separation associated with a corner vortex pattern. Figures 9 and 10 provide additional visual information for this fin-cone geometry by showing top views of the unswept and swept fin, respectively. The viewing angle is along a cone surface normal. In Figure 9, the existence of two separation lines is apparent. The primary separation line occurs about 2.2 fin leading-edge diameters (fin thickness, d) upstream of the unswept fin's leading edge. This line marks the initial flow separation of the cone boundary layer due to the adverse pressure gradient caused by the fin bow shock. This behavior of separation about 2d upstream appears to be characteristic of turbulent boundary-layer separation ahead of blunt fins of height and thickness greater than the local boundary-layer thickness over a Mach number range of about 1.2 to 2.1 independent of Reynolds number (Ref. (13)). The behavior apparently carries over from fin-plate to fin-cone geometries for the conditions indicated.

In Figure 9 a secondary separation line occurs about 0.7d upstream. The region between the primary and secondary separation lines is usually called "separated flow" while the region between the

(13) Westkaemper, J. C., "Turbulent Boundary-Layer Separation Ahead of Cylinders," AIAA Journal, Vol. 6, No. 7, Jul 1968, pp. 1352-1355

secondary separation line and the fin is called "reattached flow" ((5), (14)). A local spot from which there is apparent outward flow occurs about 1d upstream. A similar flow attachment point was observed by Winkelmann ((4), (5)) and will be noted later in the heat-transfer data. Lastly, in Figure 9 there is evidence of "herringbone" oil-flow patterns outboard of the fin. These patterns are indicative of vortical patterns trailing off downstream from the fin centerline interaction region which includes horseshoe vortices ((3), (4)).

In Figure 10 both primary and secondary separation occur within about 0.3d upstream of the swept fin. (Evident in the figure is an epoxy-plaster plug in the fin leading edge, which was necessitated by loss of a Teflon plug in an earlier test. The plug had originally provided access to the fin thermocouple.) The reduced lateral extent of outboard disturbance is evident by merely sweeping the fin a sufficient amount.

Figure 11 shows the oil-flow side view for the 0.060-inch gap. The flow is beginning to interact with the fin-hinge corner. The flow has moved into the gap somewhat, because Figure 12, which is a top view of the gapped unswept fin, shows primary separation to occur now about 1.7d. Secondary separation occurs about 0.5d upstream. The herringbone patterns from the fin hinge are most evident. The top-view oil-flow photograph for the swept fin in Figure 13 shows clearly how the flow in the gap begins to interact with the fin hinge. Primary separation still occurs ahead of the leading tip.

Figure 14 shows the oil-flow side view for the 0.125-inch gap. The flow interacts strongly with fin-hinge corner resulting in pronounced regions of high shear on the sides of both fins. In Figure 15, which is a top view of the gapped unswept fin, primary separation now occurs only about 1d upstream. The secondary separation line is not well defined near the fin leading edge due to the complex flow pattern associated with the gap. When the flow in the gap interacts with the fin hinge, a separation line appears which has a very interesting and unusual changing curvature as it moves outboard. The changing curvature is probably the result of its interaction with the vortical patterns from the upstream separation regions. Once again the "herringbone" patterns are very evident. The top-view oil-flow photograph for the gapped swept fin, Figure 16, shows clearly how the flow now interacts with the fin hinge, creating an outboard disturbance region comparable to that of the unswept flush-mounted fin. Also note that primary separation does not occur until the flow is in the gap.

---

(14) Young, F. L., Kaufman, L. G., and Korkegi, R. H., "Experimental Investigation of Interactions Between Blunt Fin Shock Waves and Adjacent Boundary Layers at Mach Numbers 3 and 5," ARL Report 68-0214, Dec 1968

HEAT-TRANSFER MEASUREMENTS

Keeping in mind the oil-flow patterns, consider now the heat-transfer results. The reduced phase-change paint data are presented as lines of constant heat-transfer coefficient, h, so-called iso-heating contours. Figures 17 and 18 show side and top views, respectively, of the flush-mounted unswept fin for the lowest Reynolds number. Figures 19 and 20 show top views for the higher Reynolds numbers. The amount of detail is somewhat a function of the rated melting temperature of the paint used. Side-view data are not presented for the two higher Reynolds numbers. These data are considered not to be as reliable because the fins generally are believed not to have behaved as semi-infinite slabs based on the embedded thermocouple temperature indications. Note that in Figures 18-20 the viewing angle is about 10 degrees forward of a normal to the cone surface at the fin leading edge. (This angle view was used in an attempt to obtain more detail about the leading-edge heating. The slight inclination was a physical constraint of the tunnel windows and model position. The additional leading-edge detail was not achieved due to the rapid heating rates.) Regions of high heating comparable to that near the leading edge are shown to occur in a crescent-shaped region at the fin "foot" and at the flow reattachment point about 1d upstream. High heating at this point 1d upstream identifies it as a high-shear region, or as a point where flow is entrained and brought into contact with the cone surface. This appears to be contrary to Winkelmann's conclusion (5) that this reattachment point is a low-shear or "dead air" region.

Isoheating contours for the swept fin are shown in side and top views in Figures 21 and 22, respectively, for the low Reynolds number condition. Both the level and extent of interference heating are greatly reduced. The dotted lines on the leading edge of the fin in Figure 21 indicate where the plug was located. The maximum h-value is down about 25 percent on the leading edge and that on the cone is down about 40 percent from the unswept fin case. This is purely a sweep effect.

Figure 23 shows a higher Reynolds number case. Only limited data are available for the highest Reynolds number as shown in Figure 24.

Figures 25 and 26 show the low Reynolds number case for the 0.060-inch gapped unswept fin. The severity of heating in the fin-hinge corner begins to approach that of the fin leading edge and fin foot region. Figures 27 and 28 show top views for the higher Reynolds numbers for this configuration.

Figure 29 displays the low Reynolds number isoheating contours for the side of the swept fin gapped at 0.060 inch. The top view is shown in Figure 30, where it is evident that severe flow interaction is occurring just under the leading tip and in the vicinity of the fin-hinge corner. Top views for the higher Reynolds numbers appear in Figures 31 and 32.

Figures 33 and 34 show isoheating contours for the 0.125-inch gapped unswept fin. The fin hinge clearly shows up as having an interaction flow field with heat transfer as severe as that on and around the fin leading edge. The heating level at primary separation remains at about the same level as for the flush-mounted fin. Now, both the fin "foot" region (a misnomer since the fin is gapped here) and the hinge region are comparable areas of high-interference heating. The two higher Reynolds numbers cases are shown in Figures 35 and 36.

Heat-transfer data for the 0.125-inch gapped swept fin are shown in Figures 37 and 38. From Figure 37 it may be seen that the immediate leading-edge segment and the hinge have heating levels comparable to the unswept fin case. In contrast, however, Figure 38 indicates a marked decrease in the interference heating level on the cone to about 60 percent of that for the gapped unswept fin. This would indicate that sufficient leading-edge sweep alone produces less lateral disturbance in the form of a separated flow region and results in lower interference heating levels in the disturbed region on the centerbody. Figures 39 and 40 provide data for the two higher Reynolds numbers.

In Figures 17 through 40 the accuracies of the heat-transfer coefficients vary according to factors in the data-reduction scheme as discussed in Reference (11). Generally, the data are considered to be accurate within a 20 to 30 percent range. The low Reynolds number data are considered the most reliable.

CONE SURFACE-PRESSURE DISTRIBUTIONS

Again recalling the oil-flow patterns of Figures 8-15, consider the surface-pressure distributions measured on the cone ahead of the fins. Figure 41 shows the flush-mounted unswept fin. The surface pressures are normalized by the undisturbed cone value, which was sensed generally by several of the most upstream taps. The abscissa is distance along the fin-centerline cone ray referenced to the fin leading edge and normalized by the fin leading-edge diameter (fin thickness, d). Data are shown for three Reynolds numbers. The pressure begins to rise a little more than 2d upstream, corresponding to the point where primary separation occurs. It rises to a slight peak, then dips, and rises again to a high peak in the fin foot region about 0.25d upstream of the leading edge. The peak pressure in the fin foot region is about 10 times the undisturbed level. Winkelmann (4) observed peak pressure ratios only about six times the undisturbed value for his fin-flat-plate configuration. Lucas (15) recorded peak pressure levels about 8 to 10 times free-stream values from his blunt fin-flat-plate tests. The peak pressure region

(15) Lucas, E. J., "Investigation of Blunt Fin-Induced Flow Separation Region on a Flat Plate at Mach Numbers 2.5 to 4.0," AEDC-TR-70-265, Jan 1971

corresponds to the crescent-shaped peak heating region of Figure 13. The reattachment zone 1d upstream, which had earlier been found to be a high-heating region, corresponds here only to a point where the pressure dips after the initial rise. The pressure ratios at the point of separation and the curves in general are not construed to represent a definite Reynolds number effect. Rather, the differences are thought to be indicative of flow unsteadiness and instability associated with the separated flow region and the likely scavenging action of the horseshoe vortices ((3), (4)).

Figure 42 shows the corresponding pressure distribution on the cone ahead of the swept fin. As expected, there is almost no upstream disturbance.

Figures 43 and 44 show pressure distributions for the 0.060-inch gapped unswept and swept fins, respectively. Pressure taps existed in the gap as shown. In Figure 43 the first pressure rise peak occurs about 1.3d upstream followed by a maximum peak in the fin foot region. This maximum is less than that in Figure 41. Some abatement must occur by the flow's being able to move into the fin-cone gap. Subsequently, a peak occurs as the flow begins to interact with the fin hinge.

Figure 44 indicates that pertubations occur in the gap for the swept fin while upstream effects are still minimized by sweep.

Figure 45 shows the 0.125-inch gapped unswept fin and Figure 46 shows the corresponding swept fin. In both cases the flow moves into the gap and displays its peak pressure in the gap. In Figure 45 the peak pressure level, down from 10 to 8, occurs just inside the gap. In question here is the exact location of the peak with respect to the tap location. After this first pressure peak, the flow appears to begin to interact with the hinge, but insufficient data exist. It may be noted that the initial pressure rise is observed to begin about 1d upstream of the unswept leading edge, corresponding to the location of the primary separation line in Figure 15.

In Figure 46 an attenuated pressure peak occurs about 2d into the gap. This lower peak pressure corresponds to the lower peak heating indicated in Figure 38.

FIN LEADING-EDGE PRESSURE DISTRIBUTIONS

Figure 47 shows the leading-edge pressure distribution for both of the flush-mounted fins. Distance, z, along the cone surface normal at the plane of the leading edge is nondimensionalized by the fin leading-edge diameter, d. The pressures are normalized by the free-stream static pressure. The relative difference in the pressure levels is explained by oblique shock theory. The bulge in the pressure distribution on the unswept fin's leading edge corresponds to impingement of the separation-induced shock wave which appears in the schlieren photograph of Figure 4 to occur at about $z/d \approx 0.9$. No pressure tap exists at $z/d = 0.5$ in the swept fin because of physical limitations in fabricating the fin.

The fin leading-edge pressure data for the gapped fins are shown in Figures 48 and 49. Figure 48 is felt to be indicative of the fluctuating pressures in the immediate shock impingement area for the unswept fin.

CONCLUDING REMARKS

The interaction flow field on a fin-cone configuration was studied at Mach 5 at unit Reynolds numbers from 4.5 to 26 million per foot. The interference flow field produced peak interference heating rates and peak pressures, which are considerably higher than in non-interference regions on the cone. The problem is a non-trivial one. In fact, Hains and Keyes (Ref. (16)) have measured peak interference heating rates up to 17 times the interference-free stagnation point value and peak pressures up to eight times the freestream pitot pressure on a hemisphere in a Mach 6 freestream with the extraneous shock generated by a wedge.

The interaction flow field on fin centerline for an unswept, cylindrically blunted fin flush-mounted on a cone appears to be qualitatively similar to, and not significantly quantitatively different from, fin-flat-plate results for similar flow conditions. For example, Winkelmann (Ref. (4)), measured peak heating levels on the order of five times those outside the interference flow field in his fin-flat-plate experiments. The fin-cone flow field is also characterized by peak heating rates about five times those outside the interference region for a flush-mounted, unswept fin.

Lucas (Ref. (15)) measured peak pressures of about eight - ten times the non-interference level in the fin foot region of his blunt fin-flat-plate model. The peak pressures measured here for a flush-mounted, unswept fin-cone configuration are also about ten times the non-interference levels on the cone. Winkelmann (Ref. (4)) observed peak pressures of about six times the non-interference level on his flat plate.

Fin leading-edge sweep alone significantly reduces the severity and extent of interference heating on the centerbody. However, when a swept fin design embodies a control hinge in the form of a circular rod, the flow in the fin-centerbody gap will interact with the control hinge. This interaction results in peak heating on the centerbody comparable to that for a flush-mounted unswept fin. Whereas sweeping the control hinge is not a practical solution, the severity of the flow interaction may possibly be alleviated by providing a control hinge fairing.

(16) Hains, F. D. and Keyes, J. W., "Shock Interference Heating in Hypersonic Flows," AIAA Journal, Vol. 10, 1972, pp 1441-1447

Separation occurs about two fin leading-edge diameters upstream of a flush-mounted unswept fin independent of Reynolds number. This behavior is characteristic of cylindrically blunted fin-flat-plate and cylinder-flat-plate results over a wide Mach number range (1.2 to 21) when the fin height and thickness exceed the local boundary layer thickness (Refs. (13), (3)).

The complexity of the flow patterns indicated by these pressure, heat-transfer and flow visualization data are clear indications why such problems defy analytical treatment. Theoretical attempts at predicting the plate heating rates and peak pressures have been limited largely to semiempirical approaches (Refs. (17), (18), (19)). Recently, a two-dimensional numerical method solution was reported for blunt body flows with an impinging shock (Ref. (20)). The method is entirely numerical, and the required computing time makes it somewhat impractical for parametric analysis. Theoretical efforts at NAVSURFWPNCEN, White Oak Laboratory, included a basic study of shock-interference heating by Chien (Ref. (21)), which resulted in an efficient, approximate method for predicting the jet impingement process in the shock interference heating phenomena. Chien's method, in addition to being simple, also appears to be more rational than the earlier empirical methods.

More experimental studies are required in order to assess these predictive methods. The information here provides some of the needed data base.

---

(17) Edney, B.. "Anomalous Heat Transfer and Pressure Distributions on Blunt Bodies at Hypersonic Speeds in the Presence of an Impinging Shock," FFA Report 115, The Aeronautical Research Institute of Sweden, Stockholm, 1968

(18) Keyes, J. W. and Hains, F. D., "Analytical and Experimental Studies of Shock Interference Heating in Hypersonic Flows," NASA TN D-7139, May 1973

(19) Bertin, J. J., Graumann, B. W. and Goodrich, W. D., "High Velocity and Real-Gas Effects on Weak Two-Dimensional Shock-Interaction Patterns," Journal of Spacecraft and Rockets, Vol. 12, 1975, pp 155-161

(20) Tannehill, J. C., Holst, T. L. and Rakich, J. V., "Numerical Computation of Two-Dimensional Viscous Blunt Body Flows with an Impinging Shock," AIAA Journal, Vol. 14, 1976, pp 204-211

(21) Chien, K.-Y., "Normal Shock Impingement of a Supersonic Jet on a Plane - A Basic Study of Shock Interference Heating," NSWC/WOL/TR 75-195, Naval Surface Weapons Center, White Oak Laboratory, Silver Spring, Maryland, 1976

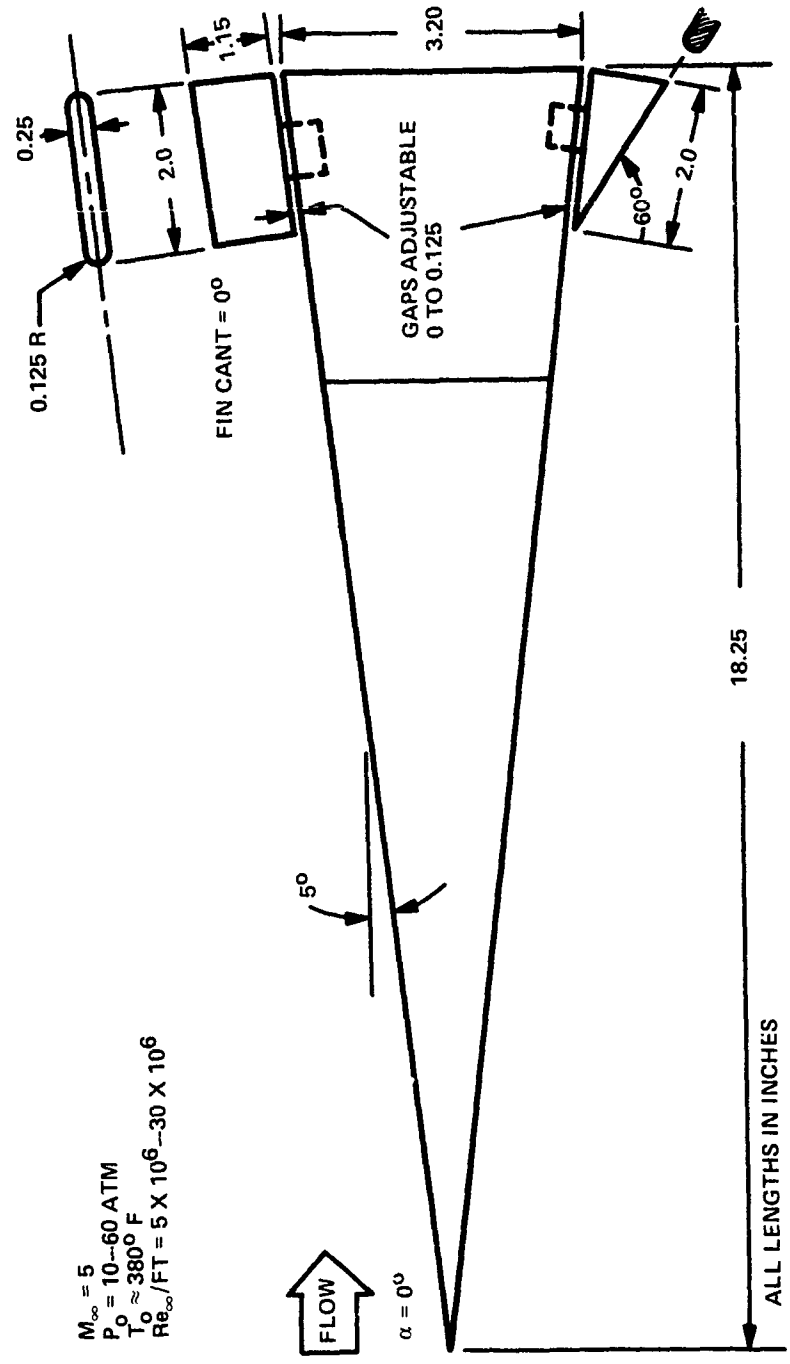

FIG. 1 SCHEMATIC DIAGRAM OF FIN-CONE MODEL

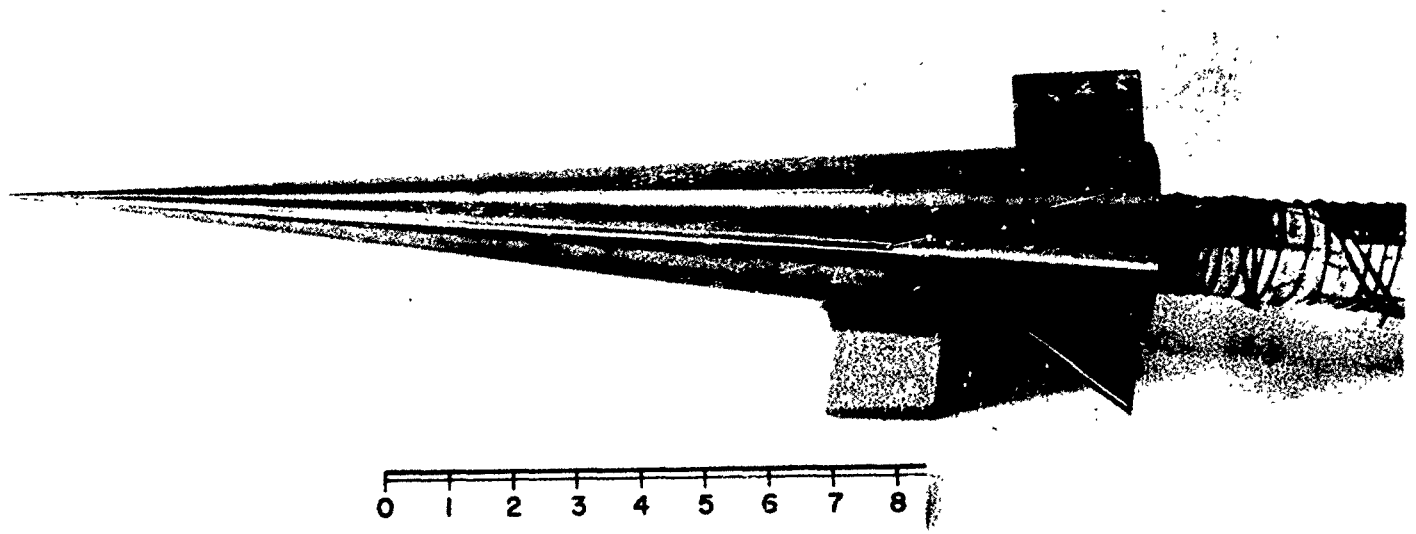

FIG. 2 STAINLESS-STEEL PRESSURE-DISTRIBUTION MODEL (SCALE IN INCHES)

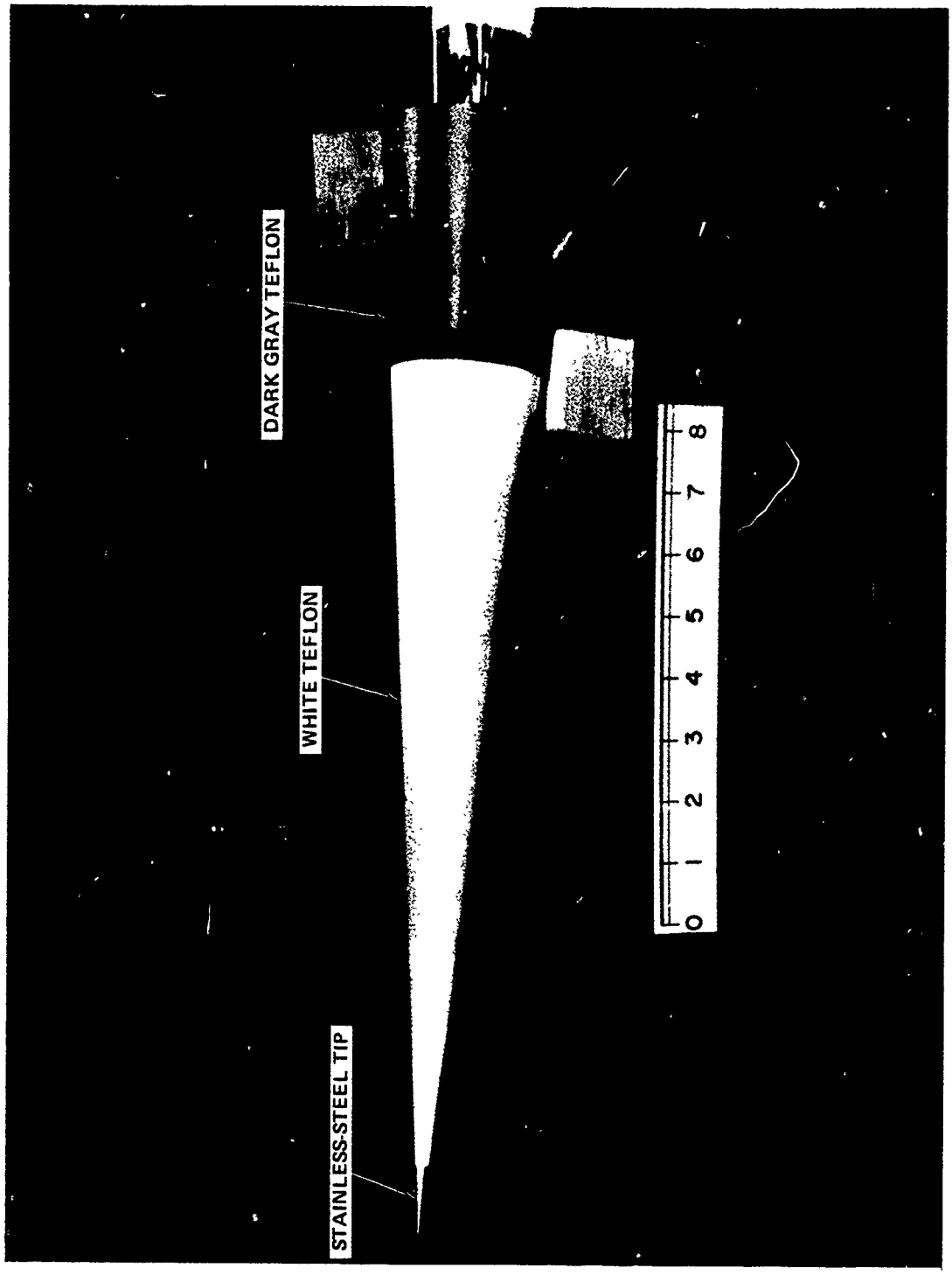

FIG. 3 TEFLON HEAT-TRANSFER AND FLOW VISUALIZATION MODEL (SCALE IN INCHES)

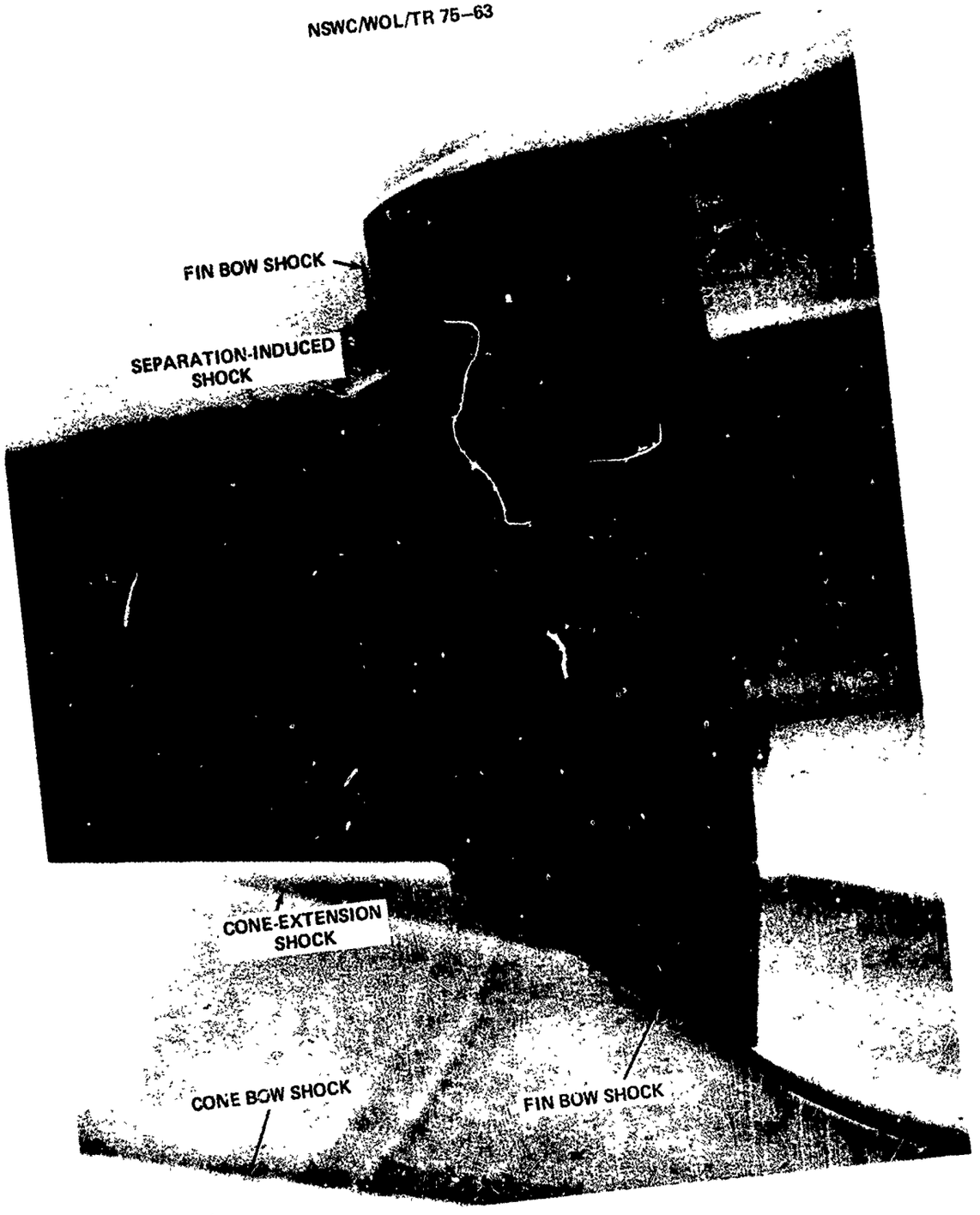

FIG. 4 SCHLIEREN PHOTOGRAPH OF FLUSH-MOUNTED FINS;
$M_\infty = 5, Re_\infty/FT = 4.5 \times 10^6$

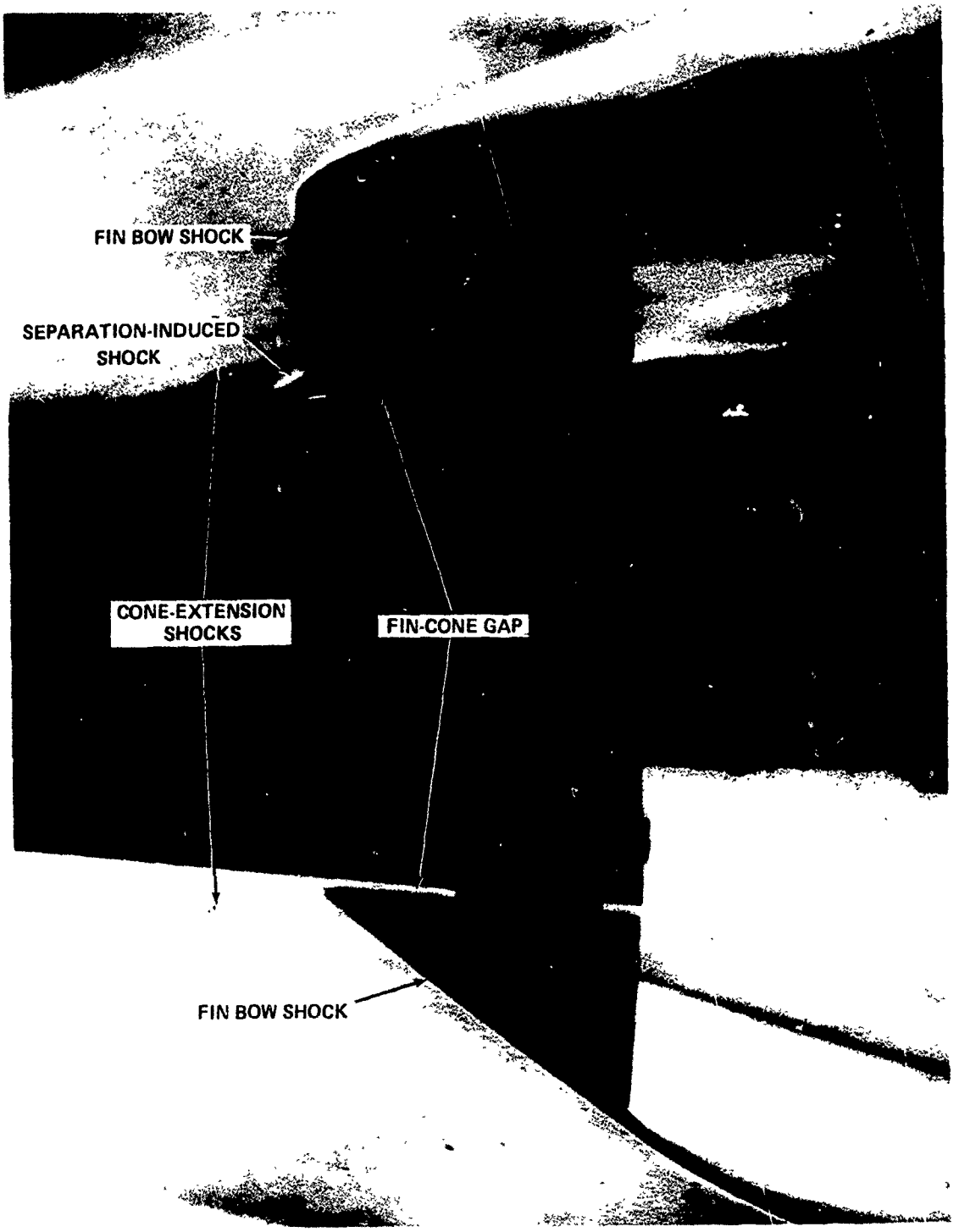

FIG. 5 SCHLIEREN PHOTOGRAPH FOR 0.060-INCH FIN-CONE GAP; $M_\infty = 5$, $Re_\infty/FT = 4.5 \times 10^6$

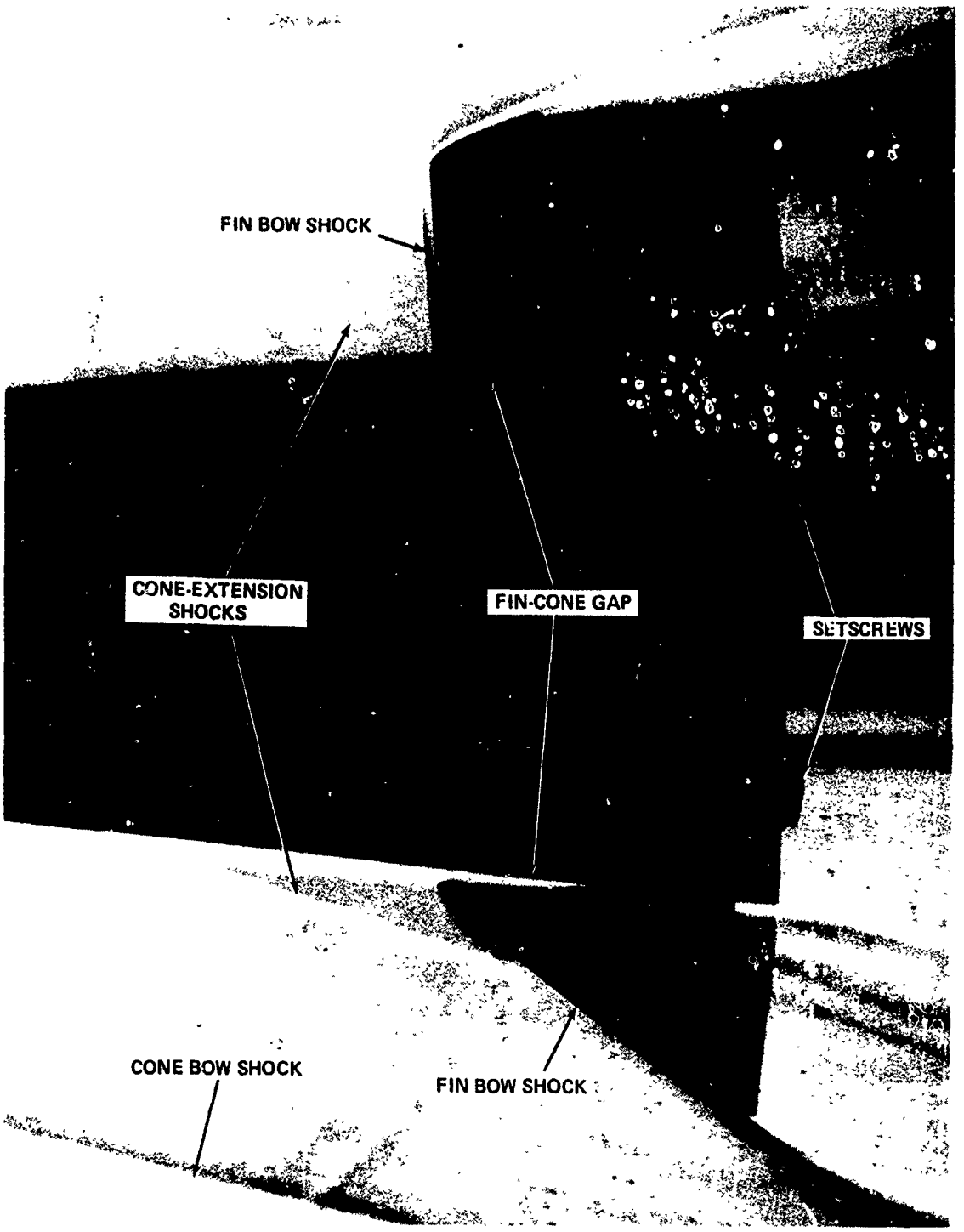

FIG. 6 SCHLIEREN PHOTOGRAPH FOR 0.125-INCH FIN-CONE GAP; $M_\infty = 5$, $Re_\infty/FT = 4.5 \times 10^6$

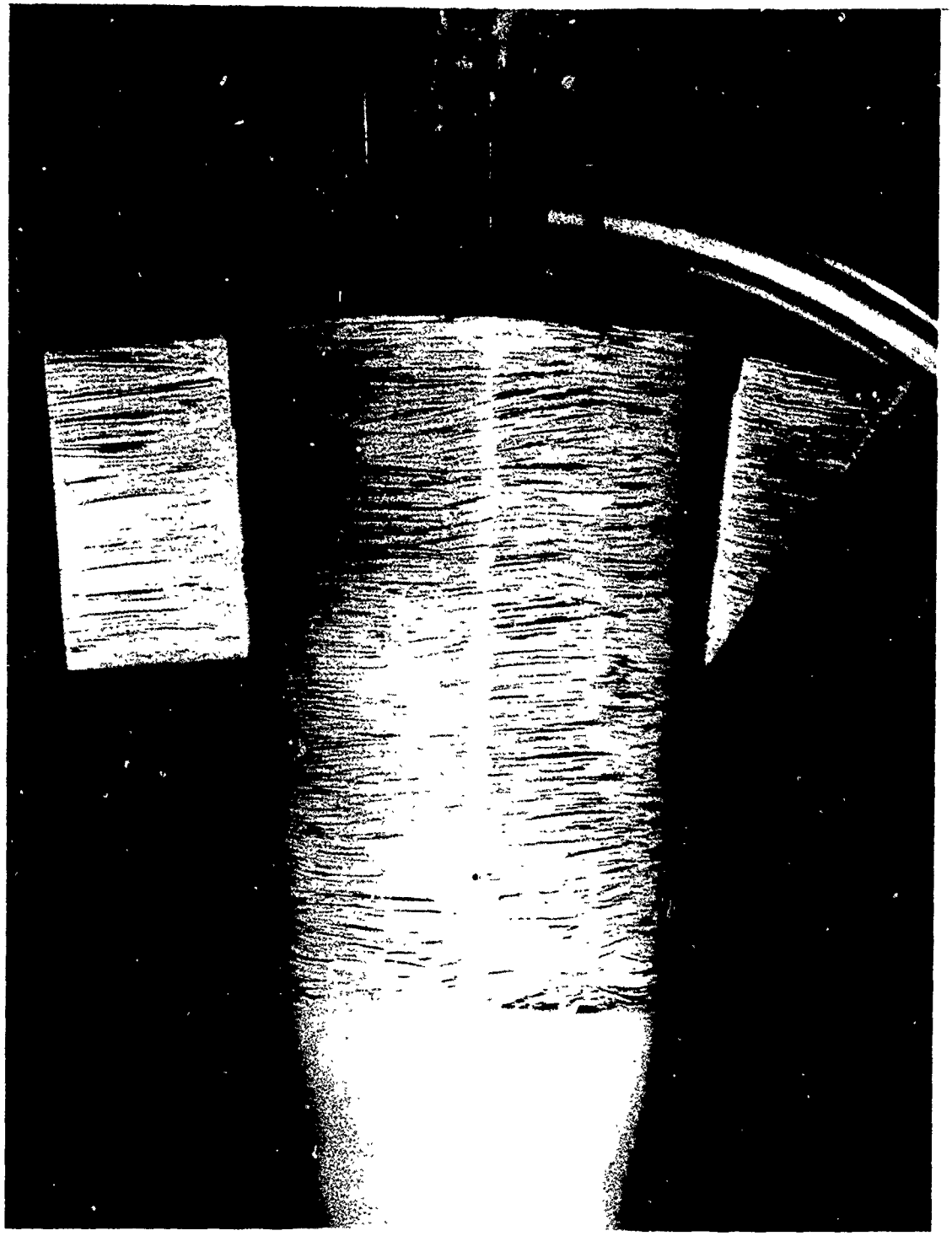

FIG. 7 SIDE-VIEW OIL-FLOW PHOTOGRAPH FOR FLUSH-MOUNTED FINS; TARE SHOT, NO FLOW

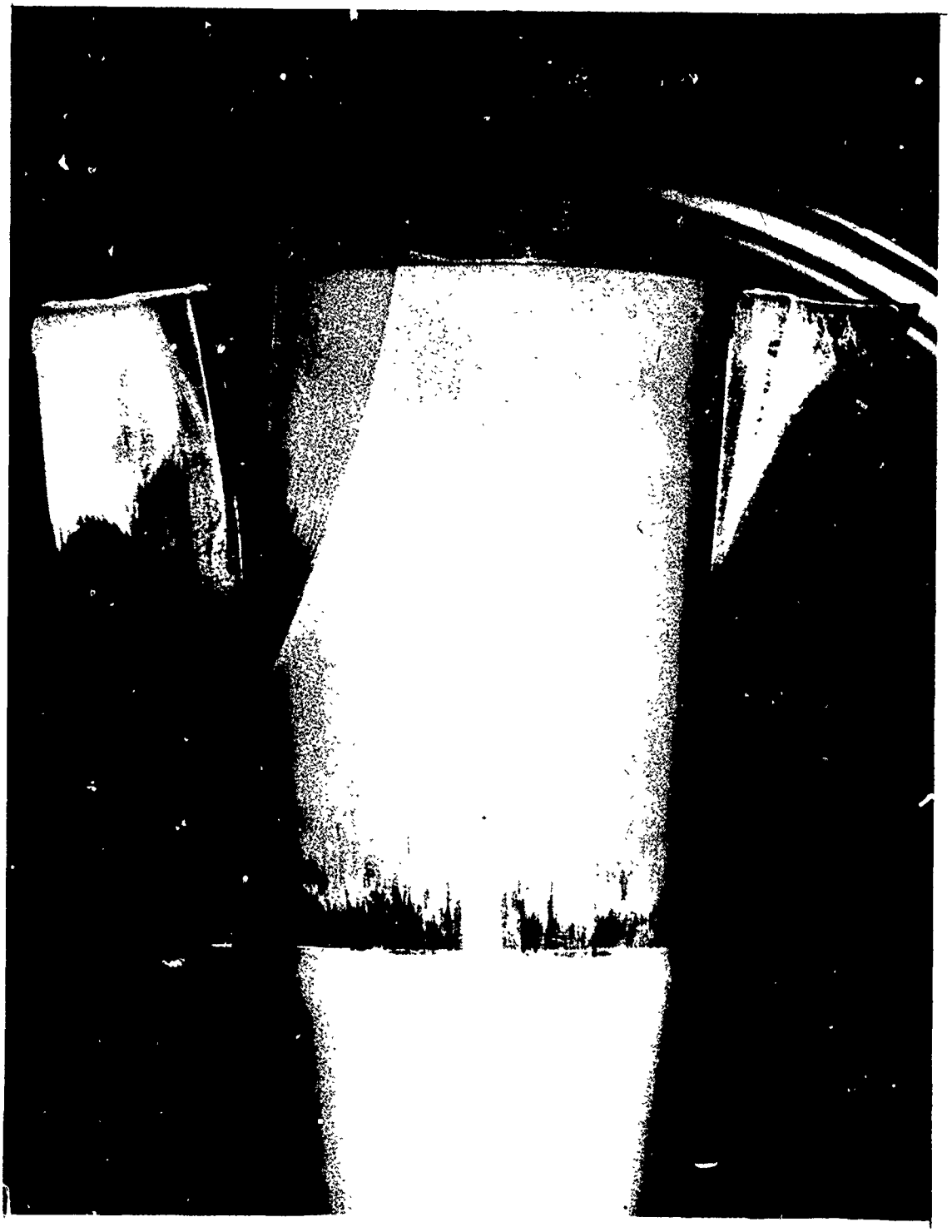

FIG. 8 SIDE-VIEW OIL-FLOW PHOTOGRAPH FOR FLUSH-MOUNTED FINS; $M_\infty = 5$, $Re_\infty/FT = 4.5 \times 10^6$

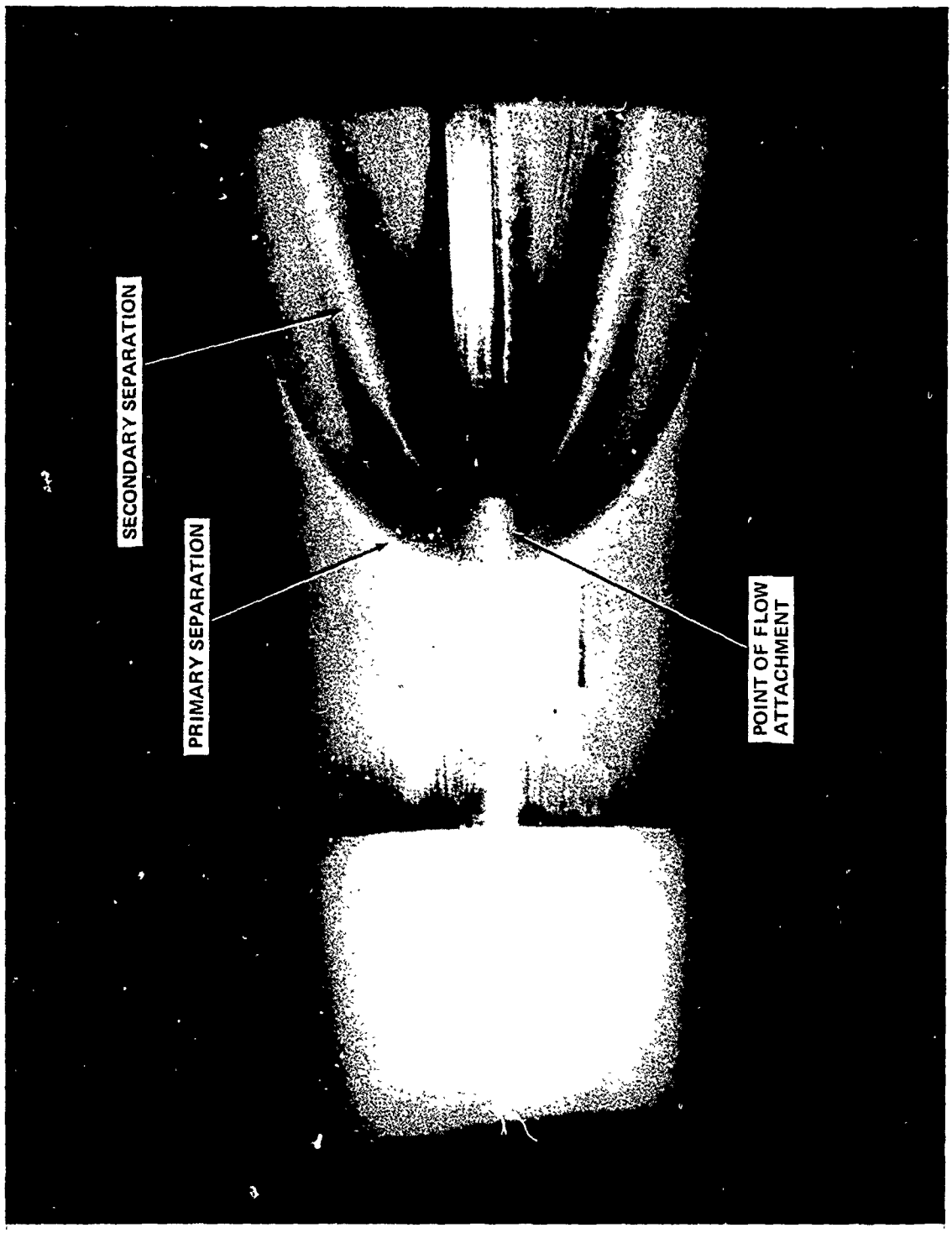

FIG. 9 TOP-VIEW OIL-FLOW PHOTOGRAPH FOR FLUSH-MOUNTED UNSWEPT FIN; $M_\infty = 5$, $Re_\infty/FT = 4.5 \times 10^6$

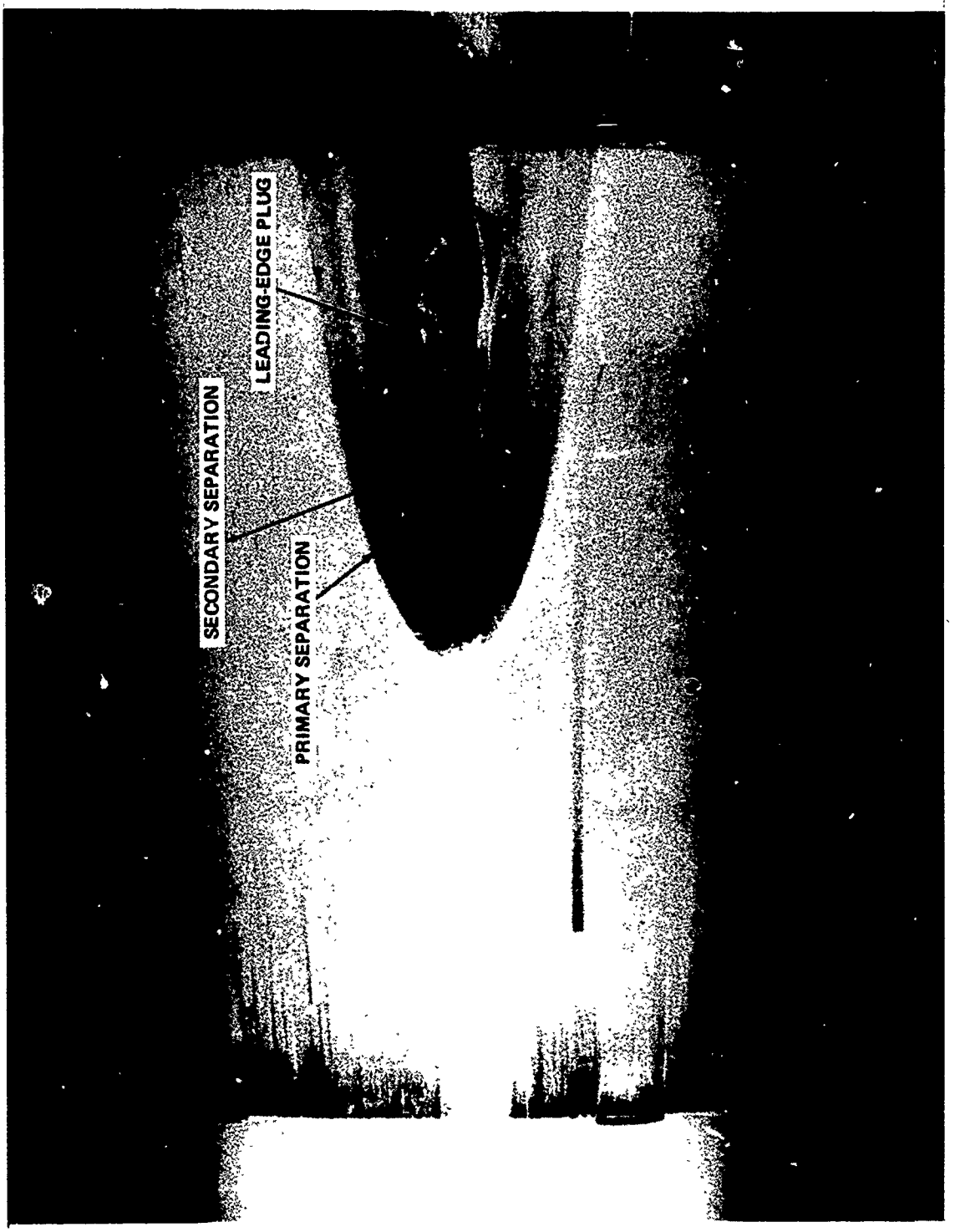

FIG. 10 TOP-VIEW OIL-FLOW PHOTOGRAPH FOR FLUSH-MOUNTED 60° -SWEPT FIN; $M_\infty = 5$, $Re_\infty/FT = 4.5 \times 10^6$

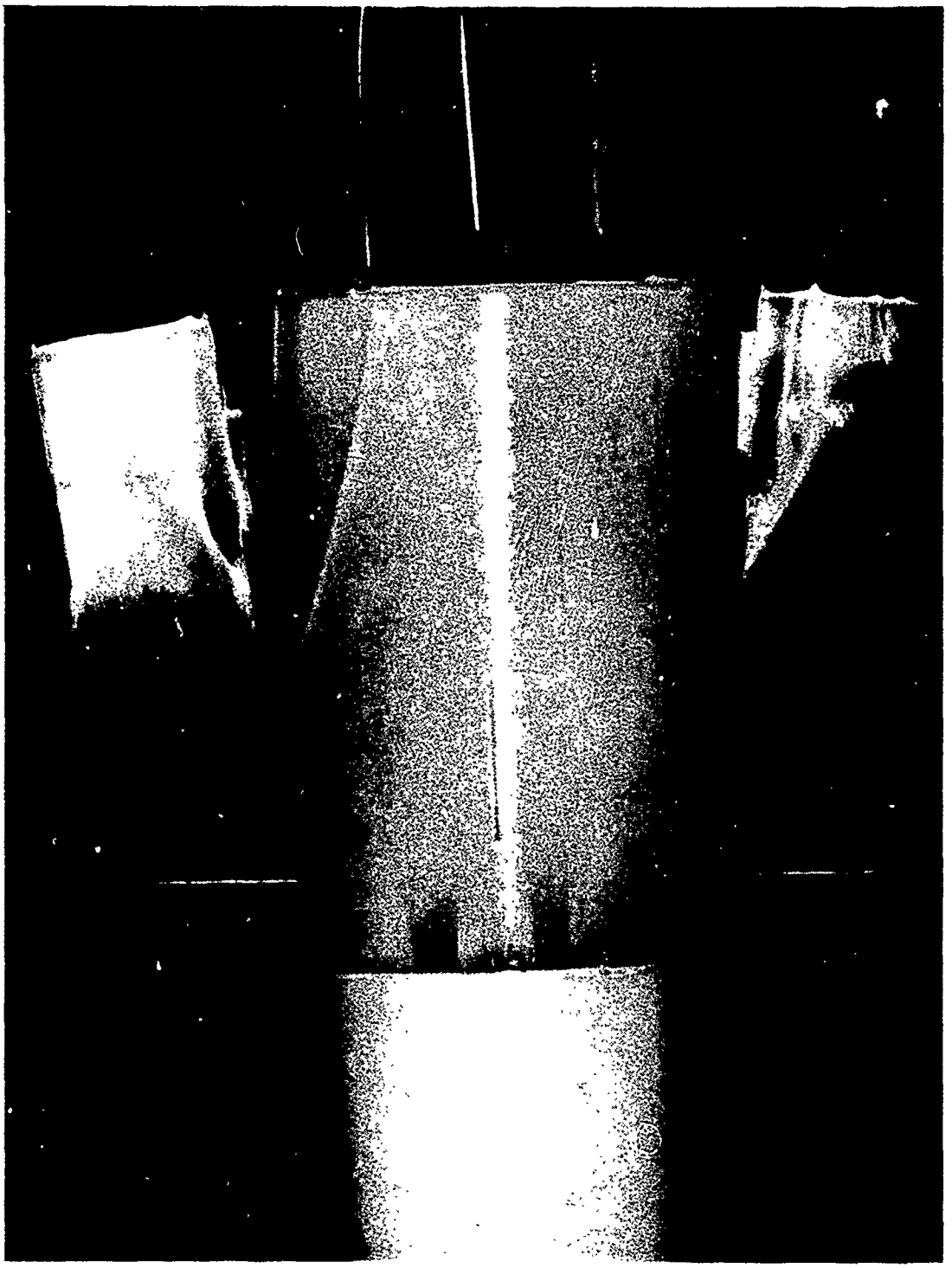

FIG. 11 SIDE-VIEW OIL-FLOW PHOTOGRAPH FOR 0.060-INCH FIN-CONE GAP; $M_\infty = 5$, $Re_\infty/FT = 4.5 \times 10^6$

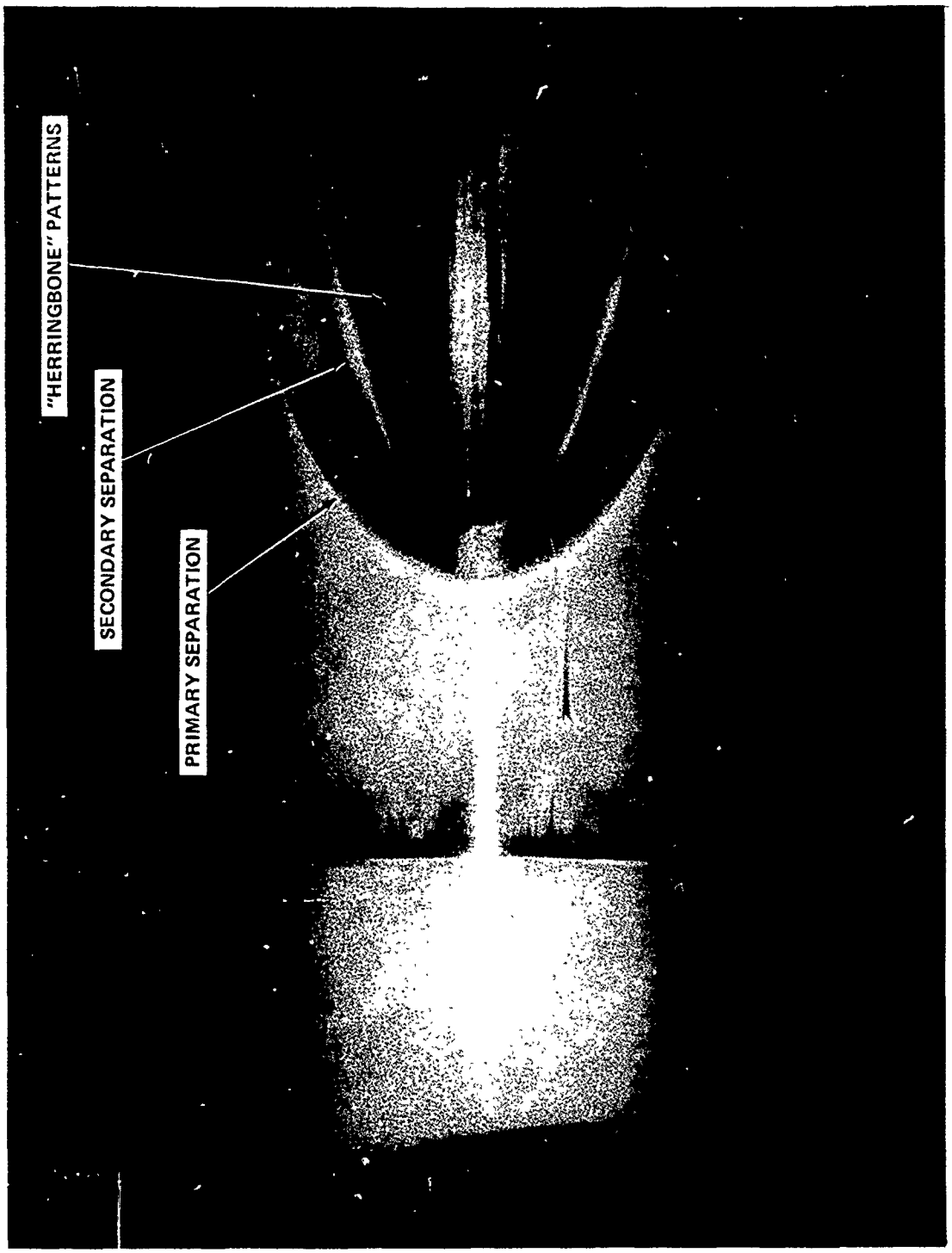

FIG. 12 TOP-VIEW OIL-FLOW PHOTOGRAPH OF UNSWEPT FIN WITH 0.060-INCH FIN-CONE GAP; $M_\infty = 5$, $Re_\infty/FT = 4.5 \times 10^6$

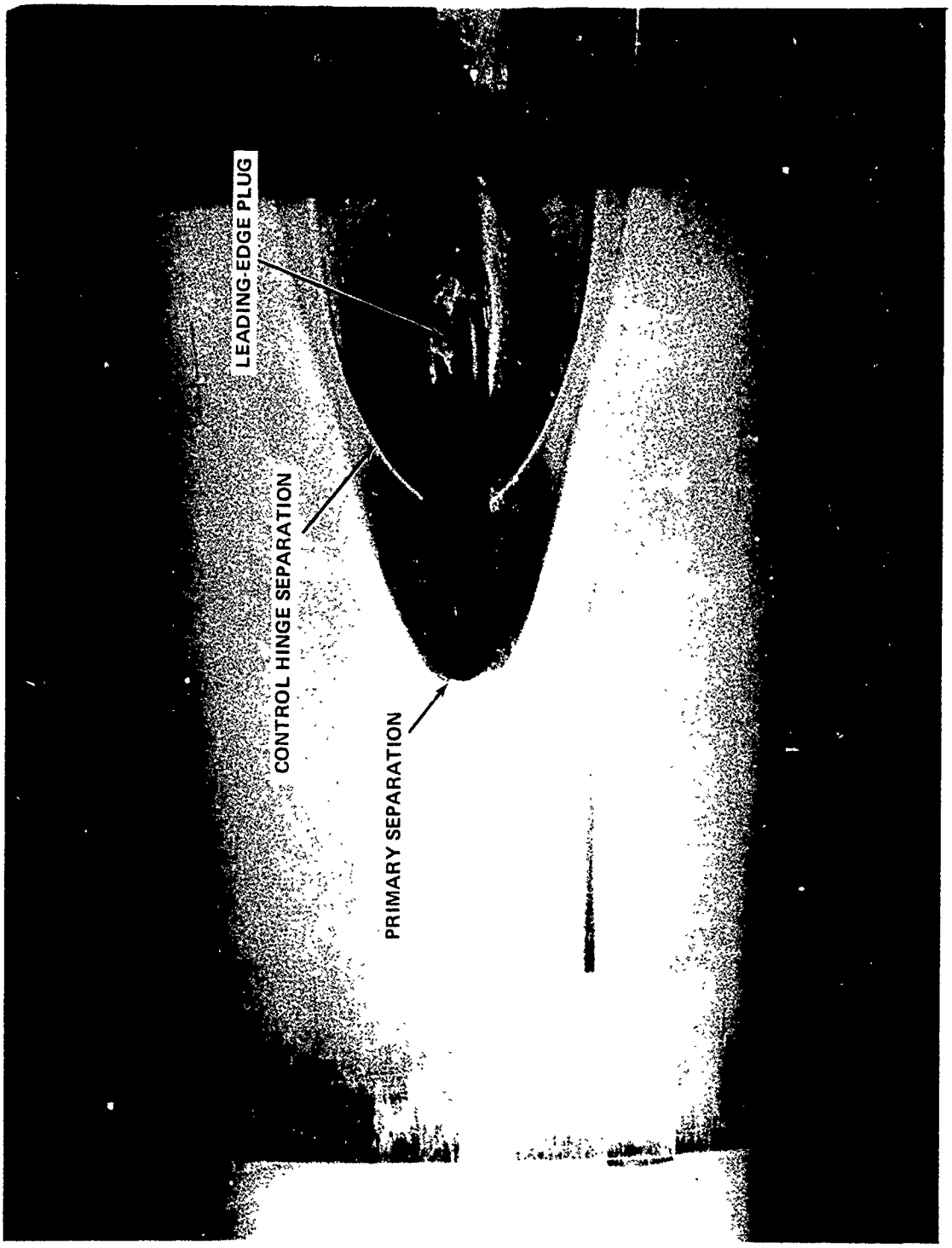

FIG. 13 TOP-VIEW OIL-FLOW PHOTOGRAPH OF 60° -SWEPT FIN WITH 0.060-INCH FIN-CONE GAP; $M_\infty = 5$, $Re_\infty/FT = 4.5 \times 10^6$

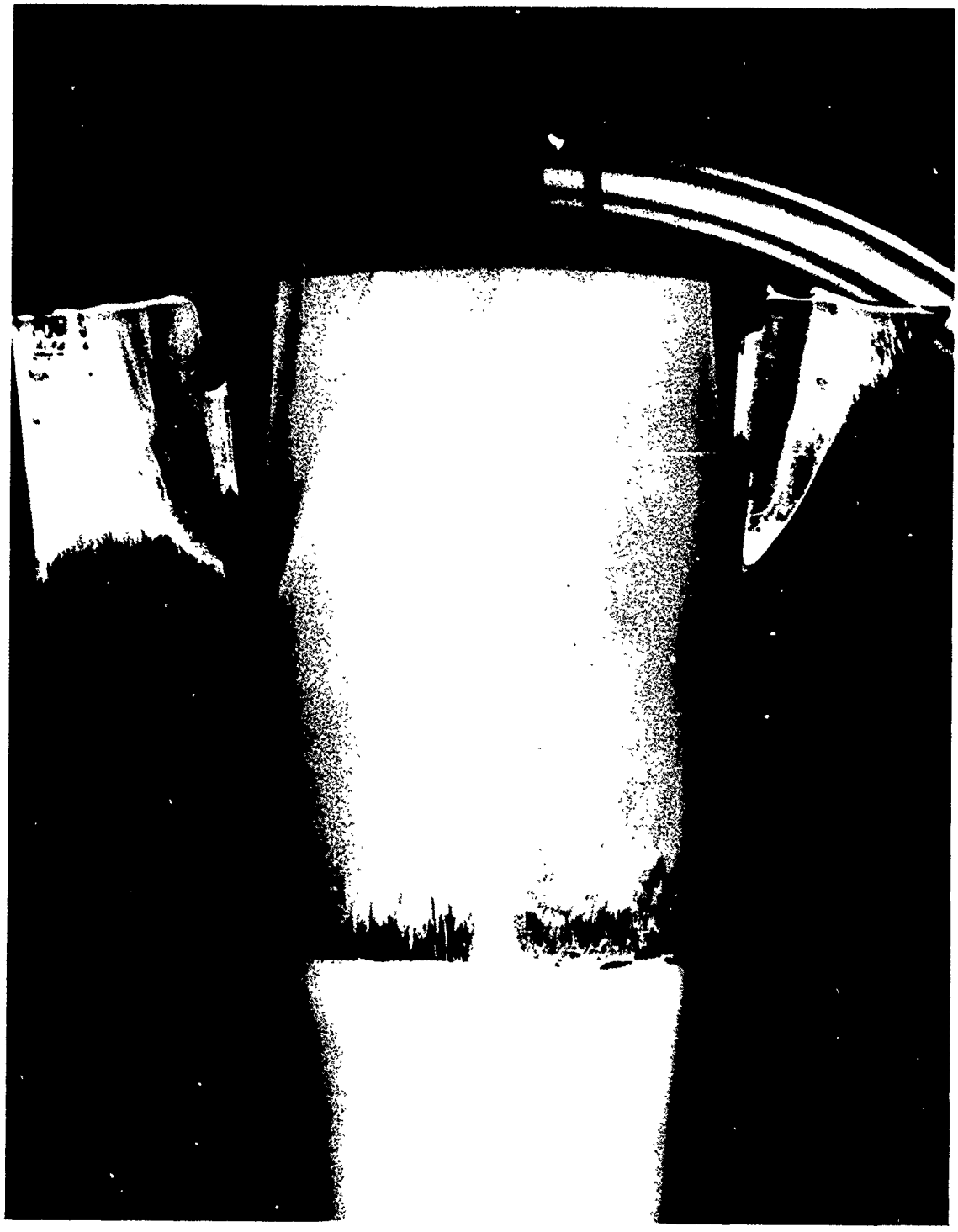

FIG. 14 SIDE-VIEW OIL-FLOW PHOTOGRAPH FOR 0.125-INCH FIN-CONE GAP; $M_\infty = 5$, $Re_\infty/FT = 4.5 \times 10^6$

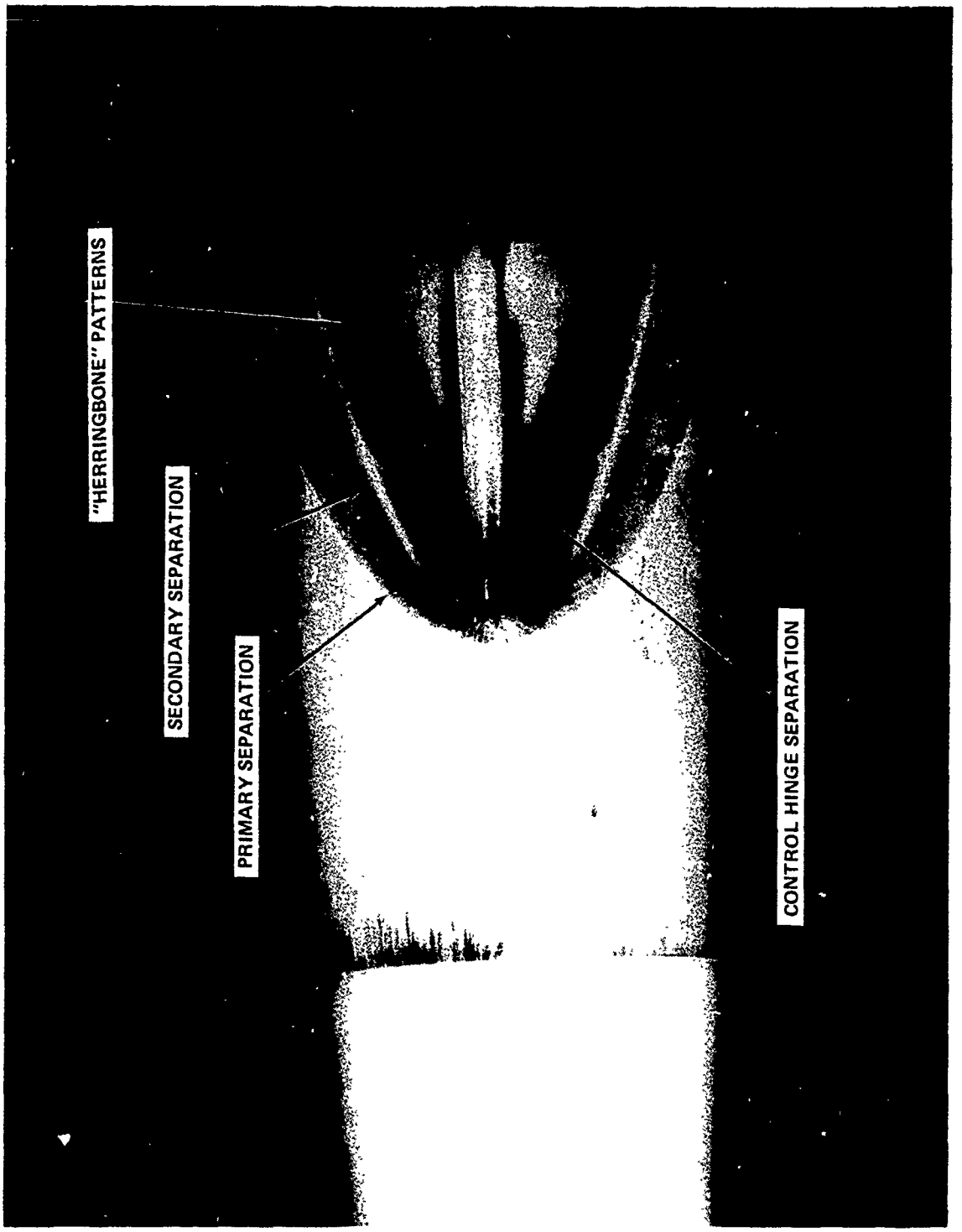

FIG. 15 TOP-VIEW OIL-FLOW PHOTOGRAPH OF UNSWEPT FIN WITH 0.125-INCH FIN-CONE GAP; $M_\infty = 5$, $Re_\infty/FT = 4.5 \times 10^6$

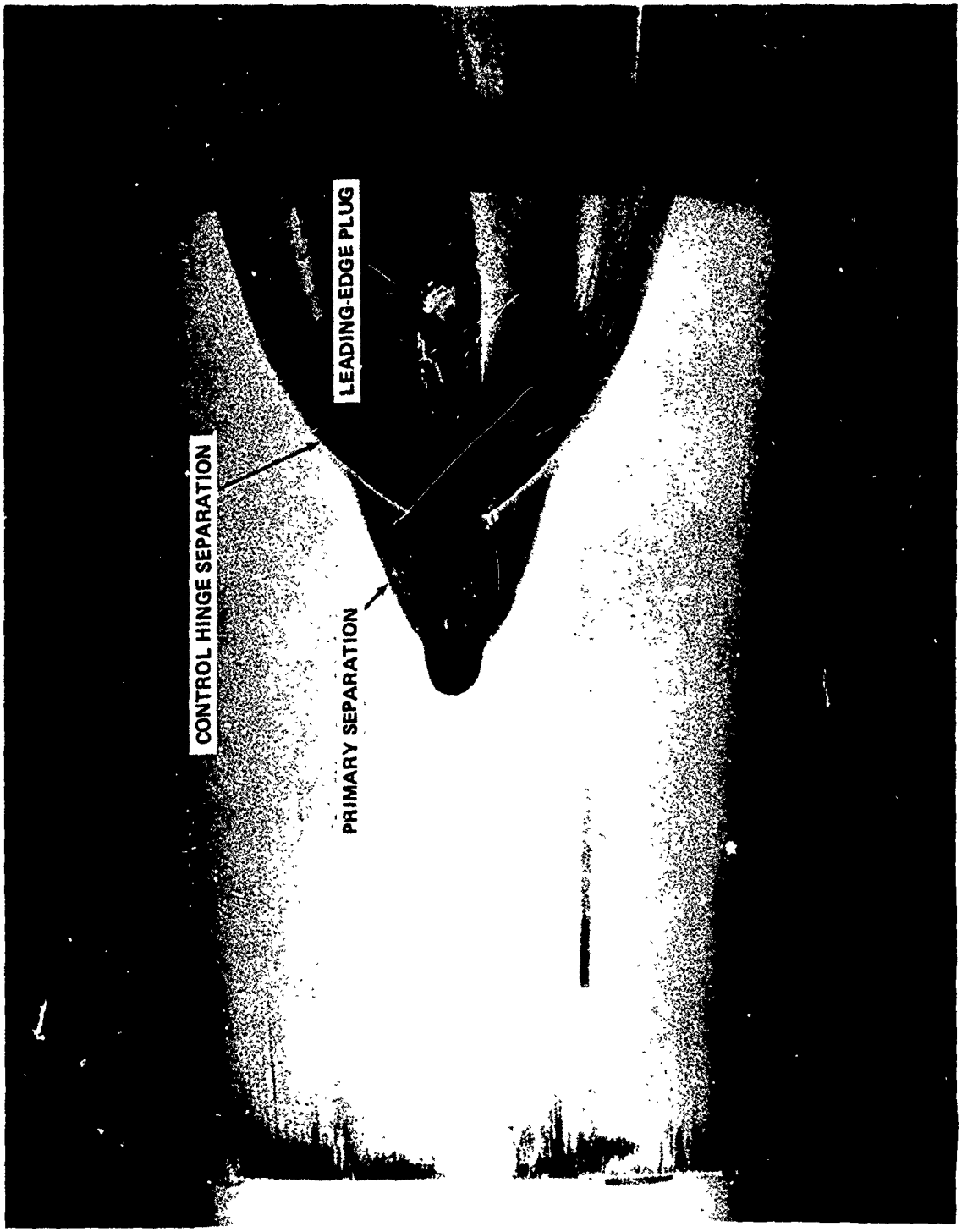

FIG. 16 TOP-VIEW OIL-FLOW PHOTOGRAPH OF 60° SWEPT FIN WITH 0.125-INCH FIN-CONE GAP; $M_\infty = 5$, $Re_\infty/FT = 4.5 \times 10^6$

$M_\infty = 5$
$Re_\infty/FT = 4.5 \times 10^6$
GAP = 0.0"

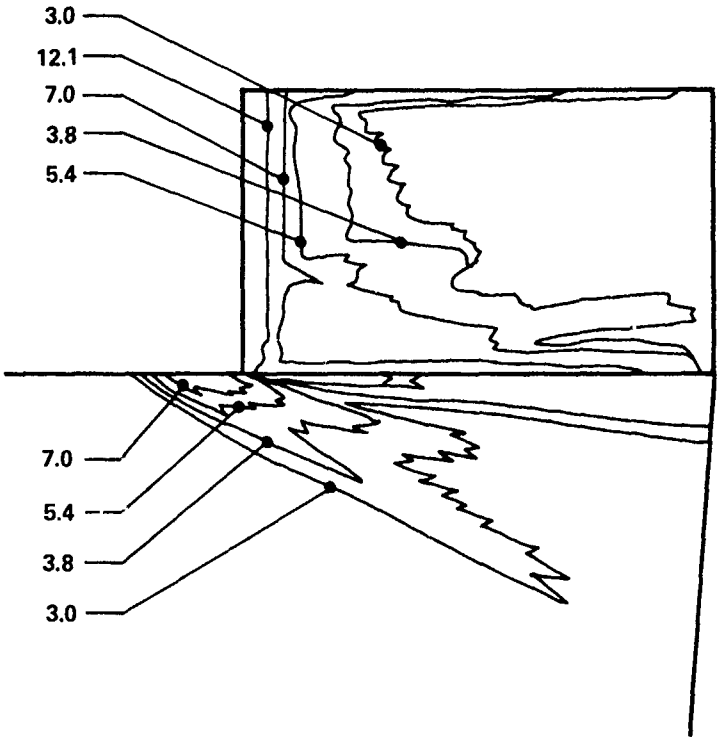

h x 10^3, BTU/FT^2–SEC–^oR

FIG. 17 ISOHEATING CONTOURS FOR FLUSH-MOUNTED UNSWEPT FIN. SIDE VIEW

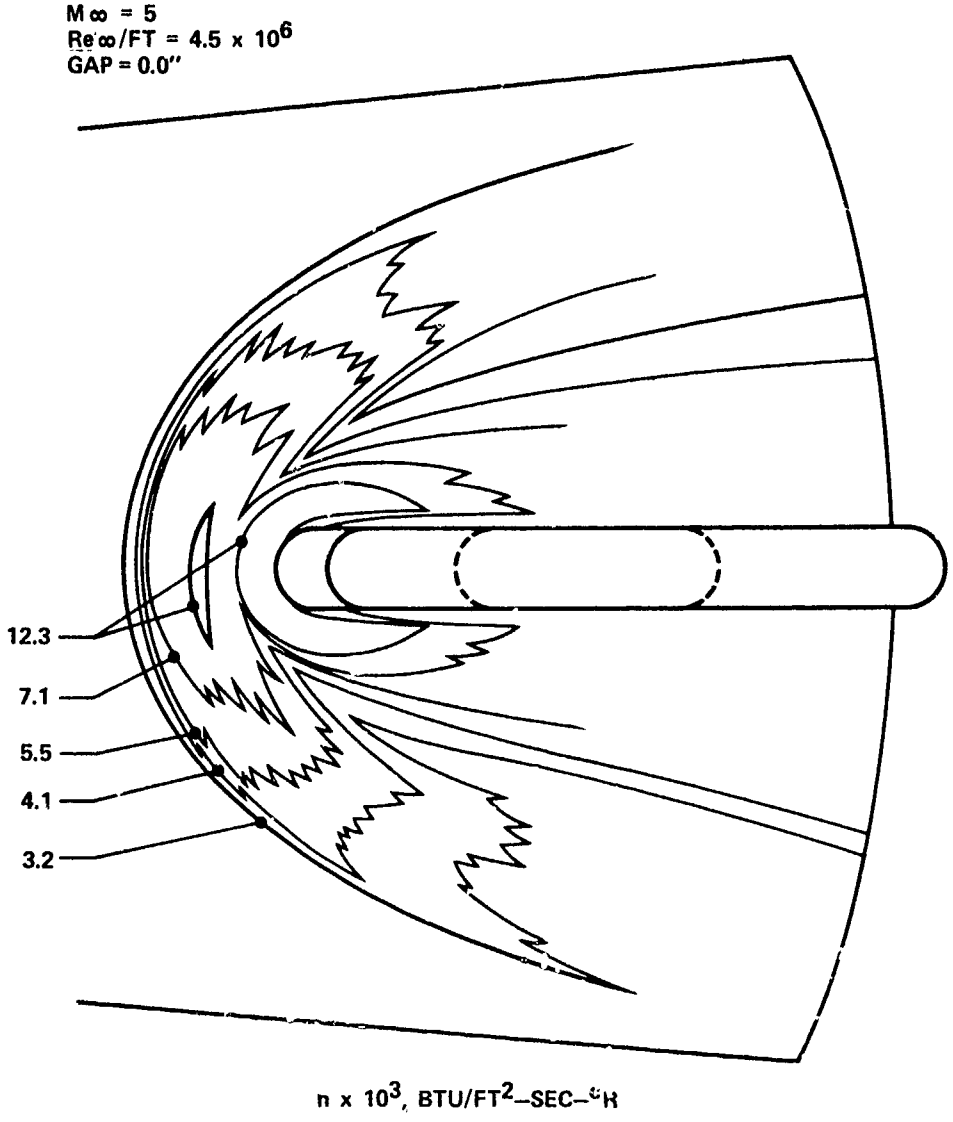

FIG. 18 ISOHEATING CONTOURS FOR FLUSH-MOUNTED UNSWEPT FIN, TOP VIEW, ABOUT 10° FORWARD OF LEADING EDGE

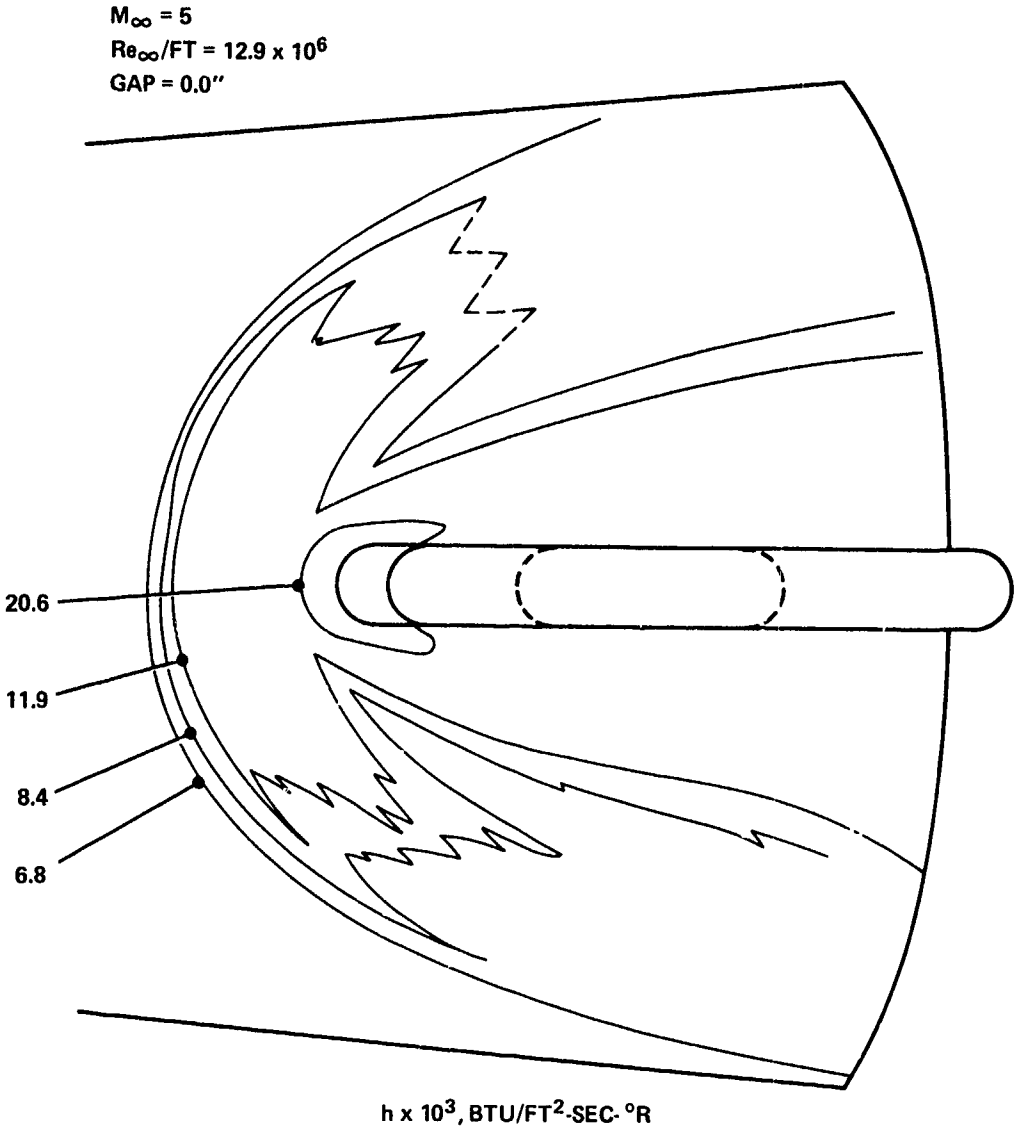

FIG. 19 ISOHEATING CONTOURS FOR FLUSH-MOUNTED UNSWEPT FIN. TOP VIEW

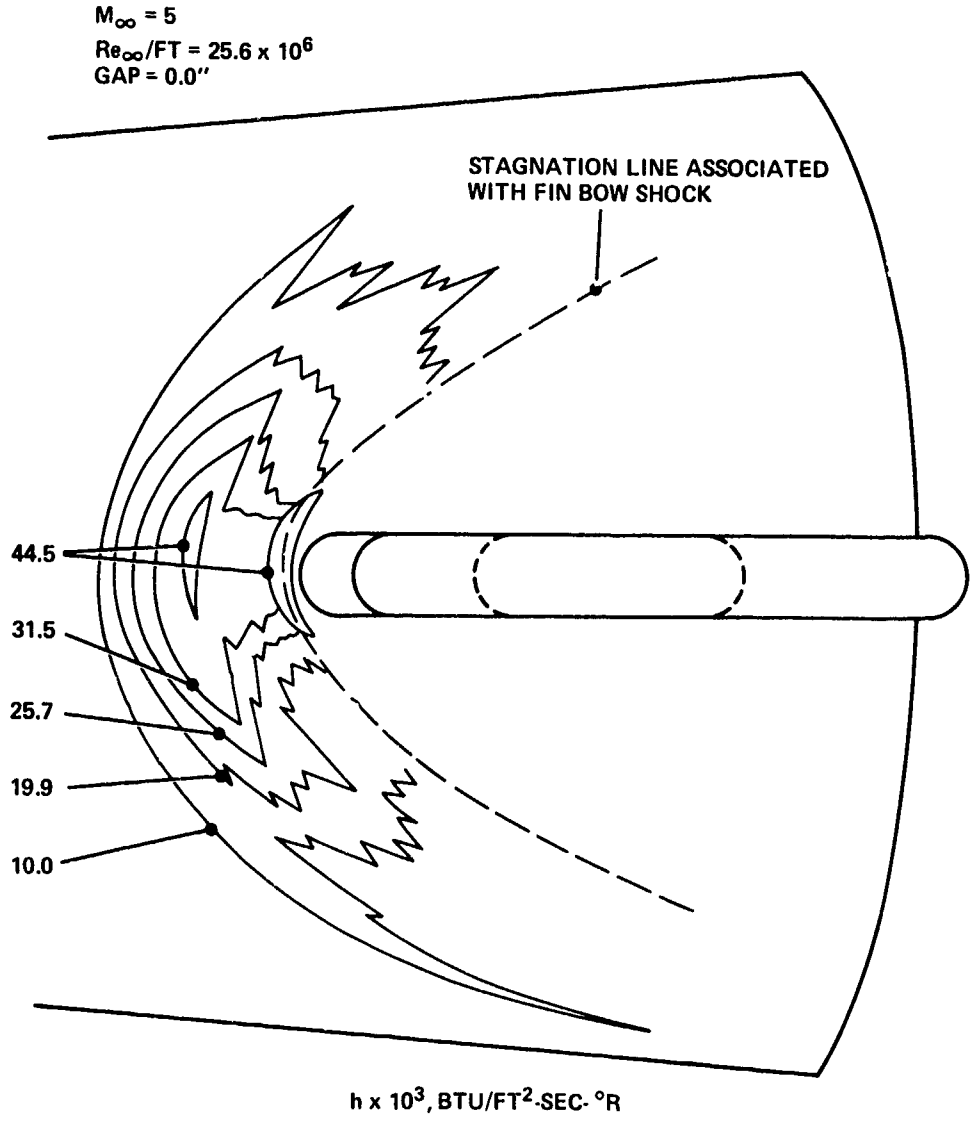

FIG. 20 ISOHEATING CONTOURS FOR FLUSH-MOUNTED UNSWEPT FIN. TOP VIEW

$M_\infty = 5$
$Re_\infty/FT = 4.5 \times 10^6$
GAP = 0.0"

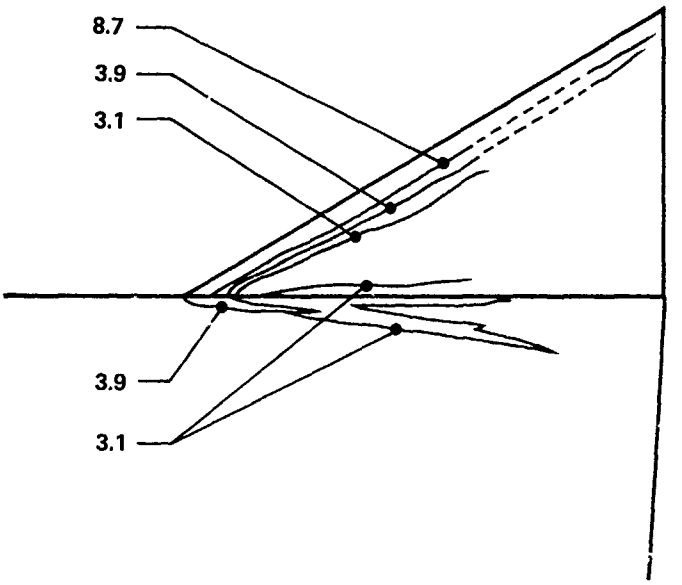

h x 10^3, BTU/FT^2–SEC–^oR

FIG. 21 ISOHEATING CONTOURS FOR FLUSH-MOUNTED 60°-SWEPT FIN. SIDE VIEW.

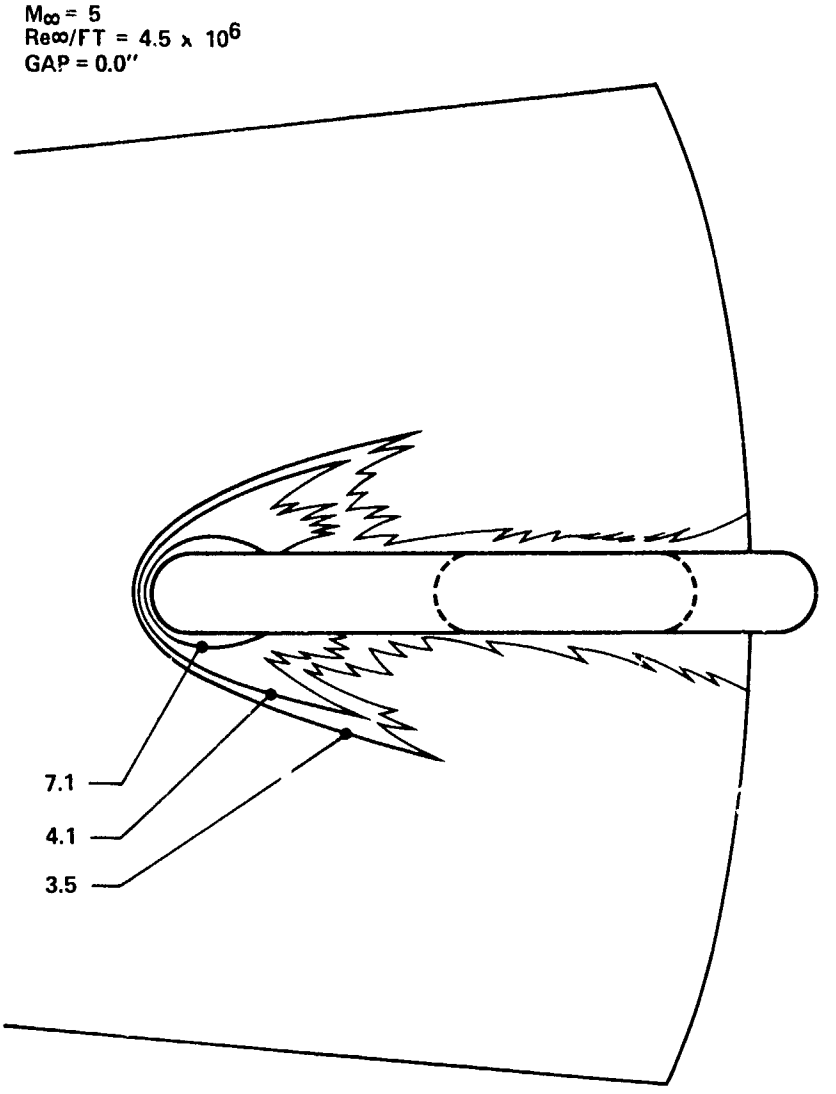

FIG. 22 ISOHEATING CONTOURS FOR FLUSH-MOUNTED 60°-SWEPT FIN. TOP VIEW

$M_{\infty} = 5$
$Re_{\infty}/FT = 12.9 \times 10^6$
GAP = 0.0"

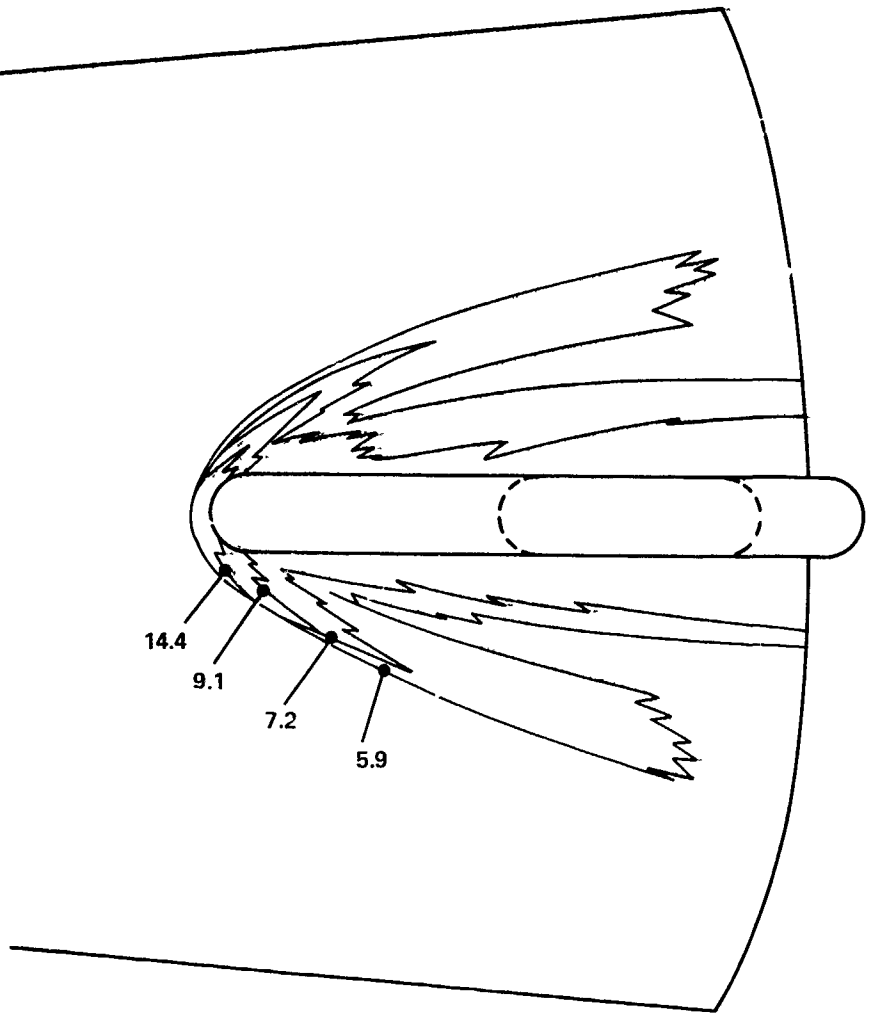

h x 10^3, BTU/FT^2-SEC-°R

FIG. 23 ISOHEATING CONTOURS FOR FLUSH-MOUNTED 60°-SWEPT FIN. TOP VIEW

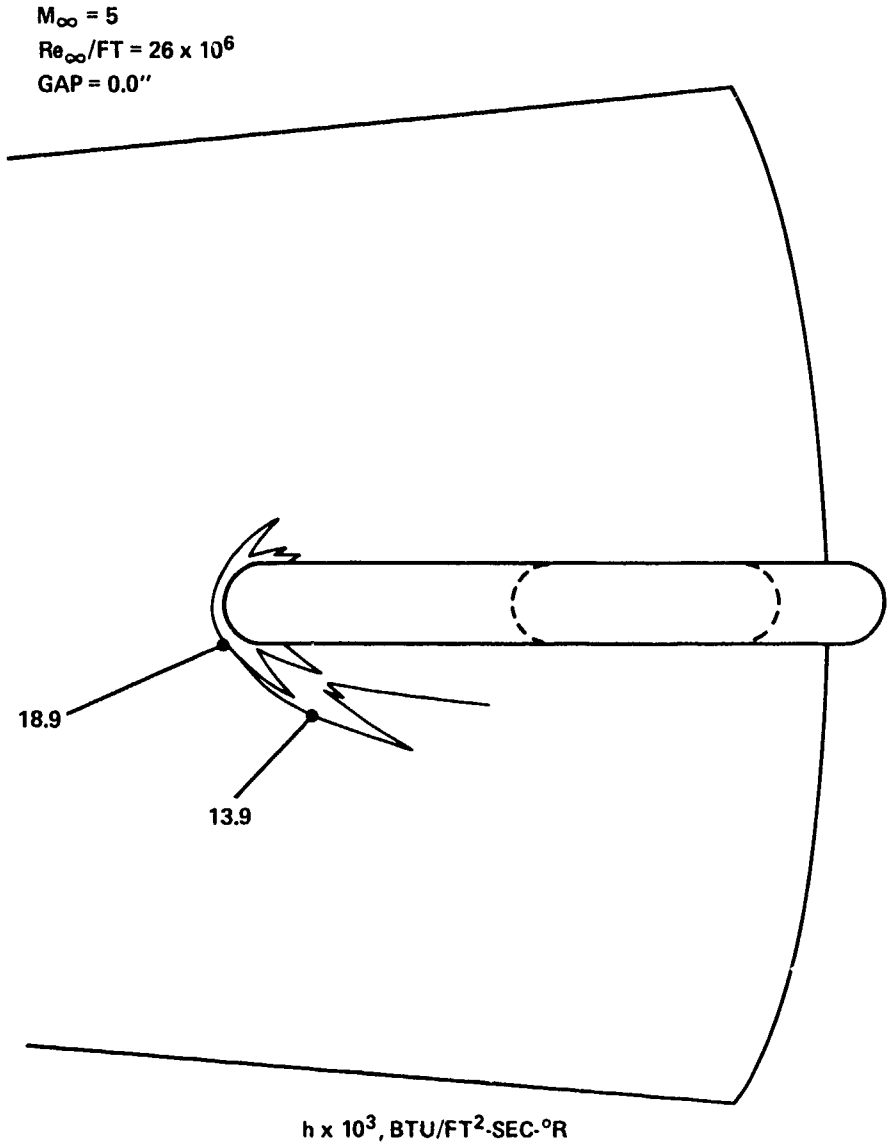

FIG. 24 ISOHEATING CONTOURS FOR FLUSH-MOUNTED 60° -SWEPT FIN. TOP VIEW

$M_\infty = 5$
$Re_\infty/FT = 4.5 \times 10^6$
GAP = 0.060"

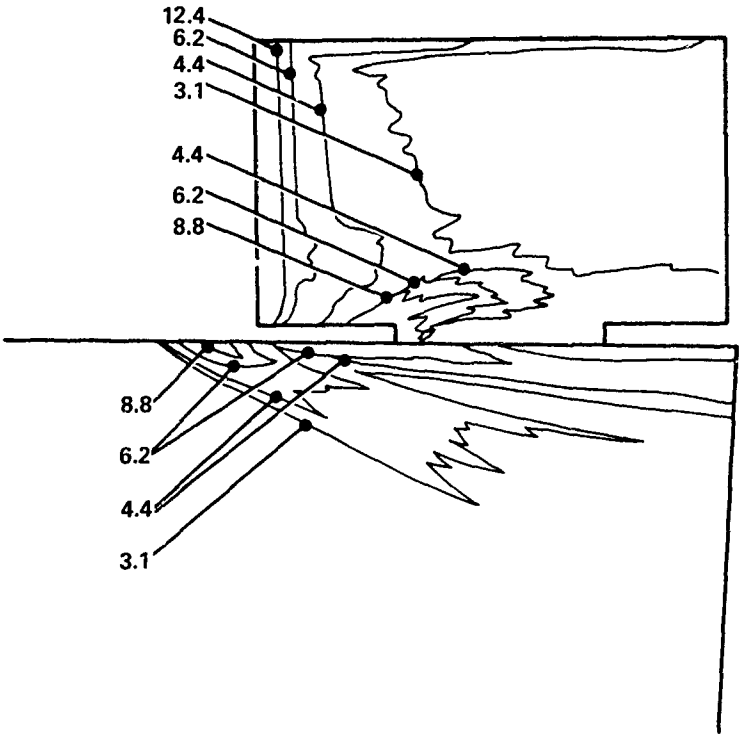

h x 10^3, BTU/FT^2-SEC-°R

FIG. 25 ISOHEATING CONTOURS FOR UNSWEPT FIN WITH 0.060-INCH FIN-CONE GAP. SIDE VIEW

$M_\infty = 5$
$Re_\infty/FT = 4.5 \times 10^6$
GAP = 0.060"

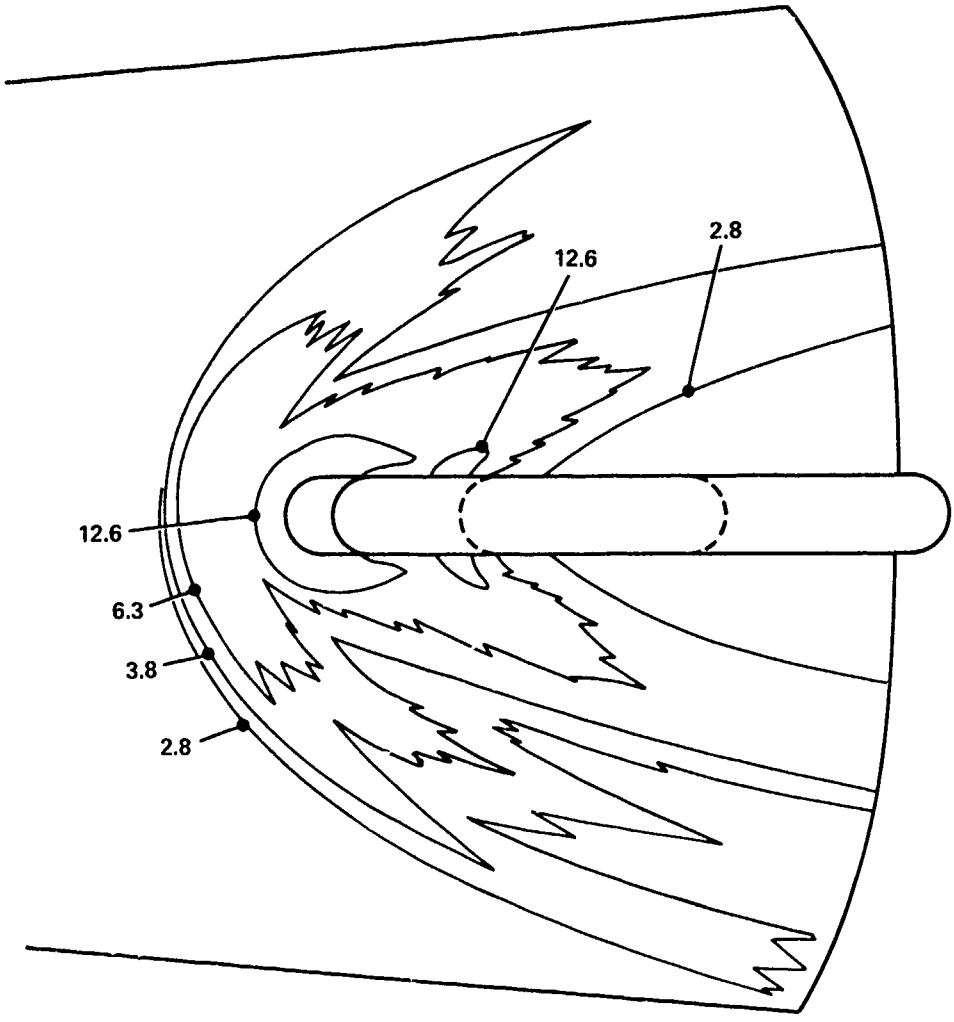

h x 10^3, BTU/FT^2-SEC-°R

FIG. 26 ISOHEATING CONTOURS FOR UNSWEPT FIN WITH 0.060-INCH FIN-CONE GAP. TOP VIEW

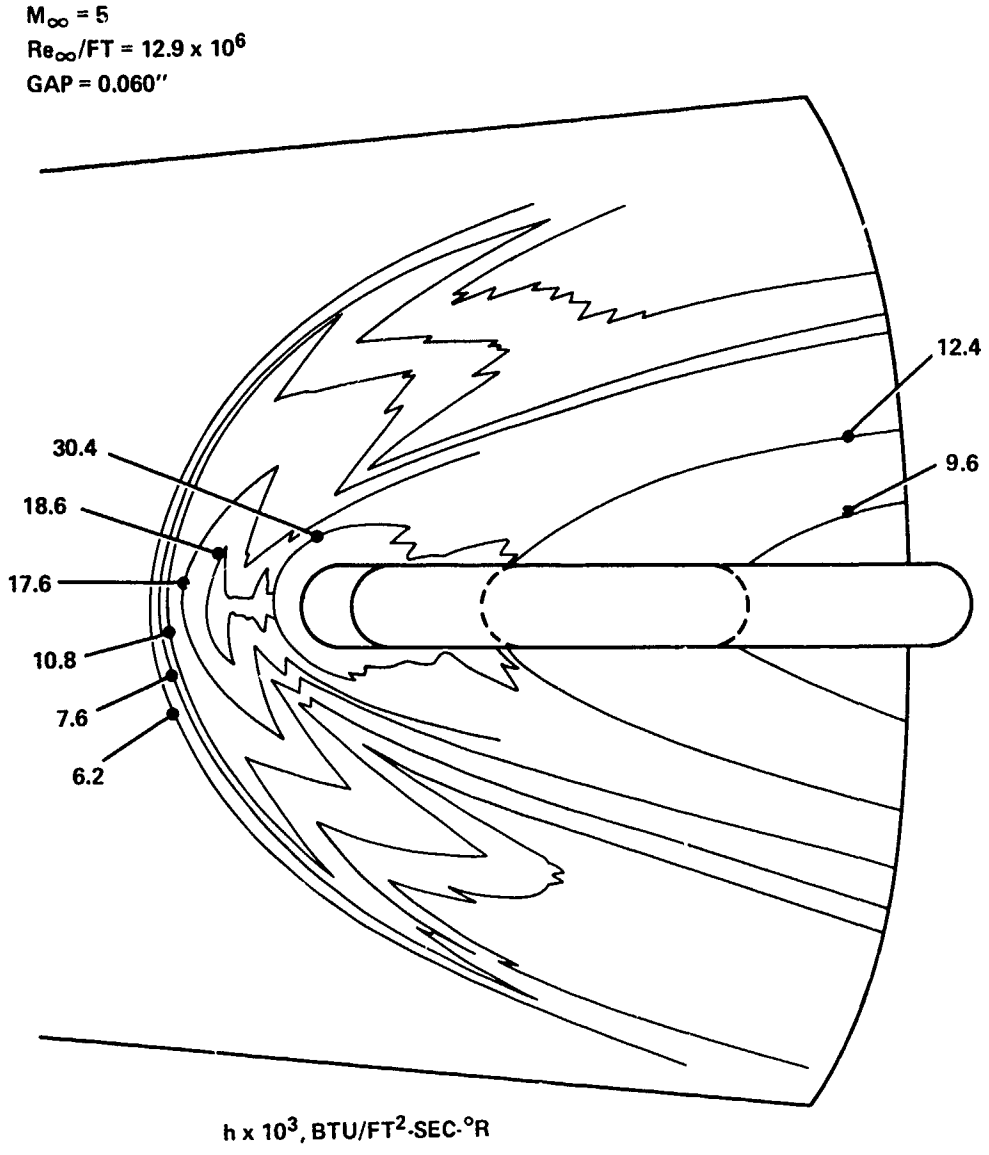

FIG. 27 ISOHEATING CONTOURS FOR UNSWEPT FIN WITH 0.060-INCH FIN-CONE GAP. TOP VIEW

$M_\infty = 5$
$Re_\infty/FT = 26 \times 10^6$
GAP = 0.060"

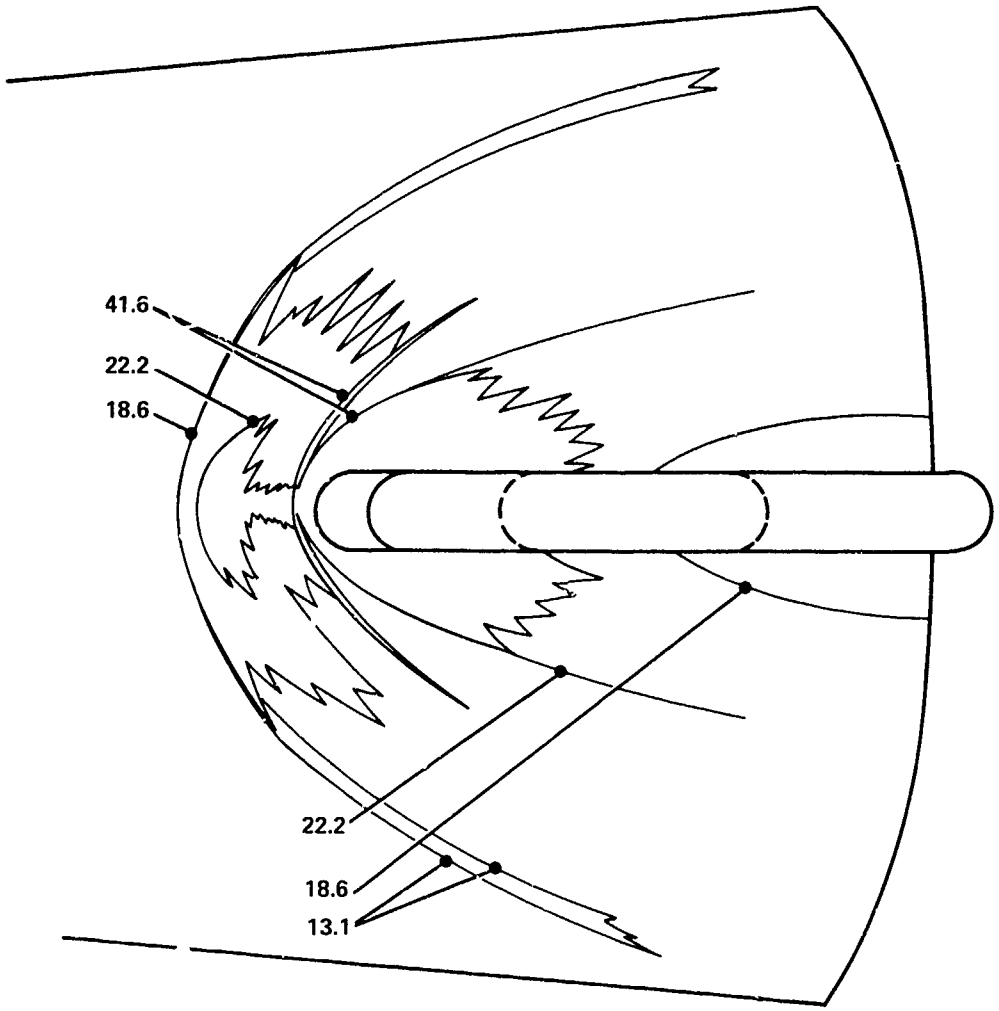

$h \times 10^3$, BTU/FT^2-SEC-°R

FIG. 28 ISOHEATING CONTOURS FOR UNSWEPT FIN WITH 0.060-INCH FIN-CONE GAP, TOP VIEW

$M_\infty = 5$
$Re_\infty/FT = 4.5 \times 10^6$
GAP = 0.060"

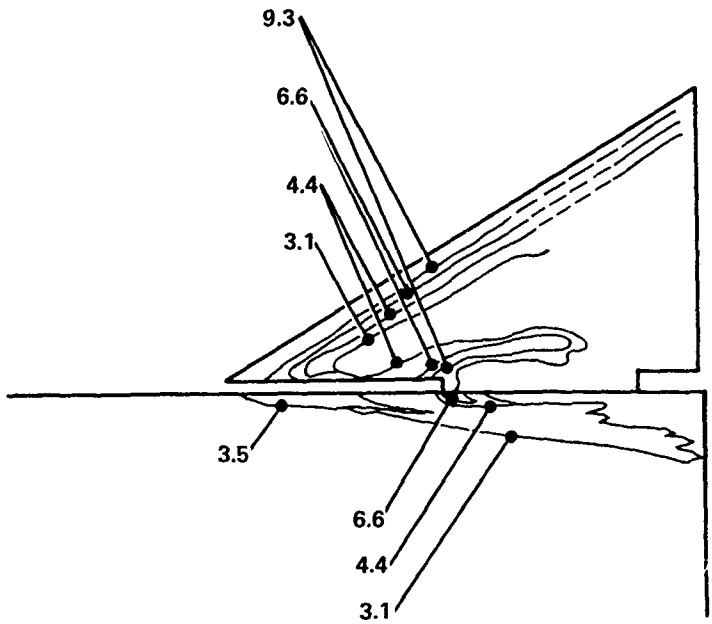

$h \times 10^3$, BTU/FT^2-SEC- °R

FIG. 29 ISOHEATING CONTOURS FOR 60° -SWEPT FIN WITH 0.060-INCH FIN-CONE GAP. SIDE VIEW

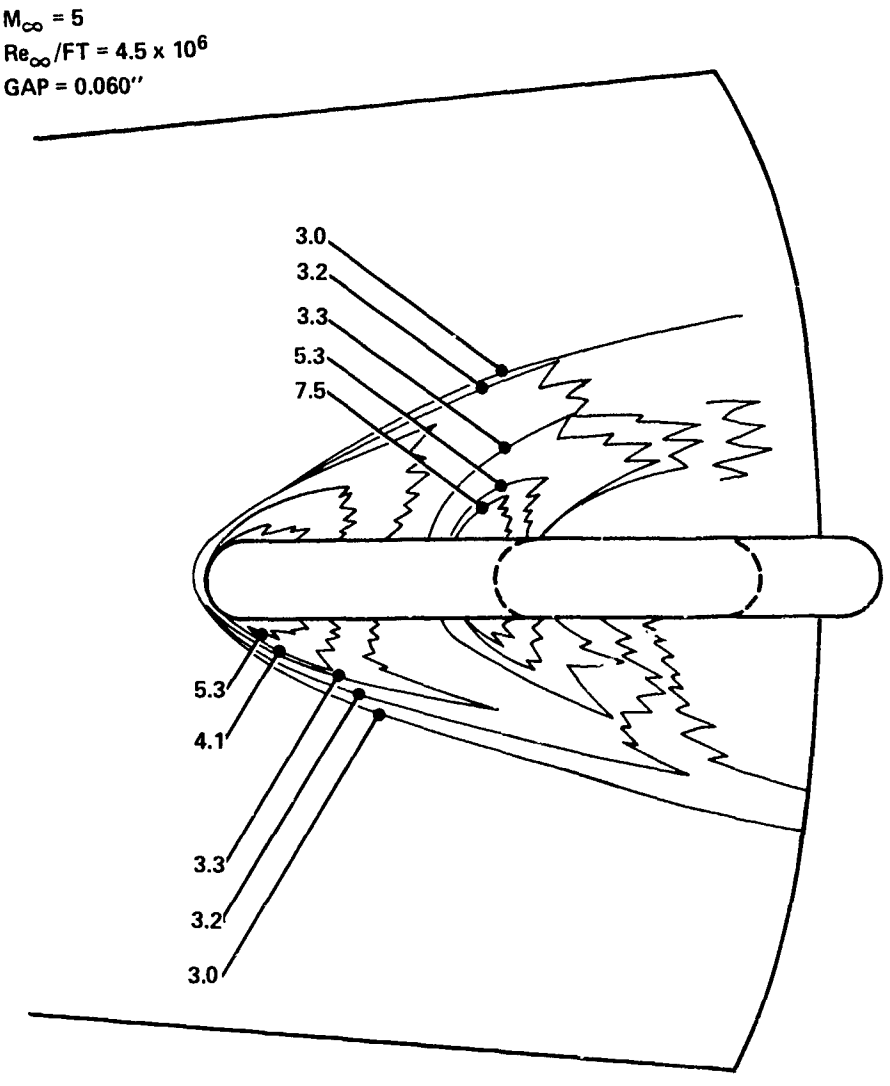

FIG. 30 ISOHEATING CONTOURS FOR 60° -SWEPT FIN WITH 0.060-INCH FIN-CONE GAP. TOP VIEW

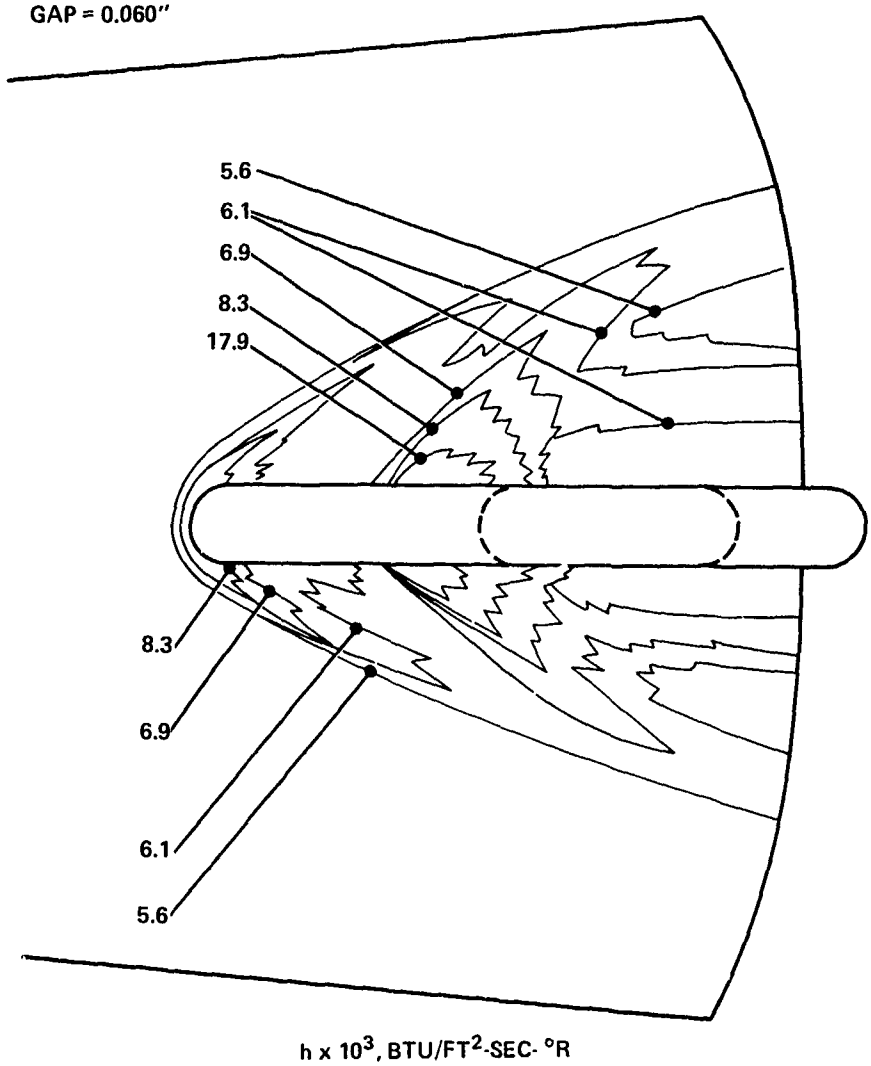

FIG. 31 ISOHEATING CONTOURS FOR 60° -SWEPT FIN WITH 0.060-INCH FIN-CONE GAP. TOP VIEW

$M_\infty = 5$
$Re_\infty/FT = 26 \times 10^6$
GAP = 0.060"

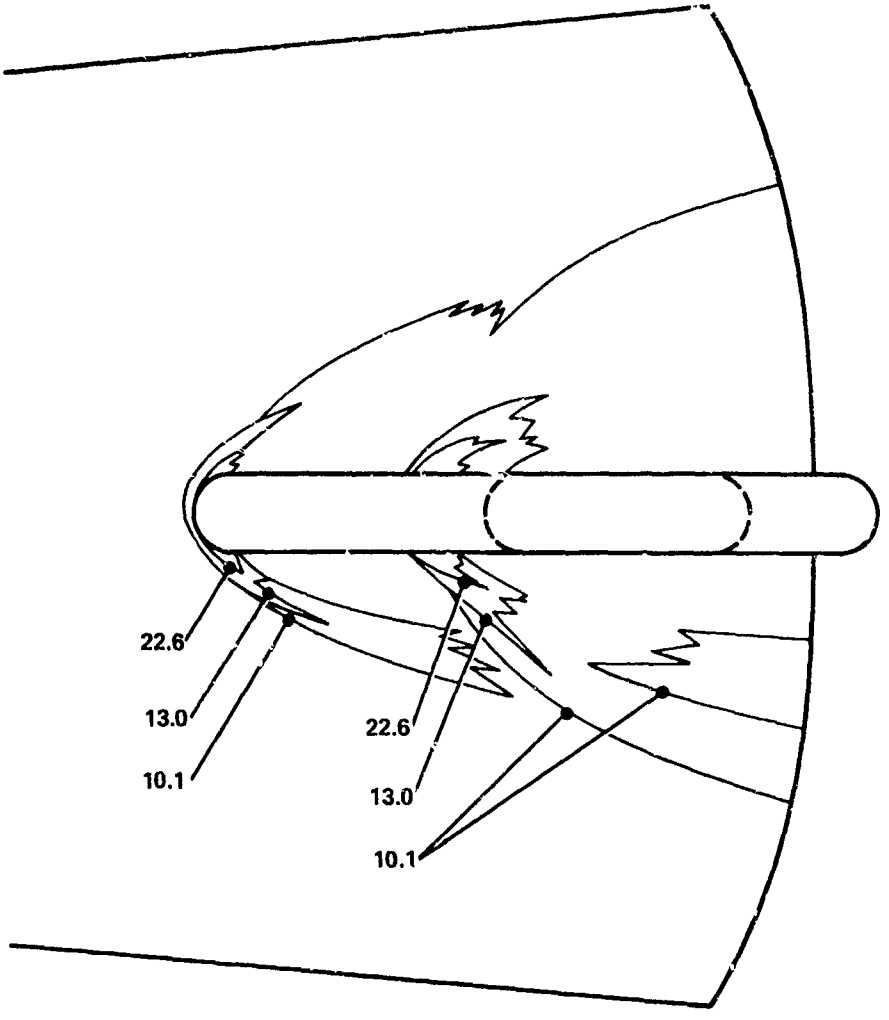

$\dot{q} \times 10^3$, BTU/FT^2-SEC-°R

FIG. 32 ISOHEATING CONTOURS FOR 60° SWEPT FIN WITH 0.060-INCH FIN-CONE GAP. TOP VIEW

$M_\infty = 5$
$Re_\infty/FT = 4.5 \times 10^6$
GAP = 0.125"

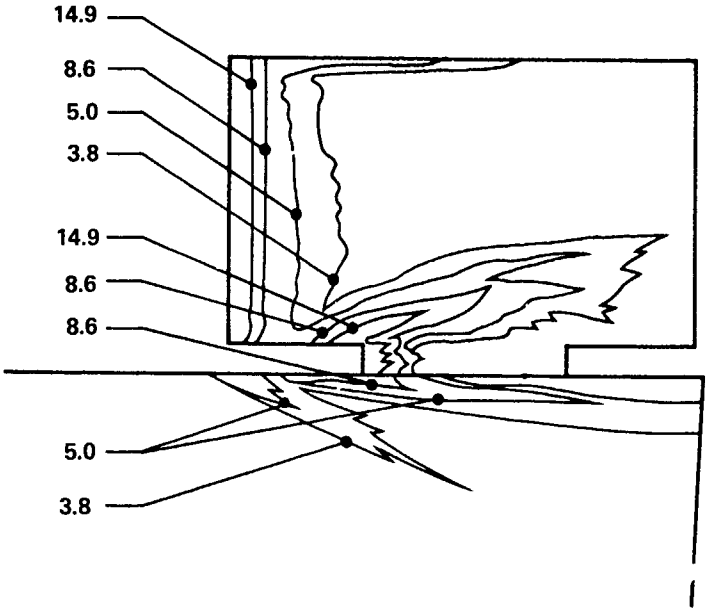

h x 10^3, BTU/FT^2–SEC–^oR

FIG. 33 ISOHEATING CONTOURS FOR UNSWEPT FIN WITH 0.125-INCH FIN-CONE GAP. SIDE VIEW

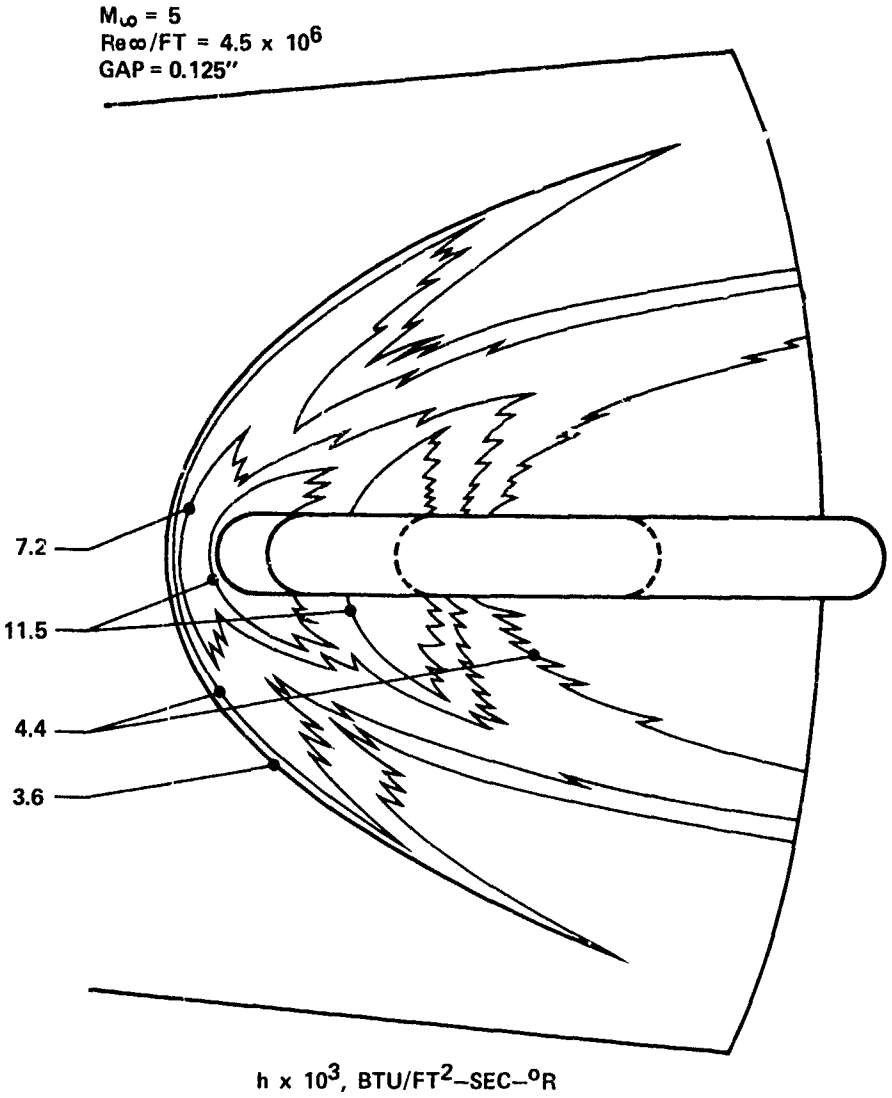

FIG. 34 ISOHEATING CONTOURS FOR UNSWEPT FIN WITH 0.125-INCH FIN-CONE GAP. TOP-VIEW, ABOUT 10^o FORWARD OF LEADING EDGE

$M_\infty = 5$

Re_∞ /FT = 12.9×10^6

GAP = 0.125"

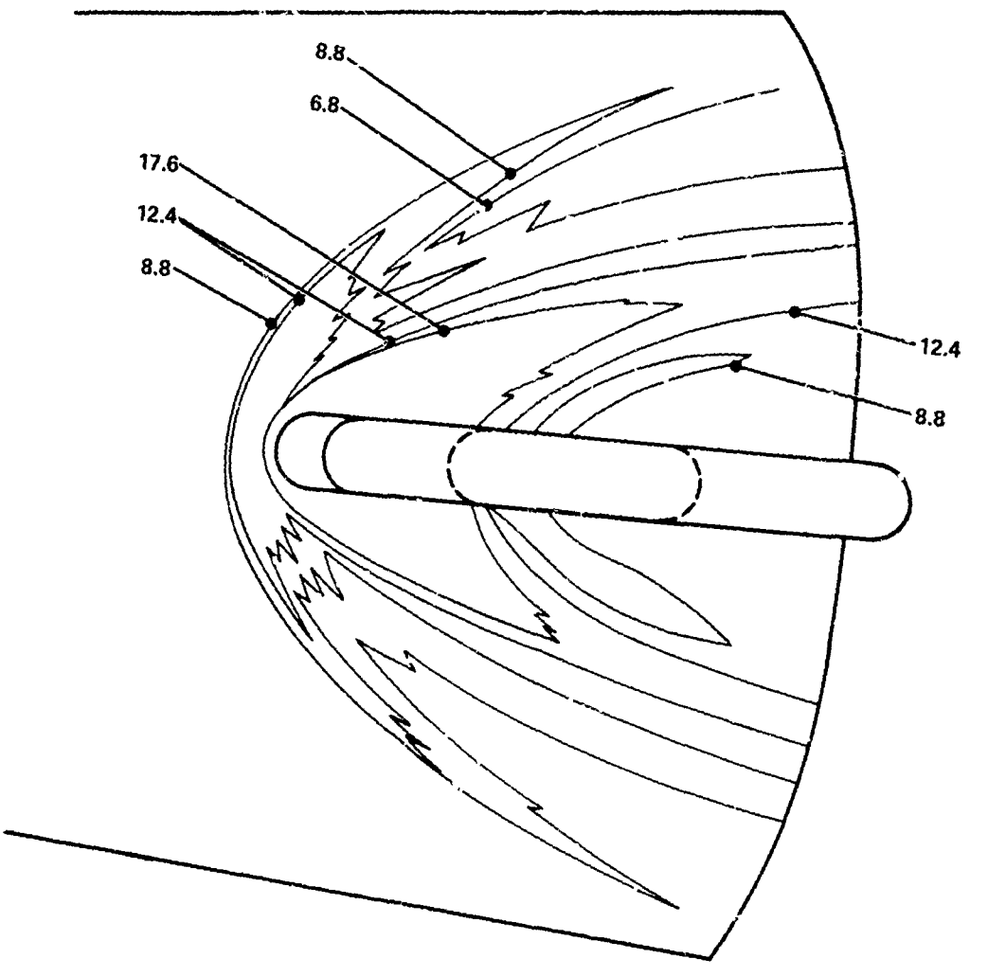

h x 10^3, BTU/FT^2-SEC-°R

FIG. 35 ISOHEATING CONTOURS FOR UNSWEPT FIN WITH 0.125-INCH FIN-CONE GAP. TOP VIEW

$M_\infty = 5$
$Re_\infty/FT = 26 \times 10^6$
GAP = 0.125"

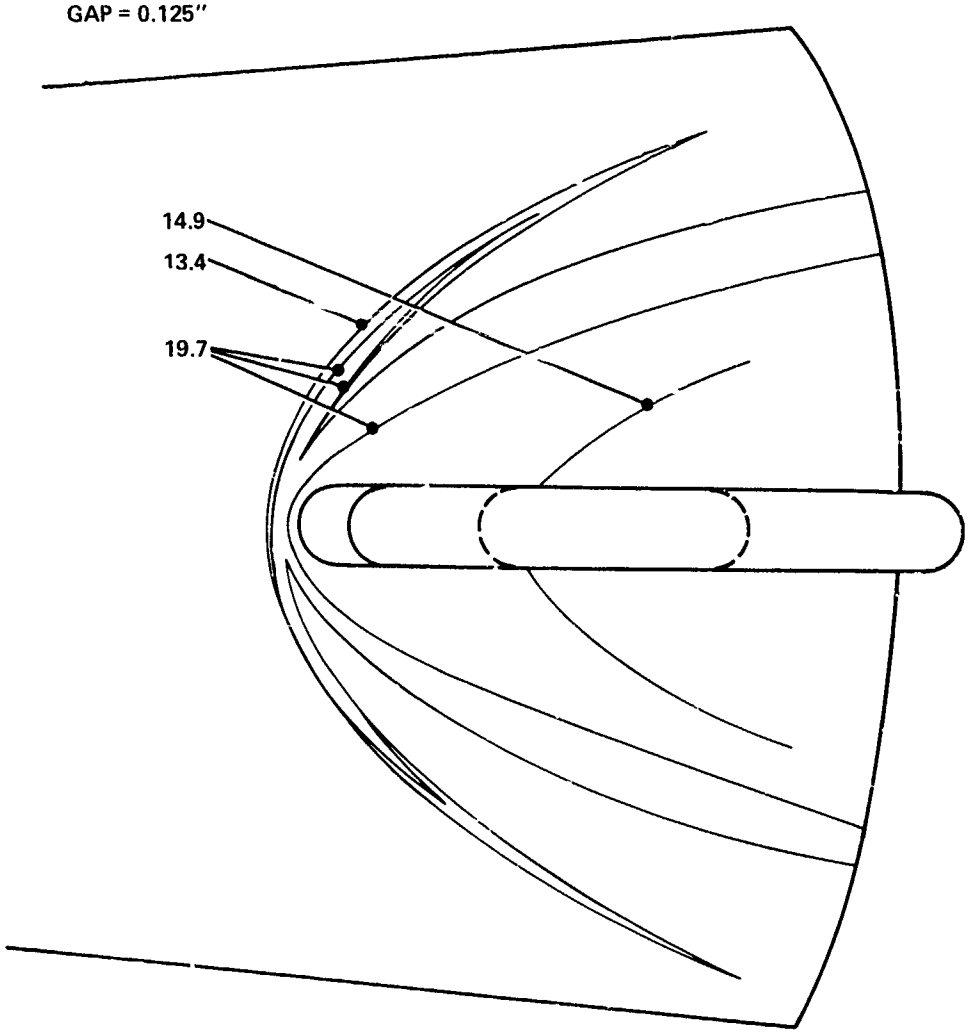

h x 10^3, BTU/FT^2-SEC-°R

FIG. 36 ISOHEATING CONTOURS FOR UNSWEPT FIN WITH 0.125-INCH FIN-CONE GAP. TOP VIEW

$M_\infty = 5$
$Re_\infty/FT = 4.5 \times 10^6$
GAP = 0.125"

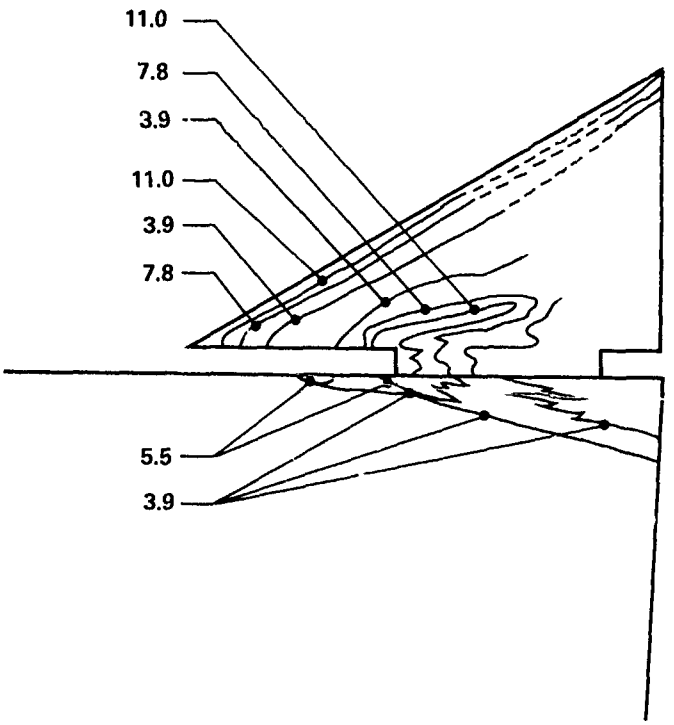

FIG. 37 ISOHEATING CONTOURS FOR 60°-SWEPT FIN WITH 0.125-INCH FIN CONE GAP. SIDE VIEW

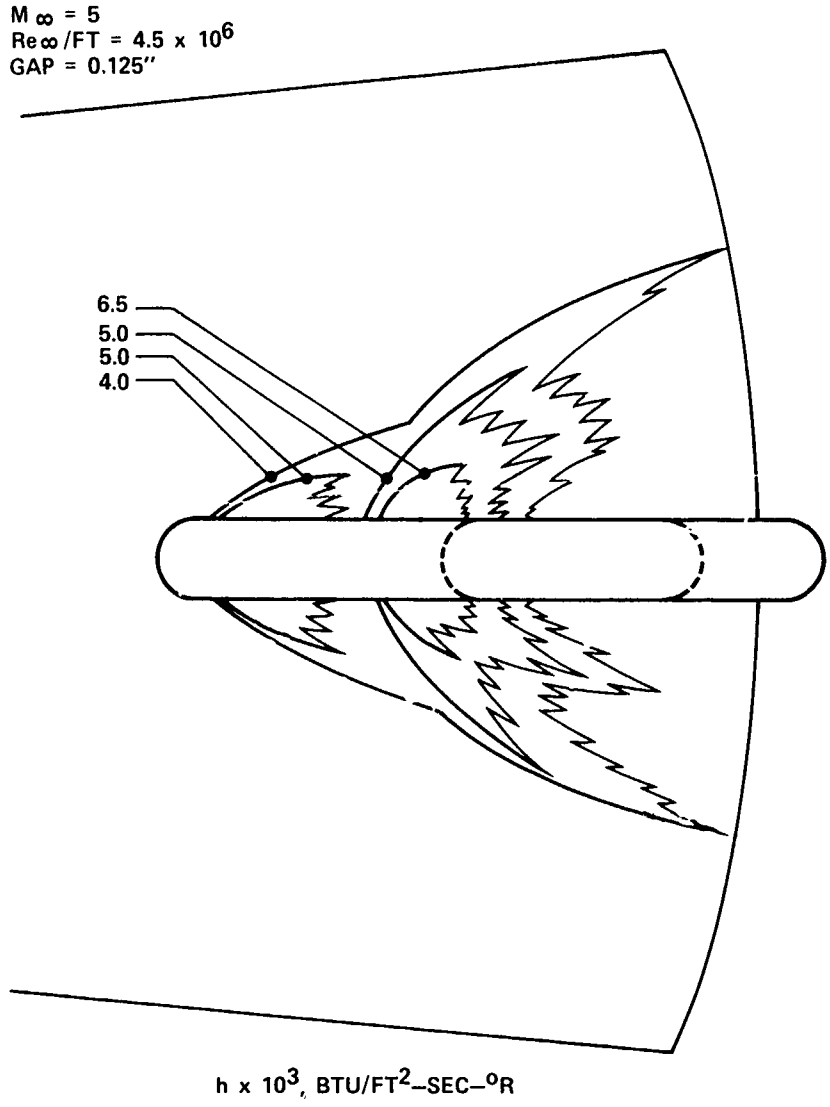

FIG. 38 ISOHEATING CONTOURS FOR 60° SWEPT FIN WITH 0.125-INCH FIN-CONE GAP. TOP VIEW

$M_\infty = 5$
$Re_\infty/FT = 12.9 \times 10^6$
GAP = 0.125"

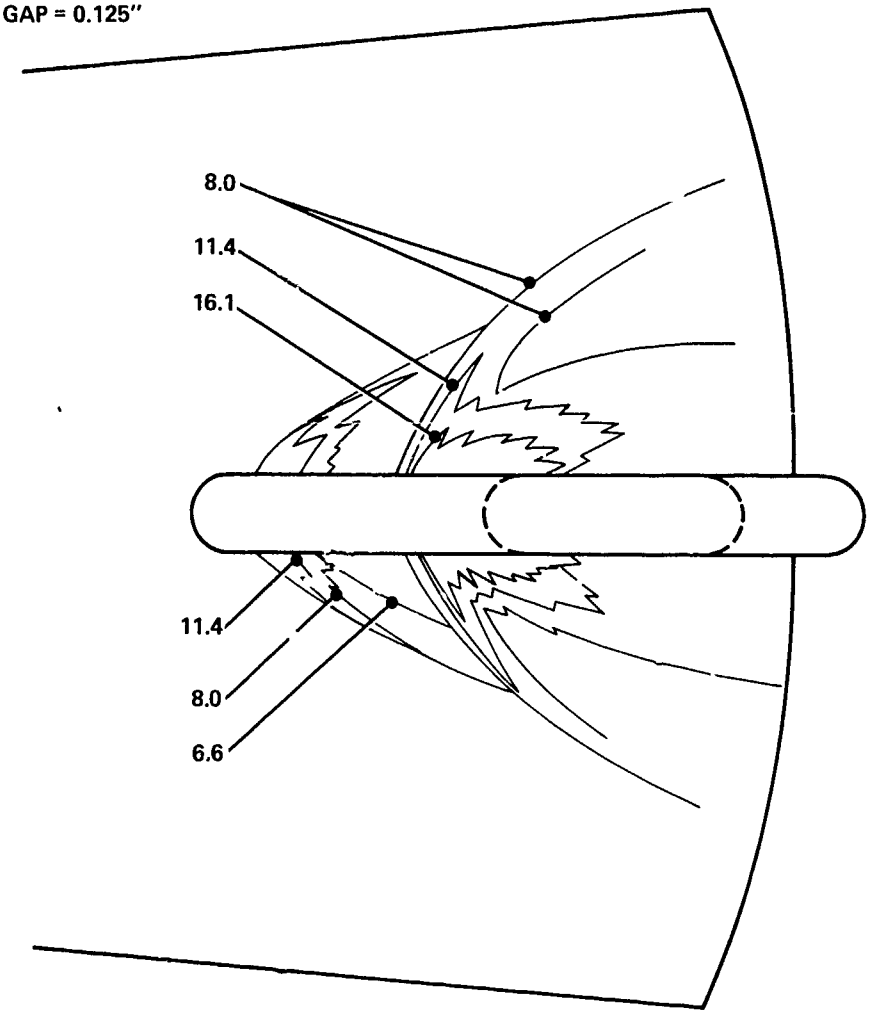

h x 10^3, BTU/FT^2-SEC-°R

FIG. 39 ISOHEATING CONTOURS FOR 60° -SWEPT FIN WITH 0.125-INCH FIN-CONE GAP. TOP VIEW

$M_\infty = 5$
$Re_\infty/FT = 26 \times 10^6$
GAP = 0.125"

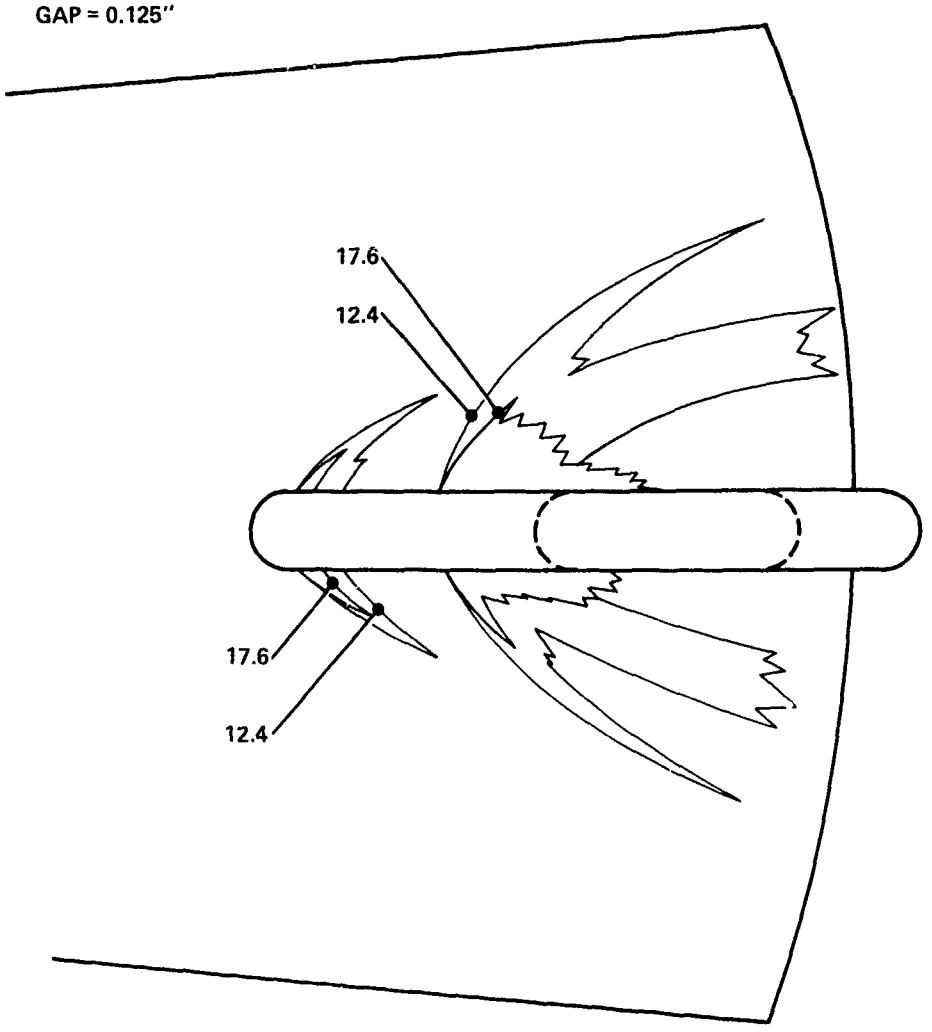

$h \times 10^3$, BTU/FT^2-SEC-°R

FIG. 40 ISOHEATING CONTOURS FOR 60° -SWEPT FIN WITH 0.125-INCH FIN-CONE GAP. TOP VIEW

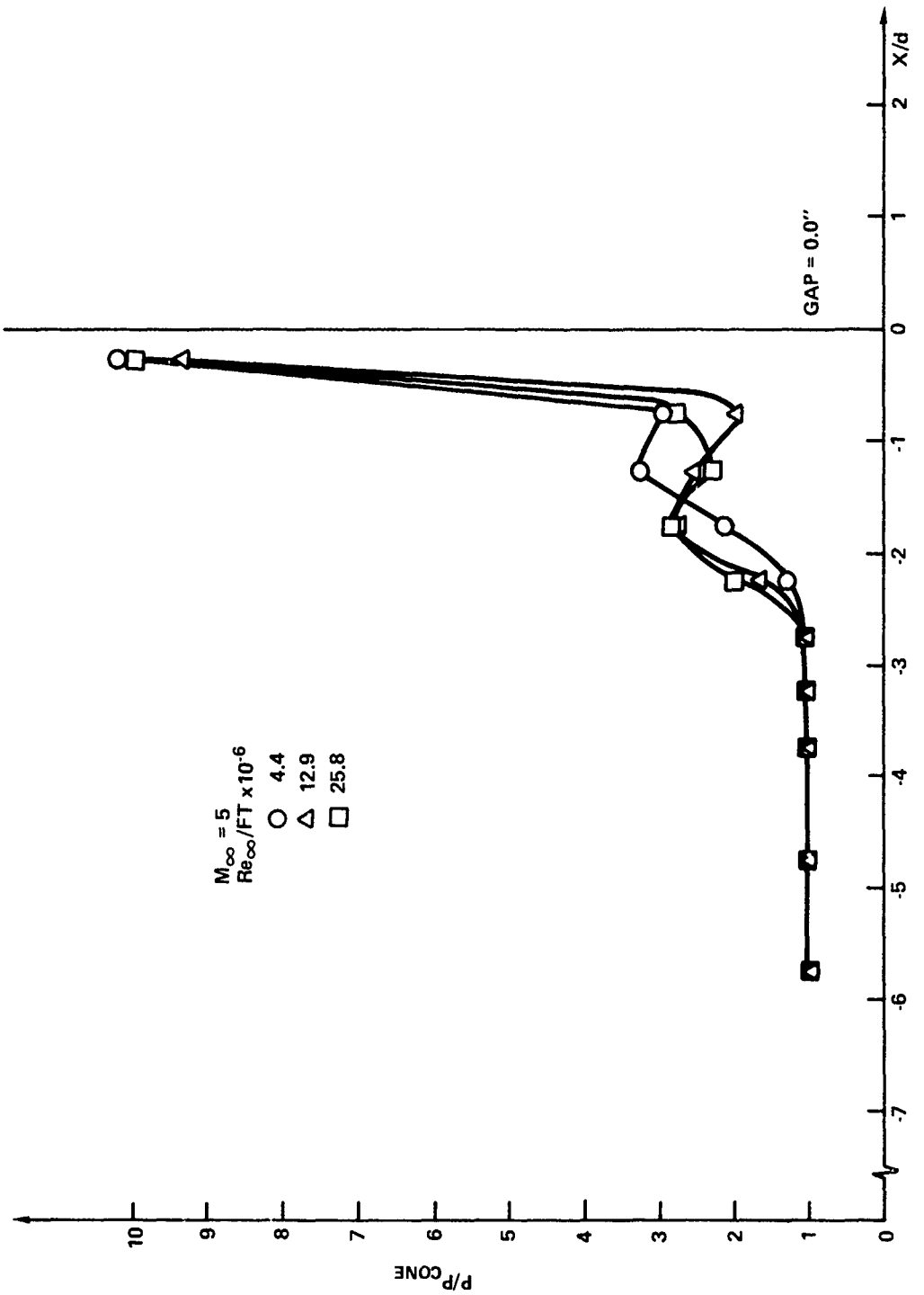

FIG. 41 PRESSURE DISTRIBUTION ON CONE AHEAD OF FLUSH-MOUNTED UNSWEPT FIN

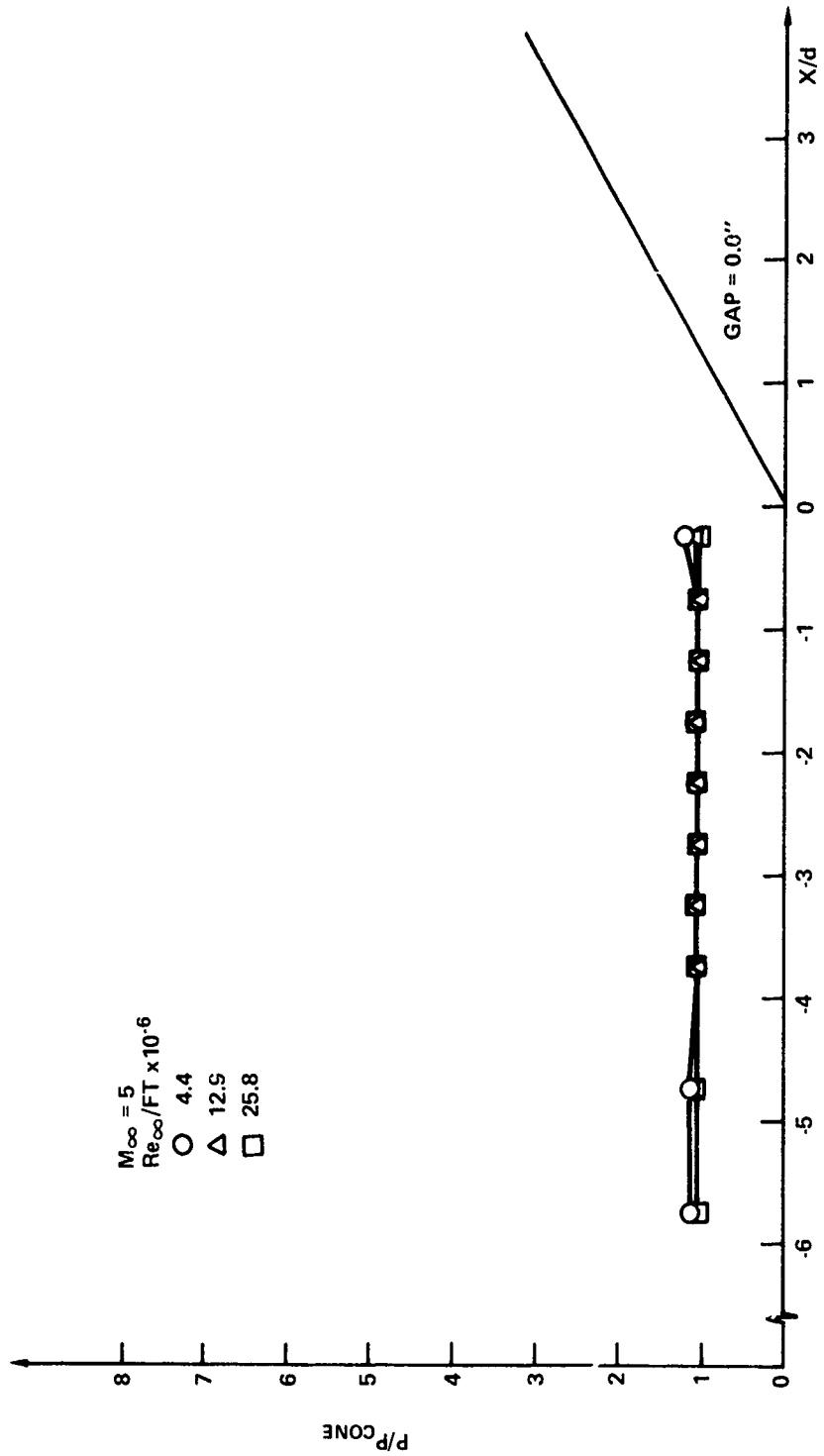

FIG. 42 PRESSURE DISTRIBUTION ON CONE AHEAD OF FLUSH-MOUNTED 60° -SWEPT FIN.

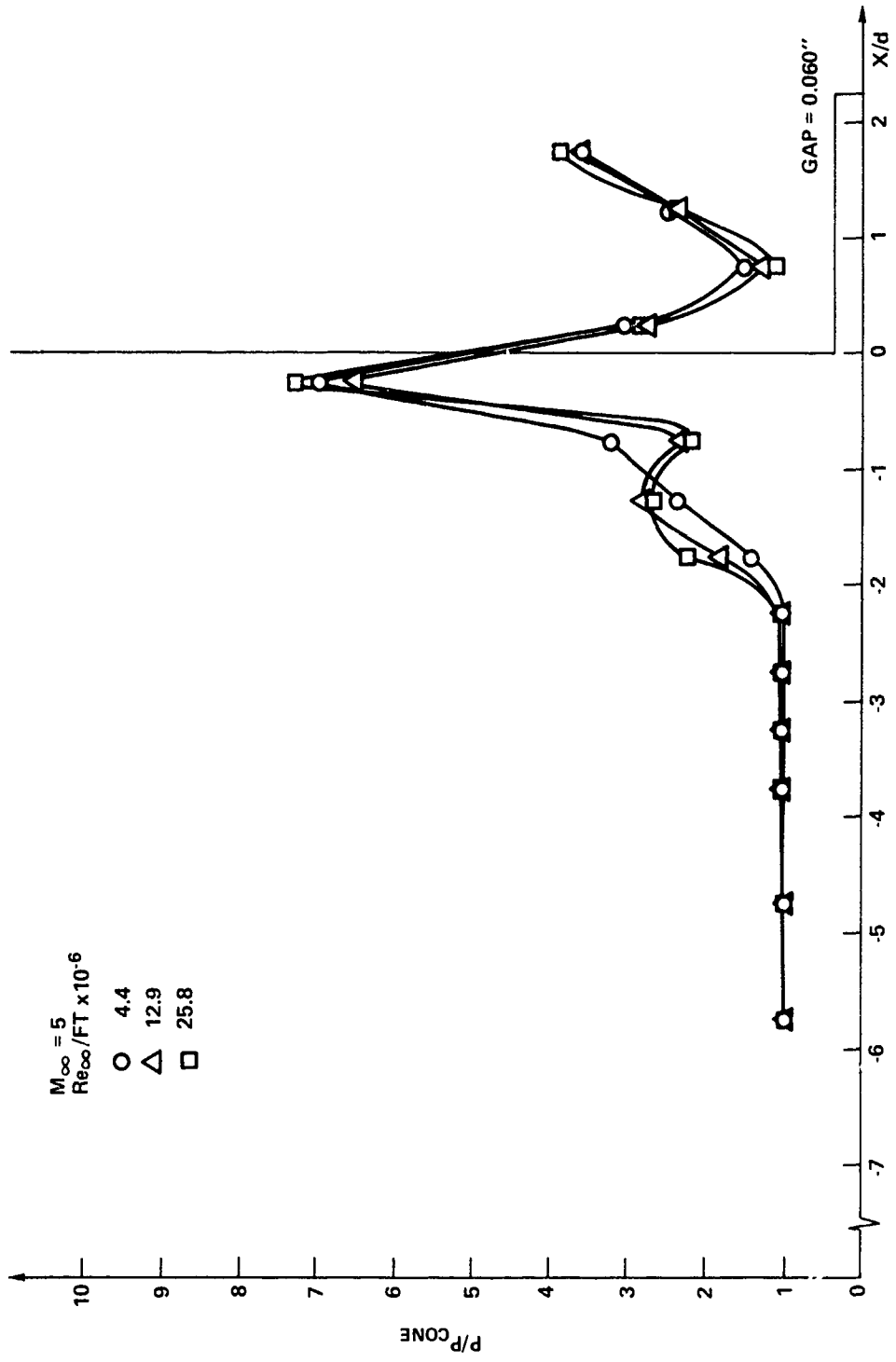

FIG. 43 PRESSURE DISTRIBUTION ON CONE FOR UNSWEPT FIN WITH 0.060-INCH FIN-CONE GAP.

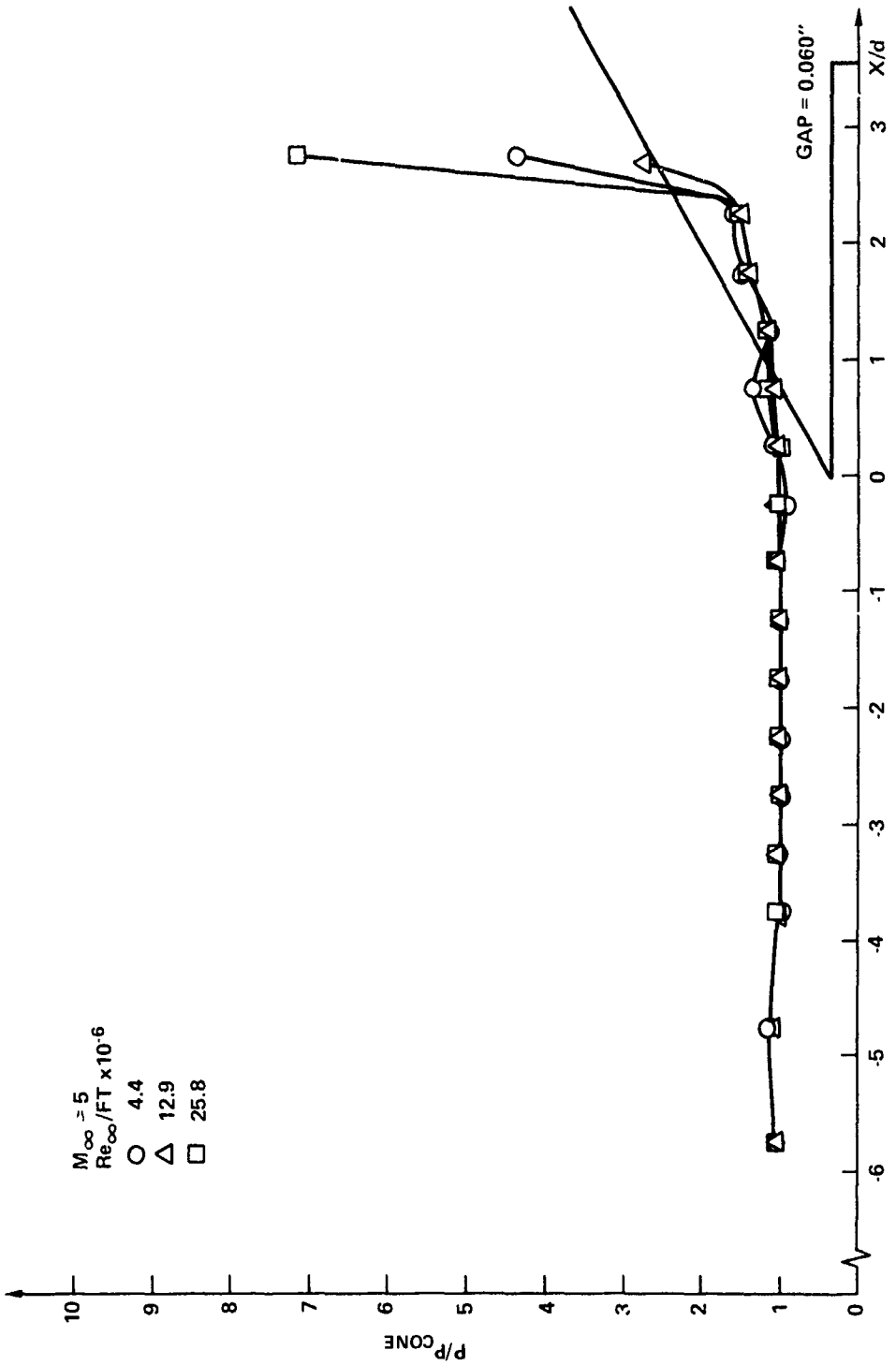

FIG. 44 PRESSURE DISTRIBUTION ON CONE FOR 60° -SWEPT FIN WITH 0.060-INCH FIN-CONE GAP.

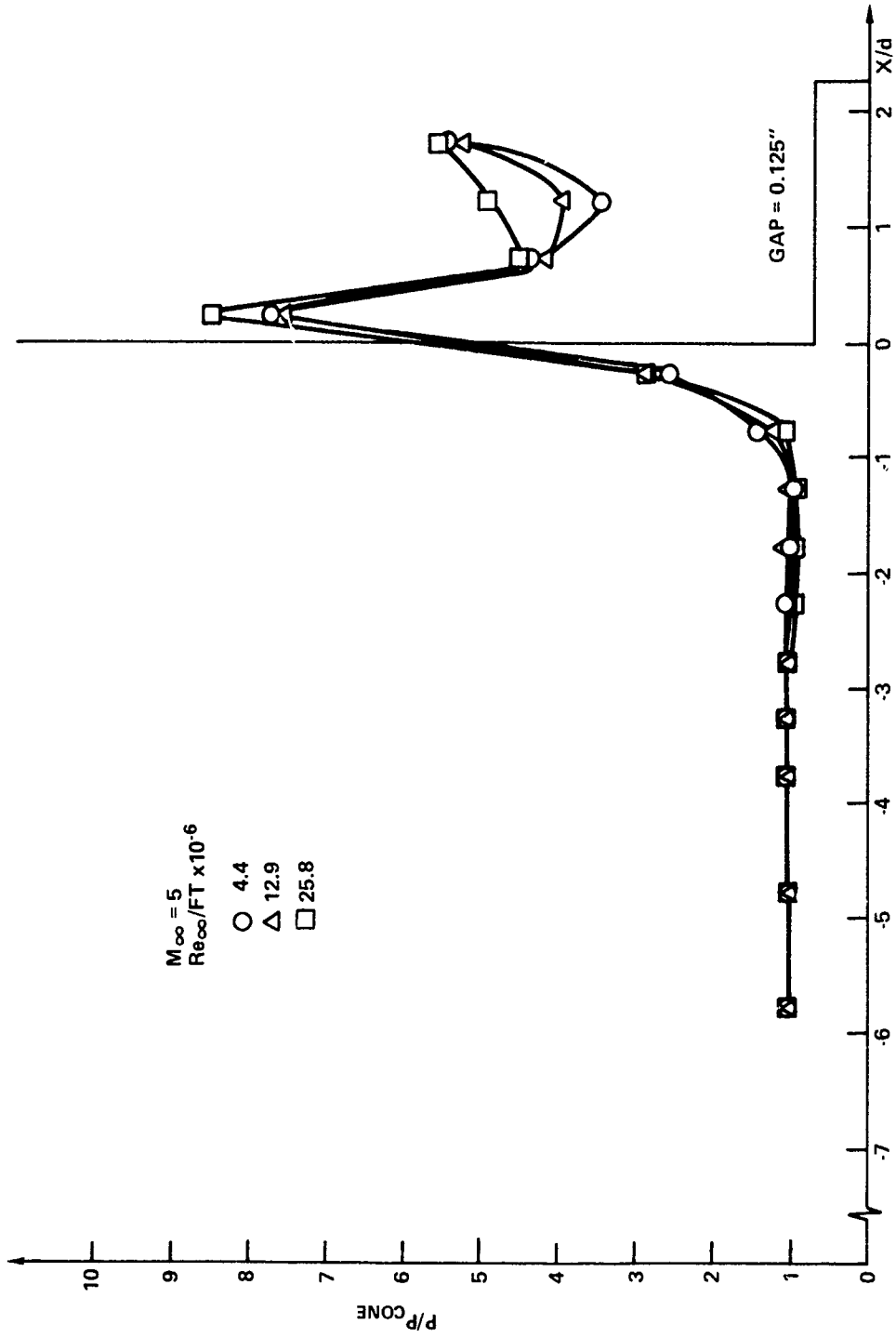

FIG. 45 PRESSURE DISTRIBUTION ON CONE FOR UNSWEPT FIN WITH 0.125-INCH FIN-CONE GAP.

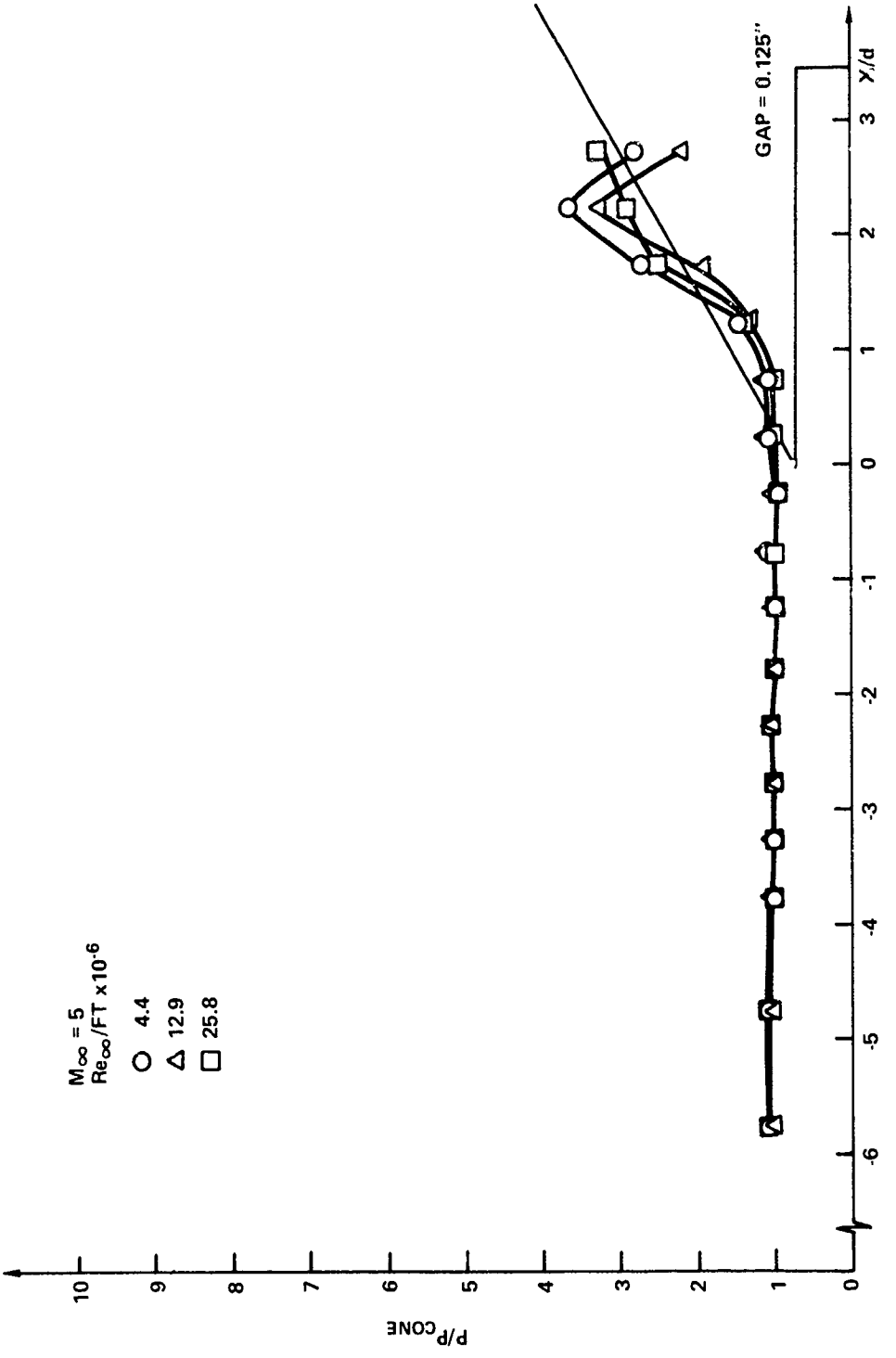

FIG. 46 PRESSURE DISTRIBUTION ON CONE FOR 60° -SWEPT FIN WITH 0.125-INCH FIN-CONE GAP

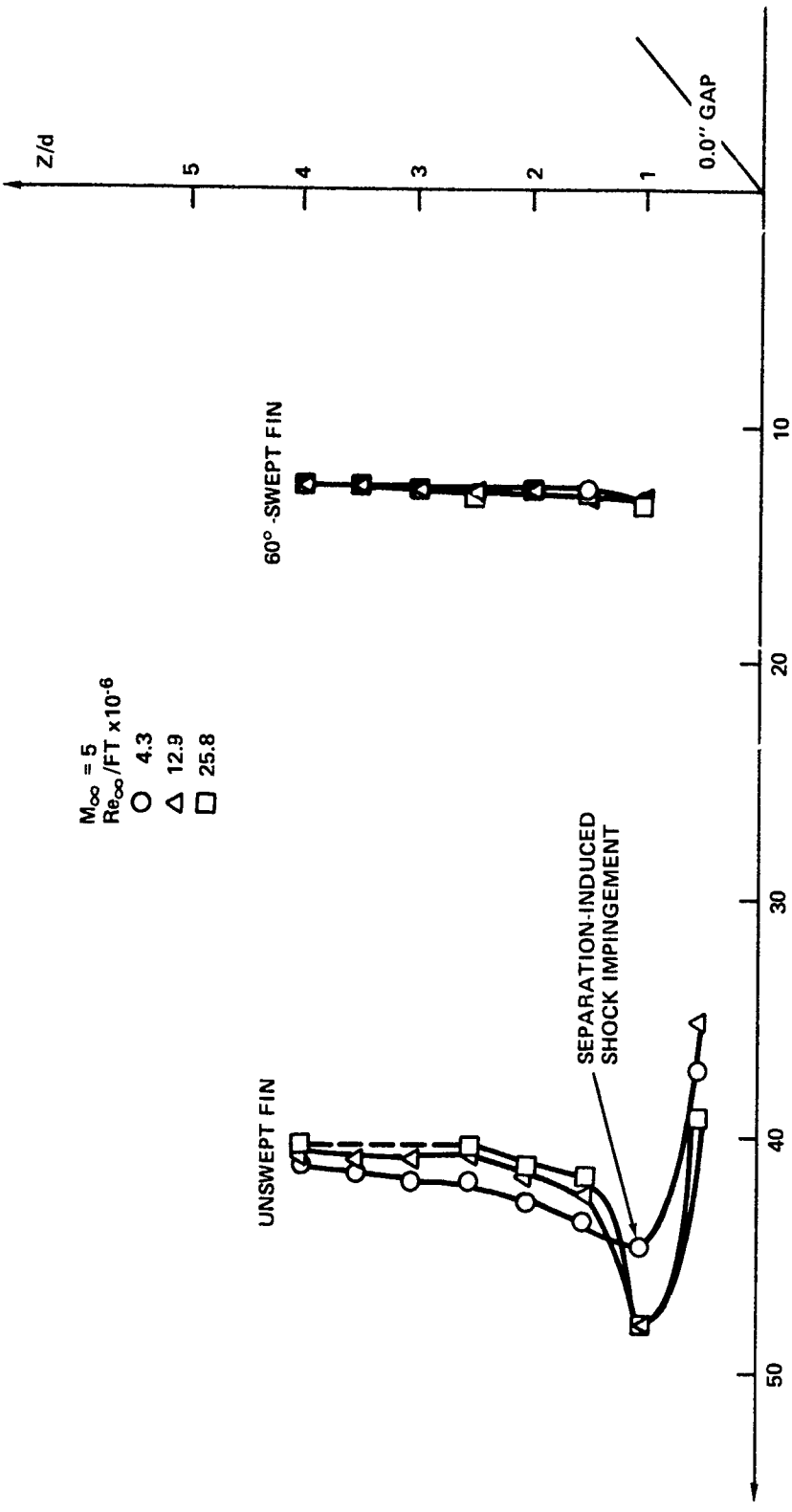

FIG. 47 LEADING-EDGE PRESSURE DISTRIBUTIONS FOR FLUSH-MOUNTED FINS

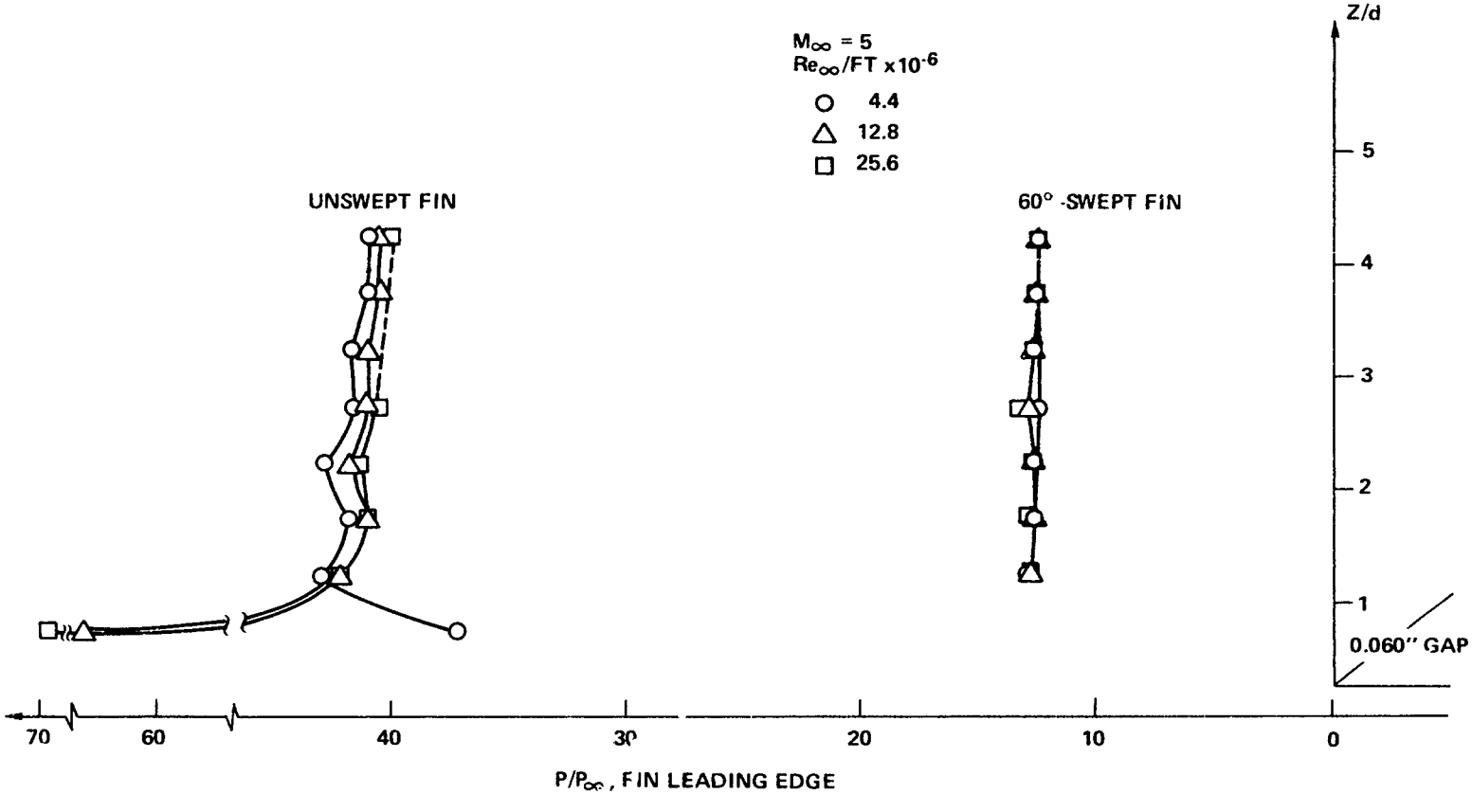

FIG. 48 LEADING-EDGE PRESSURE DISTRIBUTIONS FOR FINS WITH 0.060-INCH FIN-CONE GAP.

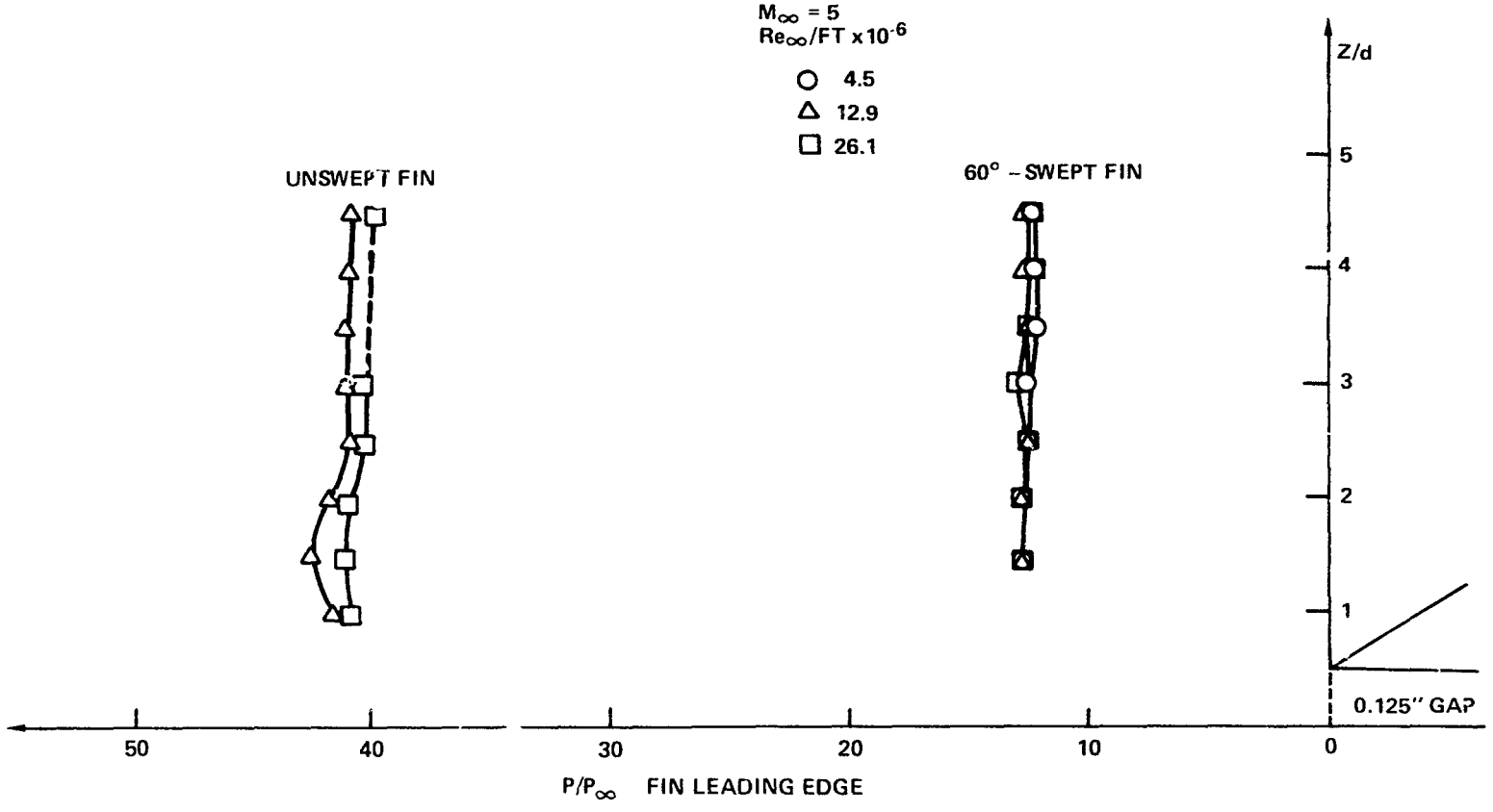

FIG. 49 LEADING-EDGE PRESSURE DISTRIBUTIONS FOR FINS WITH 0.125-INCH FIN-CONE GAP.

APPENDIX A

DETAILS OF FIN-CONE EXTENSIONS

The Teflon fin-cone extension is shown schematically in Figure A-1 with details of the location of embedded thermocouples and adjustment of the fins.

Figure A-2 shows schematically the locations of the pressure taps in the stainless-steel model.

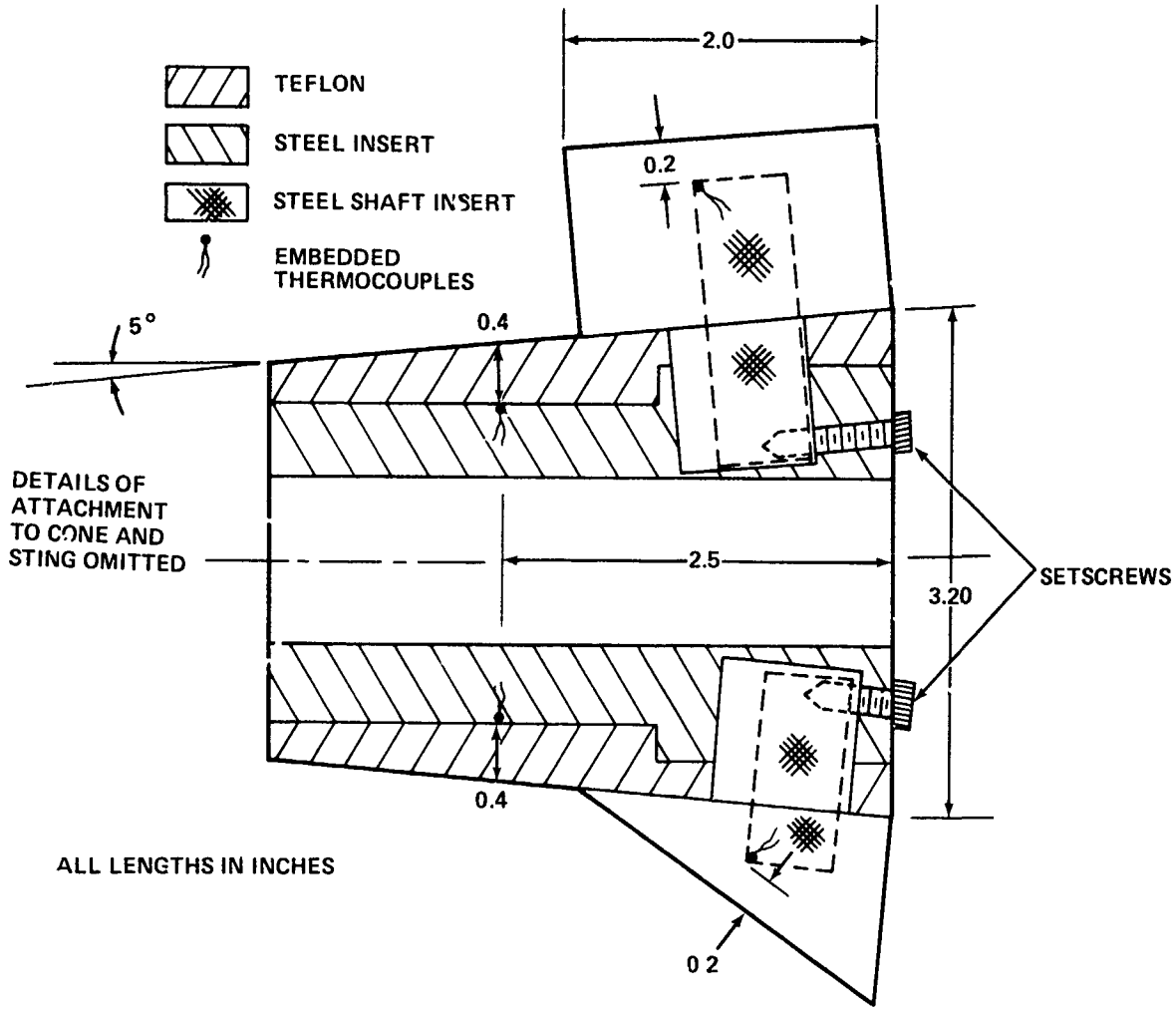

FIG. A - 1 SCHEMATIC DIAGRAM OF FINNED EXTENSION

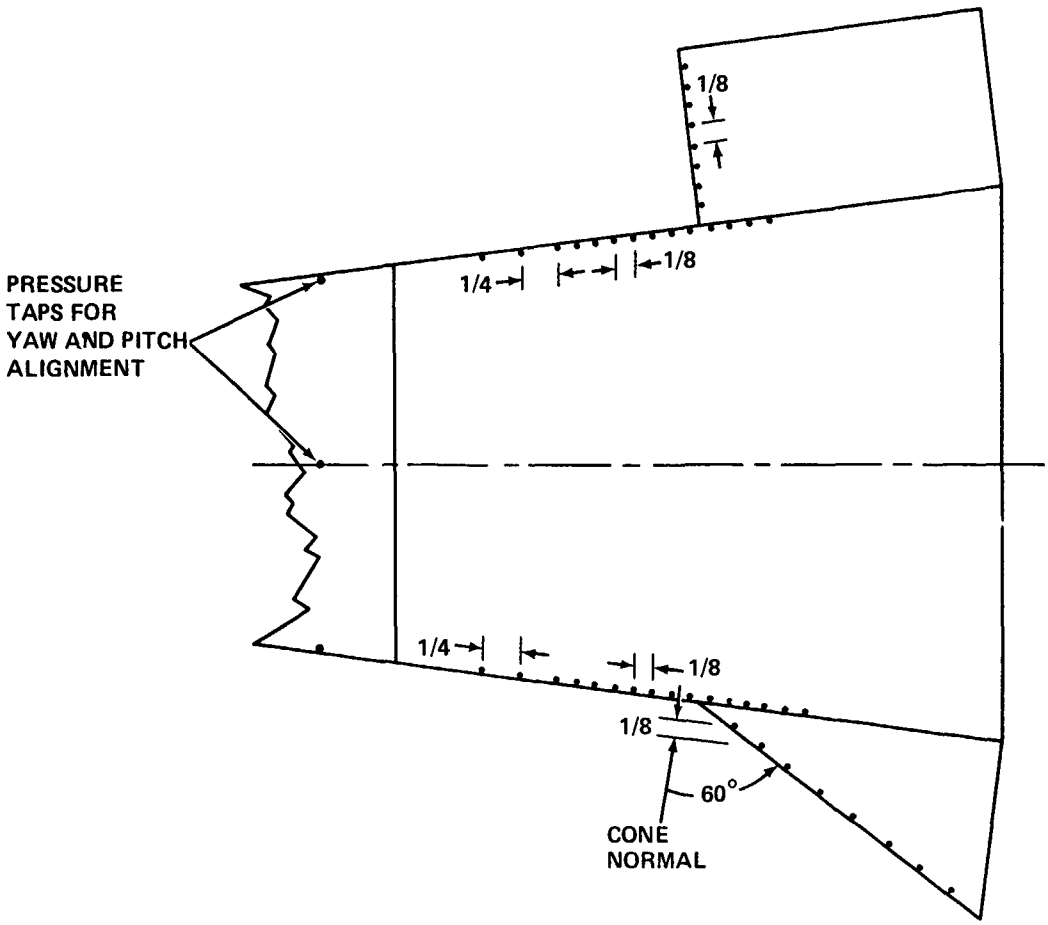

FIG. A-2 PRESSURE TAP LOCATIONS ON STAINLESS-STEEL MODEL

FLIGHT MEASUREMENTS DIVISION

EXTERNAL DISTRIBUTION LIST (A-1)

	Copies
Commander, Naval Sea Systems Command, Hqs. Department of the Navy Washington, D. C. 20360 Chief Tech. Analyst SEA 05121 SEA 033 SEA 031 SEA 09G32 SEA 035	2
Commander, Naval Air Systems Command, Hqs. Department of the Navy Washington, D. C. 20360 AIR 03B AIR 03C AIR 320 AIR 320C Dr. G. J. Mueller,AIR 310 AIR 50174	2
Office of Navy Research 800 N. Quincy St. Arlington, Va. 22217 ONR 100 Morton Cooper, 430B	2
Commander Naval Ship Research and Development Center Bethesda, Md. 20035 Central Library Br. (5641) Aerodynamics Lab. (5643)	
Commander, Naval Weapons Center China Lake, Calif. 93555 Technical Lib. (533) Code 406 R. E. Meeker (4063)	
Director, U. S. Naval Research Laboratory Washington, D. C. 20390 Library Code 6503	
NASA Langley Research Center Hampton, Va. 23665 MS/185 Technical Library Aero & Space Mech. Div. Dennis Bushnell Ivan Beckwith R. Trimpi Julius Harris	
NASA Lewis Research Center 21000 Brookpart Road Cleveland, Ohio 44135 Library 60-3 Ch, Wind Tunnel & Flight Div.	
NASA George C. Marshall Space Flight Center Huntsville, Ala. 35812 Mr. T. Reed, R-AERO-AU Mr. W. K. Dahm,	
NASA 600 Independence Ave., S. W. Washington, D. C. 20546 F. C. Schwenk, Director, Research (Code RR)	
NASA P. O. Box 33 College Park, Md. 20740	
NASA Ames Research Center Moffett Field, Ca. 94035 Dr. M. Horstman P. Kutler J. Rakich R. MacCormack L. H. Jorgensen E. J. Hopkins H. H. Album E. R. Keener	
Technical Library Director Defense Research and Engineering (DDR+E) Room 3E-1063, The Pentagon Washington, D. C. 20301 Stop 103	
Defense Documentation Center Cameron Station Alexandria, Va. 22314	12
Commander (5632.2) Naval Missile Center Point Mugu, Ca. 93041 Technical Library	
Commanding Officer USA Aberdeen Research and Development Center Aberdeen Proving Ground, Maryland 21005 STEAP-TL (Tech Lib Div) AMXRD-XSE	
Director, Stragetic Systems Project Office Department of the Navy Washingron, D. C. 20390 SP-2722	
Director of Intelligence Hdqs., USAF (AFNINDE) Washington, D. C. 20330 AFOIN-3B	2
Los Angeles Air Force Station SAMSO/DYAE P.O. Box 92960, Worldway Postal Center Los Angeles, CA 90009 Code RSSE Code RSSM	
Headquarters, Arnold Engineering Development Center Arnold Air Force Station, Tenn. 37389 Library Documents R. W. Henzel, TD Capt. C. Tirres/DYR C. Welsh	
von Karman Gas Dynamics Facility ARO, Inc. Arnold Air Force Station, Tenn. 37389 Dr. J. Whitfield, Chief L. M. Jenke W. B. Baker, Jr.	

	Copies
Commanding Officer, Harry Diamond Laboratories Washington, D. C. 20438 Library, Rm 211, Bldg. 92	
Commanding General U. S. Army Missile Command Redstone Arsenal, Ala. 35809 AMSMI-RR Ch, Document Sec. AMSMI-RDK, Mr. R. Deep AMSMI-RDK, Mr. T. Street D. J. Spring	2
Department of the Army Deputy Chief of Staff for Research, Development and Acquisition Washington, D. C. 20310 DAMA-WSM-T DAMA-AR	
Commanding Officer Picatinny Arsenal Dover, N. J. 07801 Mr. A. A. Loeb SMUPA-VC-3	
Commander (ADL) Naval Air Development Center Johnsville, Pa. 18974	
Air Force Weapons Laboratory Kirtland Air Force Base Albuquerque, N. M. 87117 Technical Library (SUL) Capt. Tolman/SAS	
U. S. Army Ballistic Missile Defense Agency 1300 Wilson Blvd. Arlington, Va. 22209 Dr. S. Alexander	
The Johns Hopkins University (C/NOw 7386) Applied Physics Laboratory Johns Hopkins Road, Laurel, Md. 20810 Document Library Dr. F. Hill Dr. L. Cronvich	2
Director, Defense Nuclear Agency Headquarters DASA Washington, D. C. 20305 STSP (SPAS) (2 cpys)	
Commanding Officer Naval Intelligence Support Center 4301 Suitland Road Washington, D. C. 20390	
Department of Aeronautics DFAN USAF Academy Colorado 80840 Col. D. H. Daley Capt. J. Williams	
Armament Development and Test Center Eglin AFB, Fla 32542 Technical Lib, DLOSL	
Headquarters, Edgewood Arsenal Edgewood Arsenal, Md. 21010 A. Flatau	
Commander U. S. Army Natick Development Center Natick, Mass. 01760 AMXNM-UBS G. A. Barnard	
AFFDL/FX Wright-Patterson Air Force Base Dayton, Ohio 45433 Dr. D. J. Harney	
AFFDL/FXG Wright-Patterson Air Force Base Dayton, Ohio 45433 Mr. M. Buck P. Ciragosian	
Naval Air Test Facility Lake Hurst, N. J. 08733 Dr. W. Sule	
Army Aviation Systems Command P. O. Box 209, Main Office St. Louis, Mo. 63166 Dr. L. Lijewski	

Copies

The Johns Hopkins University
Baltimore, Maryland 21218
Prof. S. Corrsin

University of Kentucky
Wenner-Gren Aero. Lab.
Lexington, Kentucky 40506
C. F. Knapp

Department of Aero.
Engineering, ME 106
Louisianna State University
Baton Rouge
Louisiana 70803
Dr. P. M. Miller

University of Maryland
College Park
Maryland 20740
Prof. A. Wiley Sherwood
Department of Aerospace
Engineering
Prof. Charles A. Shreeve
Department of
Mechanical Engineering
Dr. S. I. Pai, Institute
for Fluid Dynamics and
Applied Mathematics
Dr. Redfield W. Allen
Department of
Mechanical Engineering
Dr. W. L. Melnik
Department of
Aerospace Engineering
Dr. John D. Anderson, Jr.
Department of
Aerospace Engineering

Michigan State University
Library
East Lansing
Michigan 48823
Documents Department

Massachusetts Institute of
Technology
Cambridge
Massachusetts 02139
Mr. J. R. Martuccelli
Rm. 33-211
Prof. M. Finston
Prof. J. Baron, Dept.
of Aero. and Astro.
Rm. 37-461
Prof. A. H. Shapiro
Head, Mech. Engr. Dept.
Aero. Engineering Library
Prof. Ronald F. Probestein
Dr. E. E. Covert
Aerophysics Laboratory

University of Michigan
Ann Arbor, Michigan 48104
Dr. M. Sichel, Dept of Aero Engr
Engineering Library
Aerospace Engineering Lib.
Mr. C. Cousineau, Engin-Trans Lib.

Serials and Documents
Section
General Library
University of Michigan
Ann Arbor, Michigan 48104

Mississippi State
University
Department of Aerophysics
and Aerospace Engineering
P.O. Drawer A
State College, Mississippi 39762
Mr. Charles B. Clift

Copies

U.S. Naval Academy
Annapolis, Maryland 21402
Engineering Department
Aerospace Division

Library, Code 2124
U. S. Naval Postgraduate
School
Monterey, California 93940
Technical Reports Section

New York University
University Heights
New York, New York 10453
Dr. Antonio Ferri
Director of Guggenheim
Aerospace Laboratories
Prof. V. Zakkay
Engineering and Science
Library

North Carolina State College
Raleigh
North Carolina 27607
Dr. F. R. DeJarnette, Dept
Mech. and Aero.
Engineering
Dr. H. A. Hassan, Dept. of
Mech. and Aero. Engr.

D. H. Hill Library
North Carolina State
University
P.O. Box 5007
Raleigh
North Carolina 27607

University of North Carolina
Chapel Hill
North Carolina 27514
Department of Aero.
Engineering
Library, Documents Section
AFROTC Det 590

Northwestern University
Technological Institute
Evanston, Illinois 60201
Department of Mechanical
Engineering
Library

Virginia Polytechnical Institute
Blacksburg, Va. 24061
Prof. G. Inger

Department of Aero-Astro
Engineering
Ohio State University
2036 Neil Avenue
Columbus, Ohio 43210
Engineering Library
Prof. J. D. Lee
Prof. G. L. Von Eschen

Ohio State University
Libraries
Documents Division
1858 Neil Avenue
Columbus, Ohio 43210

The Pennsylvania State
University
University Park
Pennsylvania 18602
Dept. of Aero Engr.
Hammond Bldg.
Library, Documents
Section

Bevier Engineering Library
126 Benedum Hall
University of Pittsburgh
Pittsburgh
Pennsylvania 15261

COPIES

Princeton University
Aerospace & Mechanical Science Dept.
D-214 Engrg. Quadrangle
Princeton
New Jersey 08540
Prof. S. Bogdonoff
Dr. I. E. Vas

Purdue University
School of Aeronautical and
Engineering Sciences
Lafayette, Indiana 47907
Library
Dr. B. Reese, Head, Dept
of Aero. & Astro.

Rensselaer Polytechnic
Institute
Troy, New York 12181
Dept. of Aeronautical
Engineering and
Astronautics

Department of Mechanical
Industrial and Aerospace
Engineering
Rutgers - The State
University
New Brunswick, N. J. 08903
Dr. R. H. Page
Dr. C. F. Chen

Stanford University
Stanford
California 94305
Librarian, Dept. of
Aeronautics and
Astronautics

Stevens Institute of
Technology
Hoboken, New Jersey 07030
Mechanical Engineering
Department
Library

The University of Texas
at Austin
Applied Research Laboratories
P. O. Box 8029
Austin, Texas 78712
Director
Engr S.B.114B/Dr. Friedrich

University of Toledo
2801 W. Bancroft
Toledo, Ohio 43606
Dept. of Aero
Engineering
Dept. of Mech
Engineering

University of Virginia
School of Engineering
and Applied Science
Charlottesville
Virginia 22901
Dr. I. D. Jacobson
Dr. G. Matthews
Dr. R. N. Zapata
University of Washington
Seattle
Washington 98105
Engineering Library
Dept. of Aeronautics and
Astronautics
Prof. R. E. Street, Dept.
of Aero. and Astro.
Prof. A. Hertzberg, Aero.
and Astro., Guggeheim
Hall

West Virginia University
Morgantown
West Virginia 26506
Library

COPIES

Federal Reports Center
University of Wisconsin
Mechanical Engineering
Building
Madison, Wisconsin 53706
S. Reilly

Prototype Development Associates
1740 Garry Avenue
Suite 201
Santa Ana, CA 92705
Dr. J. Dunn
Dr. P. Crenshaw

Los Alamos Scientific
Laboratory
P.O. Box 1663
Los Alamos
New Mexico 87544
Report Library

University of Maryland
Baltimore County (UMBC)
5401 Wilkens Avenue
Baltimore, Maryland 21228
Dr. R. C. Roberts
Mathematics Department

Systems Research Laboratories, Inc.
2800 Indian Ripple Road
Dayton, Ohio 45440
Dr. K. Ball
Dr. C. Ingram

Institute for Defense
Analyses
400 Army-Navy Drive
Arlington, Virginia 22202
Classified Library

Kaman Sciences Corporation
P.O. Box 7463
Colorado Springs
Colorado 80933
Library

Kaman Science Corporation
Avidyne Division
83 Second Avenue
Burlington
Massachusetts 01803
Dr. J. R. Ruetenik

Rockwell International
B-1 Division
Technical Information Center
(BA08)
International Airport
Los Angeles, Ca. 90009

Rockwell International
Corporation
Technical Information Center
4300 E. Fifth Avenue
Columbus, Ohio 43216

M. I. T. Lincoln Laboratory
P.O. Box 73
Lexington
Massachusetts 02173
Library A-082

The RAND Corporation
1700 Main Street
Santa Monica
California 90406
Library - D

Aerojet Electrosystems Co.
1100 W. Hollyvale Ave.
Azusa, Ca. 91702
Engineering Library

Copies

The Boeing Company
P.O. Box 3999
Seattle, Washington 98124
87-67

United Aircraft
Research Laboratories
East Hartford
Connecticut 06108
Dr. William M. Foley

United Aircraft Corporation
400 Main Street
East Hartford
Connecticut 06108
Library

Hughes Aircraft Company
Centinela at Teale
Culver City, Ca. 90230
Company Tech. Doc. Center
6/E11, B. W. Campbell

Lockheed Missiles & Space Co.
Continental Bldg., Suite 445
El Segundo, CA 90245
T. R. Fortune
F. E. Huggin

Lockheed Missiles and Space
Company
P.O. Box 504
Sunnyvale
California 94086
Mr. G. M. Laden, Dept.
81-25, Bldg. 154
Mr. Murl Culp

Lockheed Missiles and Space
Company
3251 Hanover Street
Palo Alto, California 94304
Technical Information
Center

Lockheed-California
Company
Burbank, California 91503
Central Library, Dept.
84-40, Bldg. 170
PLT. B-1

Vice President and Chief
Scientist
Dept. 03-10
Lockheed Aircraft
Corporation
P.O. Box 551
Burbank, California 91503

Martin Marietta Corporation
P.O. Box 988
Baltimore
Maryland 21203
Science-Technology Library
(Mail No. 398)

Martin Company
3211 Trade Winds Trail
Orlando, Florida 32805
Mr. H. J. Diebolt

General Dynamics
P.O. Box 748
Fort Worth, Texas 76101
Research Library 2246
George Kaler, Mail Zone
2880

Copies

Calspan Corporation
4455 Genesee Street
Buffalo, New York 14221
Library

Air University Library
(SE) 63-578
Maxwell Air Force Base
Alabama 36112

McDonnell Company
P.O. Box 516
St. Louis, Missouri 63166
R. D. Detrich, Dept. 209
Bldg. 33

W. Brian Brooks

McDonnell Douglas Astronautics Co. - West
5301 Bolsa Avenue
Huntington Beach, California 92647
A3-339 Library
J. S. Murphy, A3-833
M. Michael Briggs

Fairchild Hiller
Republic Aviation Division
Farmingdale
New York 11735
Engineering Library

General Applied Science
Laboratories, Inc.
Merrick and Stewart
Avenues
Westbury, Long Island
New York 11590
Dr. F. Lane
L. M. Nucci

General Electric Company
Research and Development
Lab. (Comb. Bldg.)
Schenectady
New York 12301
Dr. H. T. Nagamatsu

The Whitney Library
General Electric Research
and Development Center
The Knolls, K-1
P.O. Box 8
Schenectady
New York 12301
M. F. Orr, Manager

General Electric Company
Missile and Space Division
P.O. Box 8555
Philadelphia
Pennsylvania 19101
MSD Library
Larry Chasen, Mgr.
Dr. J. D. Stewart, Mgr.
Research and Engineering

General Electric Company
AEG Technical Information
Center, N-32
Cincinnati, Ohio 45215

General Electric Company
Re-Entry & Environmental Systems
Division
3198 Chestnut Street
Philadelphia, Penn. 19101
Dr. S. M. Scala
Dr. H. Lew
Mr. J. W. Faust
A. Martellucci
W. Daskin
J. D. Cresswell
J. Pettus
L. A. Marshall
J. Cassanto
R. Hobbs
C. Harris
F. George

DISTRIBUTION (CONT)

	Copies
AVCO-Everett Research Laboratory 2385 Revere Beach Parkway Everett Massachusetts 02149 Library Dr. George Sutton	2
LTV Aerospace Corporation Vought Aeronautics Division P.O. Box 5907 Dallas, Texas 75222 Unit 2-51131 (Library)	
LTV Aerospace Corporation Missiles and Space Division P.O. Box 6267 Dallas, Texas 75222 MSD-T-Library	
Northrop Norair 3901 West Broadway Hawthorne California 90250 Tech. Info. 3360-32	
Government Documents The Foundren Library Rice Institute P.O. Box 1892 Houston, Texas 77001	
Grumman Aircraft Engineering Corporation Bethpage, Long Island New York 11714 Mr. R. A. Scheuing Mr. H. B. Hopkins Mr. H. R. Peed	
Marquardt Aircraft Corporation 16555 Saticoy Street Van Nuys, California 91409 Library	
ARDE Associates P.O. Box 286 580 Winters Avenue Paramus, New Jersey 07652 Librarian	
Aerophysics Company 3500 Connecticut Ave. N.W. Washington, D.C. 20008 Mr. G. D. Boehler	
Aeronautical Research Associates of Princeton 50 Washington Road Princeton New Jersey 08540 Dr. C. duP. Donaldson	
General Research Corporation 5383 Hollister Avenue P.O. Box 3587 Santa Barbara California 93105 Technical Information Office	
Sandia Laboratories Mail Service Section Albuquerque, N. M. 87115 Mr. K. Goin, Div. 5262 Mr. W. H. Curry, Div. 1331 Mr. A. M. Torneby, 3141 Dr. G. Stone Div. 3141	
Hercules Incorporated Allegany Ballistics Laboratory P.O. Box 210 Cumberland Maryland 21502 Library	
General Electric Company P.O. Box 2500 Daytona Beach Florida 32015 Dave Hovis, Rm. 4109	
TRW Systems Group 1 Space Park Redondo Beach California 90278 Technical Libr//Doc Acquisitions B. Pearce, Aero Dept. F. D. Deffenbaugh	
Stanford Research Institute 333 Ravenswood Avenue Menlo Park California 94025 Dr. G. Abrahamson	
Hughes Aircraft Company P.O. Box 3310 Fullerton California 92634 Technical Library, 600-C222	
Westinghouse Electric Corporation Astronuclear Laboratory P.O. Box 10864 Pittsburgh Pennsylvania 15236 Library	
University of Tennesse Space Institute Tullahoma Tennessee 37388 Prof. J. M. Wu	
CONVAIR Division of General Dynamics Library and Information Services P.O. Box 12009 San Diego California 92112	
CONVAIR Division of General Dynamics Post Office Box 80986 San Diego, California 92138 Dr. J. Raat Mail Zone 640-02 Research Library	
AVCO Missiles Systems Division 201 Lowell Street Wilmington Massachusetts 01887 E. E. H Schurmann J. Otis	
Chrysler Corporation Space Division P.O. Box 29200 New Orleans, La 70189 N. D. Kemp, Dept. 2910 E. A. Rawls, Dept. 2920	
General Dynamics Pomona Division P.O. Box 2507 Pomona, Ca. 91766 Tech. Doc. Center, Mail Zone 6-20	
General Electric Company 3198 Chesnut Street Philadelphia, Pa. 19101 W. Danskin Larry Chasen Dr. H. Lew	
Philco-Ford Corporation Aeroneutronic Division Newport Beach California 92660 Dr. A. Demetriades	

Copies

Raytheon Company
Missile Systems Division
Hartwell Road
Bedford, Ma. 01730
D. P. Forsmo

TRW Systems Group
Space Park Drive
Houston, Texas 77058
M. W. Sweeney, Jr.

Marine Bioscience Laboratory
513 Sydnor Street
Ridgecrest, Ca. 93555
Dr. A. C. Charters

University of California -
Los Angeles
Dept of Mechanics & Structures
Los Angeles, Ca. 90024
Prof. J. D. Cole

University of Wyoming
University Station
P. O. Box 3295
Laramie, Wyoming 82070
Head, Dept. Mech. Eng.

Applied Mechanics Review
Southwest Research Institute
8500 Culebra Road
San Antonio, Texas 78228

American Institute of Aeronautics
and Astronautics
1290 Sixth Avenue
New York, New York 10019
J. Newbauer

Technical Information Service
American Institute of Aeronautics
and Astronautics
750 Third Avenue
New York, New York 10017
Miss F. Marshall

Faculty of Aeronautical
Systems
University of West Florida
Pensacola, Florida 32504
Dr. R. Fledderman

Space Research Corporation
Chittenden Bank Building
North Troy, Vermont 05859
Library
J. A. Finkel

The Aerospace Corporation
P. O. Box 92957
Los Angeles, California 90009
J. M. Lyons, Bldg. 82

Chrysler Corp., Defense Division
Detroit, Michigan 48231
Dr. R. Lusardi

AERO
3020 Buckingham Drive
South Bend, Indiana 46614
Dr. J. Nicolaides

Acurex Corp. Aerotherm
485 Clyde Avenue
Mt. View, CA 94042
L. Cooper

Sandia Corporation
Livermore, CA 94550
J. K. Kryvoruka

Copies

Near, Inc.
510 Clyde Avenue
Mountain View, CA 94043

CONVAIR Division of General Dynamics
P.O. Box 80847
San Diego, California 92138
Dr. E. S. Levinsky
Mail Zone 667-1